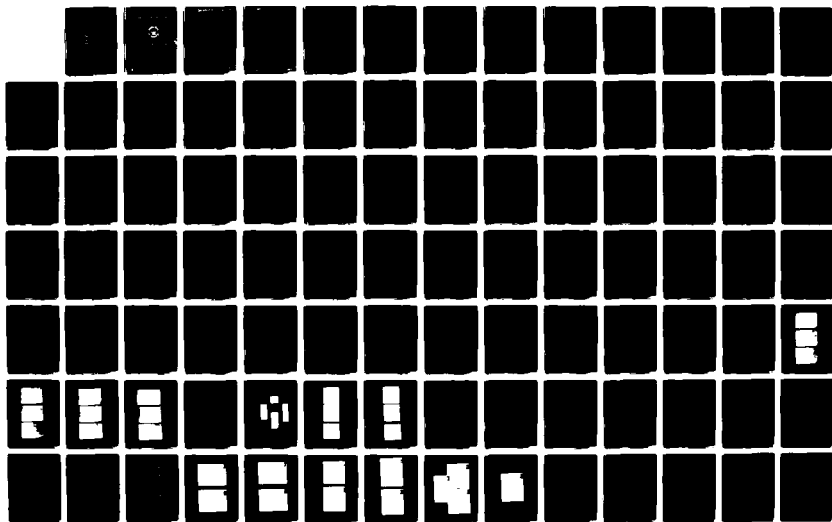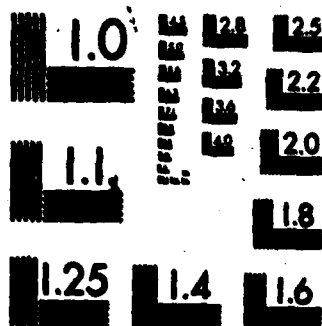AD-A129 427　FRACTURE TOUGHNESS DEGRADATION IN HY-80 AND HY-100　1/2
　　　　　　　AFTER PRESTRAINING(U) NAVAL POSTGRADUATE SCHOOL
　　　　　　　MONTEREY CA　J N MULLICAN MAR 83
UNCLASSIFIED　　　　　　　　　　　　　　　　F/G 11/6　　NL

MICROCOPY RESOLUTION TEST CHART

NATIONAL BUREAU OF STANDARDS-1963-A

NAVAL POSTGRADUATE SCHOOL
Monterey, California

THESIS

FRACTURE TOUGHNESS DEGRADATION
IN HY-80 AND HY-100 AFTER PRESTRAINING

by

James Neal Mullican

March 1983

Thesis Advisor: K. D. Challenger

Approved for public release, distribution unlimited.

83 06 17 007

SECURITY CLASSIFICATION OF THIS PAGE (When Data Entered)

REPORT DOCUMENTATION PAGE	READ INSTRUCTIONS BEFORE COMPLETING FORM	
1. REPORT NUMBER	2. GOVT ACCESSION NO. AD-A129 427	3. RECIPIENT'S CATALOG NUMBER
4. TITLE (and Subtitle) Fracture Toughness Degradation in HY-80 and HY-100 After Prestraining	5. TYPE OF REPORT & PERIOD COVERED Engineer's Thesis; March 1983	
	6. PERFORMING ORG. REPORT NUMBER	
7. AUTHOR(s) James Neal Mullican	8. CONTRACT OR GRANT NUMBER(s)	
9. PERFORMING ORGANIZATION NAME AND ADDRESS Naval Postgraduate School Monterey, California 93940	10. PROGRAM ELEMENT, PROJECT, TASK AREA & WORK UNIT NUMBERS	
11. CONTROLLING OFFICE NAME AND ADDRESS Naval Postgraduate School Monterey, California 93940	12. REPORT DATE March 1983	
	13. NUMBER OF PAGES 147	
14. MONITORING AGENCY NAME & ADDRESS(if different from Controlling Office)	15. SECURITY CLASS. (of this report) Unclassified	
	15a. DECLASSIFICATION/DOWNGRADING SCHEDULE	

16. DISTRIBUTION STATEMENT (of this Report)

Approved for public release, distribution unlimited.

17. DISTRIBUTION STATEMENT (of the abstract entered in Block 20, if different from Report)

18. SUPPLEMENTARY NOTES

19. KEY WORDS (Continue on reverse side if necessary and identify by block number)

HY-80, HY-100, Fracture Toughness, J_{1C}, Tearing Modulus, Plane Strain Fracture Strain.

$J_{sub\ 1C}$

20. ABSTRACT (Continue on reverse side if necessary and identify by block number)

This thesis is the first in a series that is attempting to discover the mechanism by which the fracture toughness (J_{1C}) of HY-series steel decreases with increasing prestrain at room temperature. This decrease in J_{1C} is a function of yield strength and plane strain fracture strain. However, this reduction in J_{1C} is shown to be caused by a reduction in the plane strain fracture strain. Fractographic ⟶

DD FORM 1473 1 JAN 73 EDITION OF 1 NOV 65 IS OBSOLETE
S/N 0102-014-6601 |

SECURITY CLASSIFICATION OF THIS PAGE (When Data Entered)

examinations have verified this reduction in the fracture strain and also have shown that regions of very low ductility exist due to alloy segregation that is present in bands. The mechanism for the degradation in the toughness is believed to be such that stress relieving following pre-straining would restore the toughness.

Accession For

NTIS GRA&I

DTIC TAB

Unannounced

Justification

By

Distribution/

Availability Codes

Avail and/or

Special

Fracture Toughness Degradation in HY-80
and HY-100 After Prestraining

by

James Neal Mullican
Lieutenant Commander, United States Navy
B.S.M.E., Georgia Institute of Technology, 1972

Submitted in partial fulfillment of the
requirements for the degrees of

MASTER OF SCIENCE IN MECHANICAL ENGINEERING

and

MECHANICAL ENGINEER

from the

NAVAL POSTGRADUATE SCHOOL
March 1983

Author _____

Approved by: _____
                                    Thesis Advisor
             _____
                                    Second Reader
             _____
             Chairman, Department of Mechanical Engineering
             _____
                         Dean of Science and Engineering

3

ABSTRACT

This thesis is the first in a series that is attempting to discover the mechanism by which the fracture toughness J_{1C}, of HY-series steel decreases with increasing pre-strain at room temperature. This decrease in J_{1C} is a function of yield strength and plane strain fracture strain. However, this reduction in J_{1C} is shown to be caused by a reduction in the plane strain fracture strain. Fractographic examinations have verified this reduction in the fracture strain and also have shown that regions of very low ductility exist due to alloy segregation that is present in bands. The mechanism for the degradation in the toughness is believed to be such that stress-relieving following prestraining would restore the toughness.

TABLE OF CONTENTS

5

LIST OF TABLES

8

LIST OF FIGURES

ACKNOWLEDGMENT

I wish to express my sincere appreciation to my thesis
advisor, Dr. Ken Challenger, for his patience and assistance
with this work; to Mr. Tom Kellogg for his invaluable assist-
ance in all phases of my laboratory work, and to Mrs. Anita
Garg for her assistance in the acquisition of the X-ray
diffraction patterns. A debt of thanks is also given to
my parents for their encouragement and confidence. Lastly,
I wish to especially thank my wife, Cindy, for her constant
support, understanding and love that sustained me in this
effort and throughout life.

I dedicate this work to Cindy and to my children, Ben
and Mary.

I. INTRODUCTION

In the 1981 fiscal year, David W. Taylor Naval Ship
Research and Development Center (DTNSRDC), Annapolis,
Maryland began the project, "Ductile Fracture Character-
ization of Prestrained HY Steel Plate". A part of this
project was to perform an analysis of the results obtained
from the J-integral elastic-plastic fracture tests of pre-
strained and as-received HY steels and to complete a
microfracture investigation of the compact tensile speci-
mens used in the J-integral tests. The J-integral test
results as reported by DTNSRDC indicated a reduction in
the fracture toughness parameter J_{1C} with increasing
amounts of prestrain in HY-80, HY-100, and HY-130 steels.
This thesis research has examined selected compact tensile
specimens from two of the HY series steels tested, speci-
fically HY-80 and HY-100. The effects of the alloying
elements and their segregation, the microstructure, and
the fracture properties on the reduction of J_{1C} have been
specifically examined and an attempt has been made to
quantify their effect on this degradation. X-ray diffrac-
tion, scanning and transmission electron microscopy,
microhardness measurements, optical metallography and
electron microprobe analysis were used in this investigation.

The purpose of this work has been to identify and to obtain
an understanding of the mechanisms responsible for the de-
gradation of J_{1C} in HY-80 and HY-100 with increasing amounts
of prestrain.

The balance of this paper presents a background synopsis
of the materials tested and the J-integral testing procedure
used by DTNSRDC and their results, a brief outline of the
laboratory techniques employed during this investigation,
a discussion of the results obtained, and conclusions and
recommendations. Appendix A provides a detailed, step-by-
step description of some of the more complicated specimen
preparation techniques employed; and Appendix B, provides
the step-by-step procedures used on some of the more
complicated equipment operated during the course of this
research.

II. BACKGROUND

A. HY STEELS

For several years after the end of World War II the Naval
Sea System Command, formerly the Bureau of Ships, was engaged
in a research program for the development of a high yield
strength material for ship and submarine construction. A low-
carbon Special Treatment Steel (STS) possessed the best com-
bination of all the desired properties, eg. high strength,
high modulus of elasticity, and low density. This "Low Carbon
STS" was used by the Norfolk Naval Shipyard in the fabrication
of several medium-sized ship type structures for testing by the
Shipyard's Underwater Explosion Research Division. The results
of this testing were extremely encouraging. At about the same
time, the University of California, under contract with the
Ship Structure Committee as part of its research program for
solution of the brittle-fracture program, used it in tests of
the highly restrained welds associated with hatch corner rein-
forcements. In these torturous tests, the low-carbon STS
showed ductile behavior at failure and much greater energy
absorption at fracture than the other quenched and tempered
steels tested. Thus, the steel had performed excellently in
small-size laboratory specimens and in large-size shipyard
specimens; fabrication under these conditions had presented
no great problems.

At the outbreak of the Korean Incident two significant ships were in preliminary design stage, the experimental submarine USS Albacore (AGSS 569) the other, the lead ship of a new class of aircraft carriers, USS Forrestal (CVA 59). Both were to have low-carbon STS used in important structural features.

The pressure hull plating of the Albacore was purchased by the Navy Purchasing Office, Washington under Contract N600-S-11751 of 22 February 1951. The yield strength was specified to be between 80,000 and 95,000 psi. At 0.2 per cent offset with a minimum elongation of 20 per cent in a 2-inch gage length. Furthermore, Charpy Keyhole impact energy, for thicknesses between 1/2 inch to 11/4 inches inclusive was required to be 40 foot pounds at -40°F. In fall, 1953, Portsmouth Naval Shipyard reported no problems worthy of mention were encountered during fabrication or construction.

On 12 June 1952, HY-80 steel (formerly called low-carbon STS) was approved for use in the side protection system in Forrestal. Plating was purchased using Military Specification MIL-S-16216A of 13 August 1952. The name HY-80 had been given to low-carbon STS on 15 August 1951 when Military Specification MIL-S-16216 was issued.

The next use of HY-80 - and the last prior to widespread adoption for submarine construction - was for the plating

16

and framing of the missile hangers in the USS Growler (SSG 577) being built at Portsmouth Naval Shipyard. HY-80 steel was used in this ship for weight-saving. The plating was purchased using Military Specification MIL-S-16216B of 20 May 1953 [Ref. 1].

Since the mid 1950's wide spread usage of HY-80 steel has occurred in the Navy. Also, as a result of the HY-80 development another high strength steel HY-100 was developed. This steel has essentially the same composition as HY-80 with the exception of a slightly higher nickel content range. Additionally HY-100 has a higher yield strength and a lower, minimum tempering temperature requirement, $1050^{\circ}F$ as compared to $1100^{\circ}F$.

Both steels were the first high-strength quenched-and-tempered steels approved for use by the US Navy for construction of large ocean vessels. They are low-carbon steels that achieve their strength and toughness through a quenching-and-tempering heat treatment. HY-80 and HY-100 shapes and plate materials are available under the following military specifications:

(1) Plate - MIL-S16216,

(2) Extrusions - MIL-S-22664,

(3) Rolled Sections - MIL-S-22958,

(4) Castings - MIL-S-23008,

(5) Forgings - MIL-S-23009.

The commercial grades of HY-80 and HY-100 plate are covered
by ASTM Specification A543 and the commercial forging mate-
rial by ASTM A541 and A508 [Ref. 2]. The chemical composi-
tion limits for HY-80 and HY-100 steel as specified by
MIL-S-16216H and A543 are shown in Table I, [Ref. 3].

In these steels, an upper limit of 0.18 per cent carbon
in HY-80 and 0.20 per cent carbon in HY-100 was established
for good weldability. Close control of phosphorus and sulfur
is required for both steels. The upper limit for these detri-
mental elements is set at 0.025 per cent individually and
0.045 per cent collectively. The deleterious effect of sulfur
occurs when it is combined with iron to form iron sulfide
which becomes a liquid during normal rolling and forging
temperatures. This tendency to hot-shortness can be success-
fully offset by the addition of manganese thus producing mang-
anese sulfide instead of iron sulfide and limiting the sulfur
content. Manganese is also added for solid solution strength-
ening. However, manganese in amounts greater than about 1.0
per cent embrittles steel during heat treatment. Therefore,
manganese is restricted to a range 0.10 to 0.40 per cent.
Molybdenum is used to increase temper resistance by retard-
ing softening during tempering of the steel at high tempera-
tures, contributes significantly to hardenability, improves
creep resistance, and improves machinability at high hard-
ness levels. Nickel is primarily responsible for the good
toughness, and the secondary effect of increasing hardenability.

18

Chromium is added for hardenability and for its contribution to improved corrosion resistance. Silicon is used primarily as a deoxidizer [Ref. 2], and [Ref. 4] through [Ref. 8].

HY-80 and HY-100 are fully killed, low alloy steels. The microstructures are a combination of tempered bainite and tempered martensite in all section thicknesses.

Procedures for the final quenching-and-tempering heat treatment used to obtain the required mechanical properties are left to the discretion of the steel manufacturer. Only two limitations are imposed by MIL-S-16216: (1) The final tempering temperature shall be not less than 1100°F for HY-80, and not less than 1050°F for HY-100. (2) The microstructure at the midsection of the plate must contain not less than 80 per cent martensite. Heat treatments for HY-80 generally consist of austenitization at approximately 1650°F followed by a water quench [Ref. 2], and tempering in the range of 1150°F to 1250°F followed by a water quench [Ref. 4].

B. J-INTEGRAL TESTING

The J-integral is a mathematical expression, a line or surface integral that encloses the crack front from one crack surface to the other, used to characterize the local stress-strain field around the crack front. For elastic-plastic (linear and nonlinear) solids for which the mathematical expression is path independent, the J-integral is equal to the value obtained from two identical bodies with

infinitesimally differing crack areas, each subject to stress, as the difference in loading work per unit difference in crack area at a fixed value of displacement, or where appropriate, at a fixed value of load [Ref. 9].

The method employed by DTNSRDC involved digitizing analog load displacement data, and on-line, real-time computer interactive determination of crack length and J by an unloading compliance method. The immediate calculation of crack length allowed the test engineer to properly space unloadings, vary test machine speed, or vary unloading length during the test to obtain results from each specimen. Further, the method provided for storage of both digitized load displacement data and J versus crack extension data for future retrieval and analysis [Ref. 10].

The schematic of the computer interactive test arrangement is shown in Figure 1. In this set up, load cell and clip gage signals are conventionally amplified and fed to a scanner which is interfaced to a digital voltmeter through an IEEE Standard 488-1975 interface. The digitized data are then made available to a microprocessor with magnetic tape cartridge and cathode ray tube (CRT) graphics capability. The test arrangement also employs a peripheral interactive graphics plotter interface with the computer. The test results reported herein utilized an Instron Model TTD universal test machine and a Tinius-Olsen test machine, both

of which are screw-type displacement-controlled devices. The computer used for this testing was a Tektronix Model 4051. The detailed steps used to conduct the single-specimen J_{1C} test can be found in [Ref. 10] and [Ref. 11].

J was calculated according to the expression [Ref. 9]:

$$J = \frac{A}{Bb} f(\frac{a_o}{w}) \ [1 - (\frac{.75 \ f(\frac{a_o}{w}) \ -1}{b})\Delta a]$$

where

A = area under load, load-point displacement record in energy units.

B = specimen thickness (for face grooved specimens $B = B$ (net)).

w = specimen width.

a_o = original crack size, including fatigue precrack.

b = initial uncracked ligament, $(w-a_o)$.

$f(\frac{a_o}{w})$ = a dimensionless coefficient value that corrects for the tensile component of loading. Values can be found in [Ref. 9]. Incrementing $f(\frac{a_o}{w})$ for crack growth, Δa, is not necessary.

This equation includes a correction for crack growth.

J_{1C} values were then computed from the intersection of the crack opening stretch line or blunting line ($J = 2(\sigma_f)(\Delta a)$) with the least squares fit of the data points which fell at least 51 microns beyond the crack opening stretch line and did not exceed approximately 1.5mm in crack growth.

In this context σ_f is the average of the material yield strength and the ultimate strength and Δa is the crack extension [Ref. 11].

The tearing moduli were calculated from an expression developed by Paris [Ref. 12]

$$T = \frac{E}{\sigma_o^2} \left(\frac{dJ}{da}\right)$$

where

T = tearing modulus

$\frac{dJ}{da}$ = slope of the J versus crack extension curve

E = elastic modulus, and

σ_o = flow stress

After testing, all specimens were heat tinted at $370^o C$ for 30 minutes to mark the extent of crack growth.

Only those retults from the DTNSRDC test that are applicable to this thesis are included in Table II and Table III. The additional information will be contained in an as yet unpublished report by DTNSRDC Annapolis, Maryland.

III. EXPERIMENTAL

The twelve specimens examined in this work were one half of the heat tinted compact specimens used in the J-integral test conducted by DTNSRDC Annapolis, Maryland. Of the twelve, six were of HY-80 steel and the remainder were of HY-100 steel. The composition and as received mechanical properties of the steels are listed in Table I. Two specimens of each alloy were tested in the as-received conditions along with at least two specimens with different prestrained conditions, nominally 3% and 5%. Table II and Table III identifies the material, the prestrain condition, and DTNSRDC test results. All samples had been cut from the T-L position in the plate and those prestrained had been pulled in the long transverse direction; Figure 2 depicts the orientation of the test specimens in the prestrained material. The heat tinted fracture surface delineated the range of the crack growth that had occurred as a result of the J-integral test, see Figures 3 through 6.

The detailed description of the experimental investigation that follows was used on each of the twelve samples previously mentioned.

Upon receipt, each sample was checked for proper identification. A new identification system using a single letter

code, Table II was established to simplify data recording and material specimen marking. The geometry of each specimen was then determined. All measurements were taken using a Starrett No. 436, 1 inch micrometer caliper and a Ralmikes Tool-A-Rama, 4 inch micrometer, No. 045-505-629 with a .001 inch dial gage No. 505-629 by Mitutoyo; except for the length of the fatigue precrack, which was acquired using a Hewlett Packard (HP) 9874A Digitizer with the data stored on a HP 9845 computer. The initial crack length, a, data is listed in Table IV; and Figure 7 shows a graphical output of the digitized fatigue precrack with a 5X magnification.

Next, the sample condition as received was recorded photographically using a Polaroid Land Camera Model 110B using Polaroid Polapan Land Film, type 42; the magnification of the sample was 1.05X. Three views of the compact tensile specimen are shown in Figure 8. Figures 9 and 10 show the fracture surfaces of all specimens used at 1.05X. Differences in the fracture surfaces were first noted at this point.

The fractographic investigation then began with the recording of the fracture surface at 7X using an American Optical Instrument Division Model AO Microscope with a Polaroid Land Instrument Camera Model ED-10; Figures 3 through 6 present these results. Before additional fractographic studies could be made the samples had to be sectioned, this was accomplished using a Buehler LTD CAT No. 10-1010-260, SER No. 299C3175 saw using a Buehler LTD wafering blade.

At this juncture, macrohardness scans were done on each of the samples. A Rockwell Hardness Tester by Wilson Mechanical Instrument Division of American Chain and Cable Co. Inc., Model 1JR, Tester No. 1JB-821 with C BRALE identer, with a 60 Kg load for an A scale reading was used. A minimum of 5 recordings were made on four different surfaces of the sample to ensure an accurate macrohardness value for each sample. The macrohardness versus J_{1C} and versus tearing modulus are shown in Figures 11 and 12.

With the macrohardness data completed, the next step was to continue with the fractography. A section of the fracture surface was cut from the original sample. Before this piece could be mounted for use in a scanning electron microscope, an oxidized layer had to be removed. The processes used to remove this oxide layer is described in detail in Appendix A under "Fracture Surface Cleaning by a Cellulose Acetate Replica Process". The clean fracture surface pieces were then mounted using Colloidal Silver by PElco-Ted Pella Co. on SEM pads and allowed to dry for use in a S4-10 Stereoscan Scanning Electron Microscope (SEM). Operating procedures used in this investigation on the SEM are contained in Appendix B.

After completion of the scanning electron microscopy, several pieces of the original sample were sectioned for micro-structural studies, microhardness examinations, and to examine the material perpendicular to the fracture surface. Each

piece was mounted in a 1 inch Phenolic block using a Buehler
LTD SPECIMEN MOUNT PRESS and Buehler Phenolic Powder. Once
the mounting had cooled, the specimen was then prepared for
testing by a surface polishing sequence starting with 80 and
180 grit paper on a Buehler SURMET II Belt Sander, then hand
sanding using 240, 320, 400, and 600 grit paper by Buehler
on a MET/CHEM M 985 table, and final polishing was done on
Buehler polishing wheels using 15.0, 6.0, and 1.0 micron
diamond paste. Each sample was then checked for inclusions
and then etched using various etchants. The etchant found
to work best in this case was a 2 per cent nital solution.
It was also determined that swabing the surface was preferred
to dipping and swirling. Observations of the microstructures
were made on a ZEISS Universal Large Research Microscope at
magnifications of 64X, 250X, 650X, and 1060X. A microhard-
ness scan of the etched surface was conducted using a Buehler
Microhardness Tester, CAT No. 1600-1000, Serial No. 77-M-263
with a 32/2 Diamond pyramid indenter and with a 200g load.
One sample from both HY-80 and HY-100 were specially prepared
for an electron microprobe analysis using wavelength disper-
sive spectroscopy (WDS). The WDS was done by STRUCTURE PROBE
in Metuchen, New Jersey. Each sample was mounted in the phe-
nolic mounts and polished as before except that the final
polishing was done using 1.0 and 0.5 micron Aluminum Oxide
grit. Also the mounts were cut so that the height of the
mount was less than 8mm.

Following the microstructural investigation, transmission electron microscopy was undertaken. The process for the development of thin foils is covered in Appendix A. Appendix B addresses the procedures used in operating the Servomet Spark Machine, the Stuers Tenupol and Polipower, and the JEOL Transmission Electron Microscope (TEM). The low speed diamond saw used to cut the thin strips was a South Bay Technology Inc. Model 650 with a Buehler diamond wafering blade, low concentration no. 11-4254.

Thin foil samples were prepared by twin jet electropolishing using 700ml ethanol, 120ml distilled water, 100ml glycerol, 80ml perchloric (70-72%) solution at $-3^{\circ}C$ with a flow rate of .5 on the Tenupol and a voltage of 24v and a resultant current of approximately 155 to 165 ma. The current versus voltage plots for this electrolyte can be seen in Figure 13.

The X-ray diffraction was done on two samples to see if any retained austenite was present in these samples. This was done on a Philips XR6 3100 X-ray generator with a Norelco Data Control and Processor Unit using Cu K_{α} radiation and a Graphite monochromator between the specimen and the detector.

IV. RESULTS

A. J-INTEGRAL RESULTS

The results of the test conducted by DTNSRDC indicate a reduction in the value of J with prestrain for a given crack extension. The values of J versus crack extension of HY-80 specimens P (0%), D (3%), and B (7.5%) are plotted in Figure 14. Figure 15 contains a plot of J versus crack extension for HY-100 specimens I (0%), S (3%), W (5%). The stress versus strain curves resulting during the prestraining for both HY-80 and HY-100 are plotted in Figures 16 and 17 respectively. The reduction in J with prestrain resulted in a reduction in the calculated values of J_{1C} for both HY-80 and HY-100 with increasing prestrain. In HY-80 the average value of J_{1C} for 0% prestrain was 824 (in-lbs/(in*in)) whereas for 7.5% prestrain the average value of J_{1C} was 553 (in-lbs/(in*in)). Similarly in HY-100 the average value of J_{1C} for 0% prestrain was 999 (in-lbs/(in*in)); while for 5% prestrain the average value of J_{1C} was 701 (in-lbs/(in*in)). Additionally, there was a reduction in the tearing modulus as calculated from the change in the slope of the J versus Δa or R curve beyond J_{1C} and an increasing value of material flow stress with increasing prestrain. In reference [Ref. 13] the tearing instability using compact specimens is addressed in more detail. The average tearing modulus dropped

from 51.8 in HY-80 0% prestrain sample to 12.4 in the 7.5% prestrained sample. While in HY-100 the average tearing modulus went from 24.4 in the 0% prestrained samples to 14.7 in the 5% prestrained samples. The results for each sample tested are recorded in Tables II and III. Figure 18 is graphical representation of the reduction in the average values of the J_{1C} for HY-80 and HY-100 versus per cent prestrain; and Figure 19 is a graphical presentation of the reduction in the average values of the tearing modulus for HY-80 and HY-100 versus the per cent prestrain.

B. MICROSTRUCTURAL INVESTIGATION

The x-ray diffraction patterns for HY-80 and HY-100 specimens, Figure 20, show that retained austenite is below the detection range of the equipment used, less than 0.1 per cent retained austenite. The major peaks that were recorded all correspond to BCC iron. It should also be noted that BCT (martensitic structures) were not observed presumably due to both the lack of tetragonality in this low carbon martensite and to the high tempering temperatures.

The micrographs of Figures 21 and 22 support the results of the x-ray diffraction analysis, in that the microstructure is primarily tempered martensite with a small percentage of lower bainite. It can be discerned in Figure 23 that certain areas are more readily attacked by the 2% nital etchant. All micrographs are taken from surfaces that are parallel to the

29

fracture surface. The indicated segregation in the lightly etched micrographs of Figures 21 and 22 were reinforced when the same surfaces were heavily etched, Figure 23. Obvious segregation/banding is shown in Figure 24. In HY-80 the widths of the dark regions vary from .001 inches to .007 inches with the average widths as follows: sample L(0%) = .003 inches, sample D(3%) = .003 inches, sample B(7.5%) = .003 inches. In HY-100 the darkly etched regions have widths varying from .001 inches to .005 inches, with the average width for sample I(0%) = .003 inches, for sample S(3%) = .001 inches, and for sample W(5%) = .001 inches. When these same samples were repolished to remove the effects of etching, inclusions were noted to be higher in the HY-100 than in the HY-80. Also, the inclusions tend to form in a line parallel to the rolling direction in the dark etched regions. Figures 25 and 26 are examples of the regions that contain inclusions.

The small indentations visible in Figures 23 and 24 are the result of the diamond pyramid hardness (DPH) scans. A minimum of thirteen indentations were taken per sample with at least six being in the light regions and the remainder in the dark etching regions. A higher hardness exists in the dark regions supporting alloy segregation. The average DPH in HY-80; for sample P(0%) is 206.8 in the light regions and is 224.1 in the dark regions, for sample D(3%) is 228.6 in the light regions and is 253.3 in the dark regions, and

for sample B(7.5%) is 242.3 in the light regions and is 273.3
in the dark regions. Similarly in HY-100, the average DPH
for sample I(0%) is 226.6 in the light regions and is 252.2
in the dark regions, for sample S(3%) is 247.9 in the light
regions and is 274.1 in the dark regions, and for sample W(5%)
is 253.3 in the light regions and is 274.0 in the dark regions.
The variations in DPH is shown graphically for HY-80 samples
L(0%), C(3%), and B(7.5%) in Figures 27, 28, 29 and for HY-100
samples I(0%), S(3%), and W(5%) in Figures 30, 31, 32. Tables
V and VI list the results of the DPH scans respectively for
HY-80 and HY-100. Additionally, there is an increase in the
hardness of both the light and the dark regions with increasing
prestrain. In HY-80, the light regions average DPH increased
from 206.8 242.3, while in the dark regions the average DPH
increased from 224.1 to 273.3. This is graphically shown in
Figures 33, 34, 35, and 36 for HY-80 and HY-100. It should,
also, be noted that the range of variation of hardness within
the sample is increasing with prestrain and that the dark
regions are strain hardening at a different rate than the
light regions. HY-100 shows the same results as above with
the average DPH in the light regions going from 226.6 to
253.3 and the DPH in the dark regions going from 252.2 to
274.0. In both HY-80 and HY-100 it appears that the major-
ity of the strain hardening occurs as a result of the first
3% of strain. Graphical presentation of the increasing DPH

31

with prestrain is shown in Figures 37 and 38 for HY-80 and HY-100 respectively. This observation is verified by the stress-strain curves recorded during prestraining.

The results of the Rockwell A hardness scans agreed with the trends seen in the Diamond Pyramid Hardness scan in that hardness was increasing with prestrain. The effect of the increasing hardness on the tearing modulus and on J_{1C} are shown in Figures 39, 40, 41, and 42; average values were used to indicate trends. It appears that the slope of the J_{1C} versus hardness curve is constant; there does appear to be, as would be expected, a decrease in J_{1C} with increasing hardness within a given material. The tearing modulus however seems to be more sensitive to hardness, as seen from the reduction in the slope of the tearing modulus versus hardness curves. The plots also indicate the same relationship between both J_{1C} and tearing modulus with the hardness in both the light and the dark regions.

Conclusive evidence of alloy segregation with higher alloy content residing in the dark regions was provided by Structure Probe after completing their electron microprobe analysis. Their data was gathered around DPH indentations that identified light and dark regions. A line 150 microns in length was scanned parallel to the banding around each designated position on HY-80 specimen L(0%) and on HY-100 specimen A(0%). Counts were collected for 40 seconds and compared with the

32

appropriate background levels to establish the composition
of each line. For details on Structure Probe and their test
methods see reference [Ref. 14]. The analysis was made for
Nickel (Ni), Iron (Fe), Chromium (Cr), Molybdenum (Mo),
Vanadium (V), Silicon (Si), Sulfur (S), Carbon (C), and
Manganese (Mn) on the surface of each specimen at the desig-
nated position. Table VII includes a complete account of the
results of the electron microprobe analysis on HY-80 and
HY-100. In HY-80 specimen L(0%), the nickel varied from 3841
counts in a light region to 4331 counts in a dark region; Cr
varied from 4964 counts in a light region to 5385 counts in
a dark region; Mo varied from 79 counts in a light region to
134 in a dark region; V, S, Si counts were negligible; and
C and Mn showed no tendancies for preferential segregation
or association with a light or a dark region. Thus there
was an increase in Ni, Cr and Mo in the dark regions.
Similarly, in HY-100 specimen A(0%) the Ni varied from
6028 in a light region to 7045 in a dark region; Mn varied
from 1224 counts in a light region to 1738 in a dark region;
Cr varied from 5625 in a light region to 6395 in a dark
region; Mo varied from 114 in a light region to 195 in a
dark region; V and S counts were very low; Si counts however
varied from 39 in a light region to 160 in a dark region;
C varied from 1213 counts in a light region to 974 in a
dark region. Thus in HY-100, Ni, Mn, Cr, Mo and Si increased

in the dark regions, while C decreased. Since HY-80 and
HY-100 are normally nominally compositionally equivalent,
it was noted that HY-100 was at the upper limit of the
allowed nickel content range, while HY-80 was at the lower
limit, in agreement with the results from the manufacturer,
Table I. Also, the Cr and Mo content were higher in the
HY-100 than in HY-80. More significant was the increase in
the silicon content in HY-100 as compared with HY-80 and the
segregation of the Si in the dark regions. Additionally,
HY-100 showed the only obvious C segregation with the
largest quantities residing in the light regions.

Any difference in the actual microstructure as a result
of this segregation is not apparent in the microstructures
recorded in Figures 21 and 22 which show both light and dark
regions having similar microstructures.

The microstructure as observed by transmission electron
microscopy, also support a martensite and a bainitic struc-
ture, Figures 43 through 48. The only difference noted
between the non-prestrained and the prestrained material
is an increase in the dislocation density. A very low dis-
location density was noted in the zero prestrained micro-
structures of both HY-80 and HY-100. However, there was an
apparent increase in the dislocation density with increased
prestrain, Figure 44. The carbides seemed to be very fine
and fairly uniformly distributed. In all specimens the

carbides seemed to be uniformly distributed with a separation distance of around .000180 inches (4.57 microns) for example see Figure 46. Additionally, transformation twinning was obvious in all samples examined, Figures 45 and 48. There appeared to be little variation in the extent of twinning as a function of prestrain.

C. FRACTURE INVESTIGATION, RESULTS OF

Optical observation and low magnification examinations indicate that fibrous fracture occurred during the J-integral test. Examination of the fracture surfaces, using the scanning electron microscope, showed that increasing levels of prestrain produced more change in the topography of the HY-80 than the topography of the HY-100. In the HY-100, the only significant changes with prestrain were a slight increase in the size and number of elongated tear-ridges, oriented in the rolling direction, and a slight decrease in the depth of the microvoids. In HY-80, more obvious variations with prestrain occurred. A noticeable increase in the number of elongated tear ridges (or large coalesced microvoids) was observed with increasing prestrain. Also, the shape of the microvoids are more rounded and appear to be more shallow with increasing prestrain.

The overall fracture mode for the specimens was ductile rupture (microvoid coalescence) showing a dimpled fracture appearance, interspersed with large elongated coalesced

microvoids generating elongated tear ridges. The primary
sites for void initiation were probably large and small
inclusions and large carbides, separated in many areas by
smaller voids nucleated at small carbide particles. The
large elongated voids probably nucleated around inclusions
where a low interface cohesive strength would be expected.
Figures 49, 50, and 51 show the fracture surfaces of three
HY-80 specimens specifically P(0%), D(3%), B(7.5%). Figures
52, 53, 54 show the fracture surfaces of HY-100 specimens
I(0%), T(3%), and W(5%). The micrographs shown in Figures
55 and 56 are cross-sectional views of the crack. These
support the results of the scanning electron microscopy in
that the fractures are fairly consistent with increasing
prestrain in HY-100 and that the fracture surface is chang-
ing more in the HY-80. It also, appears that with increas-
ing prestrain the fracture process follows a more zig-zag
course. Additionally, it appears that the depth of the
voids decreases with increasing prestrain at the beginning
of crack growth with the initiation of the J-integral test.
References [15] through [17] have indicated similar fracture
surfaces in similar materials.

Additionally, the widths of the elongated ruptures are
of the same order of magnitude as the dark etched regions
observed in the microstructural investigation. In HY-80,
the average width of the ruptures in specimen L(0%) is

0.007 inches, in specimen D(3%) is 0.004 inches and in specimen B(7.5%) is 0.004 inches. Likewise, in HY-100 the average width of the ruptured areas for specimen I(0%) is 0.003 inches, for specimen S(3%) is 0.004 inches, and for specimen W(5%) is 0.005 inches.

The small equiaxed microvoid separation averages approximately 0.0004 inches in all the specimens examined. Since the average carbide spacing was found to be about 0.0002 inches using the TEM, this supports the idea that the smaller microvoids are nucleated by the carbides.

V. DISCUSSION

Begley and Landes, [Ref. 18], have stated that the energy
line integral, J, is applicable to elastic material or elastic-
plastic material when treated by a deformation theory of
plasticity. Rice [Ref. 19] has proven that the J-integral
is path independent and that it may be interpreted as the
potential energy difference between two identically loaded
bodies having similar crack sizes. Since paths can be chosen
close to the crack tip, the energy line integral represents
an average measure of the near tip deformation field and
thus can be used as a failure criterion.

In the linear elastic case and also for small scale yield-
ing, J is equal to G (strain energy release rate), the crack
driving force. For any non-linear elastic body, J may be
interpreted as the energy available for crack extension.

For irreversible deformation (plastic) an energy inter-
pretation of J cannot be applied to crack extension; however,
J is still equal to the potential energy difference. The
physical significance of J for elastic-plastic materials is
that it is a measure of the characteristic crack tip elastic-
plastic field [Ref. 18].

The J approach is normally limited to problems of plane
strain or generalized plane stress. Another limitation is

that unloading is not permitted if the deformation theory of plasticity is to be a realistic approximation of elastic-plastic behavior. Typically J-integral failure criterion is limited to the case of plane strain. As a consequence of the inadmissability of unloading and subcritical crack growth the critical value of J, J_{1C} fracture criterion refers to crack initiation rather than propagation, [Ref. 18].

For a valid plane strain fracture toughness test using J-integral criterion, the specimen thickness must be greater than a minimum value. Specifically

$$B \geq \alpha \ \frac{J_{1C}}{\sigma_y}$$

where

$\alpha = 50$

B = specimen thickness

σ_y = yield stress

This criterion was met by all the samples tested by DTNSRDC and examined in this work.

In order to logically attempt to establish what mechanism/mechanisms were active that were causing the reduction in J_{1C} and the tearing modulus with increasing prestrain, an analytical approach was used.

J. F. Knott [Ref. 20] has shown that the line integral, J, on a circle of infinite radius surrounding the notch tip

becomes identical to the strain energy release rate, G, for a linear elastic body. The critical value of J, J_{1C}, that occurs at crack initiation is defined as follows:

$$J_{1C} = G_{1C} = \frac{K_{1C}^2}{E} (1 - \nu^2) \text{ in plane strain} \qquad (1)$$

where

K_{1C} = critical stress intensity factor for plane strain mode I loading.

ν = Poissons ratio

E = Youngs Modulus

A plastic-zone crack-length correction for K is required when a large plastic zone is created ahead of the crack-tip. This correction to K_{1C} is

$$K_{1C} = \sigma_f \sqrt{\pi(a + \frac{K_1^2}{6\pi\sigma_y^2})} \qquad (2)$$

where

σ_f = applied stress at fracture

a = crack length

σ_y = yield stress

$K_1 = \sigma_f \sqrt{\pi a}$

substituting for K_{1C} from equation (2) into equation (1)

$$J_{1C} = (\frac{1 - \nu^2}{E}) \pi a [\sigma_f^2 + \frac{\sigma_f^4}{6\sigma_y^2}] \qquad (3)$$

40

From this relationship a function in J_{1C} could only occur as a result of an increase in yield stress or a reduction in the applied stress at fracture, if Poissons ratio, Youngs Modulus, and crack length were assumed constant or nearly so.

It is known, [Ref. 8], that the yield strength of a material may be given by:

$$\sigma_y = \sigma_T + \sigma_{ST} + K_y d^{-\frac{1}{2}}$$

where

σ_T = short-range order Peierls stress effects (<10 Å)

σ_{ST} = long-range order dislocation stress field effects (100Å-1000Å)

K_y = "locking parameter," which measures relative hardening contribution of grain boundaries

d = grain size

From the micrographs shown in Figures 21 and 22 the grain size d is a constant within a given material; thus the grain size contribution to the yield stress is considered constant. Additionally, the Peierls stress would also be constant with increasing prestrain. Therefore, if σ_y is to increase in HY-80 and HY-100 as is shown in the assumed stress-strain curves plotted in Figures 16 and 17; then σ_{ST} must be increasing.

41

It is well known that:

$$\sigma_{ST} \propto \tau = k\,G{\cdot}b\,D^{\frac{1}{2}} \qquad\qquad (4)$$

where:

τ = effective internal stress

k = constant

G = shear modulus (constant)

b = burger vector (constant)

D = dislocation density.

The transmission electron micrographs, Figures 44 and 47, confirm an increase in the dislocation density with increasing prestrain which must be responsible for the increased yield stress. Insufficient data on the exact dislocation densities precludes the application of equation (4) to explain the increased yield stress but the trend is clearly correct.

Knowing that σ_y does increase with prestrain, σ_y values were extrapolated from Figures 16 and 17 for the prestrained conditions reported by DTNSRDC. These values of yield stress were substituted into equation (3) in an effort to quantify the effect of increasing yield stress on J_{1C}. Poissons ratio and Youngs Modulus were assumed constant. The crack length used for all calculations was the depth of the machined crack plus the depth of the fatigue precrack as measured using micrometers and the HP 9874 digitizer. The calculations

42

indicate that approximately 16% for HY-100 and 29% for HY-80 of the measured reduction in J_{1C} is due solely to the increase in yield stress. Table IV shows the results of these calculations. This table also indicates the amount that the applied stress at fracture must decrease to account for the remainder of the reduction in J_{1C}.

To quantify the effect of the prestrain on the fracture process Barsom and Pellegrino, [Ref. 21], have shown that there exists a relationship between K_{1C} and the plain-strain fracture strain, $\epsilon_{f,ps}$. The crack-tip strain, ϵ, is related to the crack opening displacement, δ, by

$$\epsilon = \alpha \ \delta^m \tag{5}$$

where α is a proportionality factor and m is a constant much less than one, because of crack blunting and work hardening. M is nominally 0.25 for low carbon steels based on a comparison of data by Hertzberg, [Ref. 8].

The crack opening displacement (COD, δ) is approximately related to K_1 by the expression:

$$\delta = \frac{K_1^{\ 2}}{E\sigma_y} \tag{6}$$

combining equation (5) and (6) at the critical values. Then

$$K_{1C} = A \ \sqrt{\sigma_y} \ \epsilon_{f,ps}^{\ \frac{1}{2m}} \tag{7}$$

43

where

A = constant for a given steel

with the assumed experimental value for m equation (7) becomes

$$K_{1C} = A \sqrt{\sigma_y} \ \varepsilon_{f,ps}^2 \qquad (8)$$

substituting K_{1C} from equation (8) into equation (1)

$$J_{1C} = (\frac{1 - \nu^2}{\alpha^4}) \ \sigma_y \ \varepsilon_{f,ps}^4 \qquad (9)$$

Knott, [Ref. 22], has also shown that

$$J_{1C} = n \ \sigma_0 \ \delta \qquad (10)$$

where

n = geometrical factor (values range from 1-3)

σ_0 = materials flow stress.

assuming $\sigma_0 = \sigma_y$ in low strain hardening materials and taking $n = 1$ based on the findings of Robinson and Tetelman, [Ref. 23] taken from direct measurements of COD as a function of K for several steels, and combining equations (9) and (10):

$$\delta = (\frac{1 - \nu^2}{\alpha^4}) \ \varepsilon_{f,ps}^4 \qquad (11)$$

44

This relationship has been verified by using the experimental data by B. A. Fields et al [Ref. 24]. Figure 57 is a graphical verification of this relationship.

To estimate $\varepsilon_{f,ps}$ from the DTNSRDC results, a model developed by Bates and Santhanam, [Ref. 25], for a smooth blunting notch under Type I loading is applied. They show that the average strain around the crack tip surface, $\varepsilon_{\theta ave}$ is

$$\varepsilon_{\theta ave} = \ln \left[(1 + \frac{\delta}{2\rho_o}) \; (1 + \frac{\delta}{\pi\rho_o(1+\frac{\delta}{\alpha})})^{-1} \right] \qquad (12)$$

where

   ρ_o = initial crack tip radius

   γ = crack extension due to blunting

   α = the distance that the center of curvature of the notch recedes during blunting.

Equation (12) assumes the notch has parallel flanks and a semicircular tip. For a very sharp crack (as in our case), $\gamma << \alpha$; therefore $\frac{\gamma}{\alpha} \approx 0$ and is neglected.

Bates and Santhanam, [Ref. 25], have also shown that the longitudinal strain (ε_y) at the notch tip is related to the average strain $\varepsilon_{\theta ave}$ by:

$$\varepsilon_y = \varepsilon_{\theta ave} \; (\frac{\pi}{2} - \frac{\omega}{2}) \cos(\frac{\omega}{2}) \qquad (13)$$

where $\dot{\omega}$ = flank angle of the notch. In this case for a sharp crack $\omega \approx 0$ thus equation (13) reduces to

$$\varepsilon_y = \varepsilon_{\theta ave} \left(\frac{\pi}{2}\right) \tag{14}$$

When fracture occurs $\varepsilon_y = \varepsilon_{f,ps}$ and combining this and equations (12) and (14)

$$\varepsilon_{f,ps} = \frac{\pi}{2} \ln \left[\frac{1 + \frac{\delta}{2\rho_0}}{1 + \frac{\delta}{\pi\rho_0}} \right] \tag{15}$$

Equation (10) in conjunction with equations (12) and (15) resulted in the values of δ, $\varepsilon_{\theta ave}$, $\varepsilon_{f,ps}$ recorded in Table VIII for HY-80 and HY-100 collectively. It is apparent that in both HY-80 and HY-100 J_{1C} and δ are proportional to $(\varepsilon_{f,ps})^4$ as seen in Figures 58 and 59. This implies that very small changes in $\varepsilon_{f,ps}$ will result in large changes in J_{1C} and/or COD.

If the amount of plastic prestrain, ε_p, is simply added to $\varepsilon_{f,ps}^p$: the summation results in a fairly constant value equal to the total strain, $\varepsilon_{f,ps}^{np}$, for the zero prestrain material, Table IX, (note: superscript p = prestrained and np = non-prestrained). However, in HY-80 there appears to be a trend towards lower values of $\varepsilon_{f,ps} + \varepsilon_p$ with increasing prestrain; but this may simply be due to a small sampling and

the questionable yield stress information. In HY-100, where the yield stress data is not as suspect, the $\varepsilon_{f,ps}^p + \varepsilon_p$ remains constant within a small error band with increasing prestrain. The fact that $\varepsilon_{f,ps}^p$ is reduced by prestrain suggest that some limiting ductility criterion may be applicable.

The fracture surfaces with and without prestrain support the proposed reduction in $\varepsilon_{f,ps}$. Shallower dimples and an increasing number of large elongated dimples are observed on the fracture surfaces with increasing prestrain. The increase in dislocation density created by prestraining has probably led to easier microvoid nucleation. In fact, the large elongated microvoids that appear more frequently on the prestrained fracture surfaces exhibit very limited plasticity. It appears that the prestrain may have caused decohesion of the interface between the matrix and the large inclusions associated with these microvoids. The elimination of the regions with low ductility is possible only by improved melting and processing techniques.

The mechanism by which the prestraining has reduced the fracture ductility is not completely understood. One possible explanation is that the increased dislocation density has resulted in a local increase in the residual stress surrounding each carbide particle. When this is combined with the applied stress, decohesion of the interface occurs

47

at what appears to be a lower applied stress, where in reality the local stress at the carbide matrix interface required to cause decohesion is independent of the pre-straining. Iricibar et al [Ref. 26] have shown that the strain required to nucleate a microvoid decreases linearly with the square of the hydrostatic component of stress. This would suggest that the strain required for nucleation of a microvoid would be path dependent and could be altered by not only prestrain but the method of prestraining, eg. tension versus compression. Iricibar et al [Ref. 26] have also shown that the strain required for void nucleation is dependent upon the particle size and location. Large particles located on grain boundaries have a much lower void nucleation strain than do the smaller particles in the matrix. This also supports the explanation for the appearance of more low ductility troughs (large elongated microvoids) on the fracture surfaces of the materials with increasing prestrain.

Another possible explanation is that if we view the process of ductile fracture as two steps, void nucleation and void growth, then the prestraining may effect one or both of these steps. The previous discussion is germane to the void nucleation step; however, the observation that the microvoids (dimples) on the fracture surface of the prestrained samples are shallower suggest that the void

growth behavior has been changed. The work of Tracey, [Ref. 27], clearly shows that void growth is decreased by strain hardening. Thus, a complete understanding of how prestraining has altered the ductile fracture process requires an understanding of how the strain history has affected the strain hardening rate of the material.

It can be seen from Figures 16 and 17 that the initial work hardening rate for both of these steels is high compared to that which occurs after about 1% plastic strain. Thus, it is expected that the local work hardening rate has been altered and that this must have some effect on the rate of void growth.

With the information presently available it is impossible to separate the role of void nucleation from void growth, but the evidence strongly supports a damage mechanism where the summation of the two strains (strain from void nucleation plus void growth strains) is reduced by prestrain. It is believed that microvoids may be initiated by as little as 3% plastic strain in the vicinity of large non-metallic inclusions during prestraining and that this is responsible for the large elongated microvoids in the regions containing these inclusions. But, this is not believed to have a major effect on the fracture toughness. Also, microvoid nucleation on carbide particles is not believed to have occurred during prestraining.

The major cause for the reduced fracture toughness is
believed to be a combination of residual stresses around
carbide particles resulting from the prestrain, a reduction
in void nucleation strain and a decrease in void growth
resulting from changes in the local strain hardening behavior.
In either case, the total strain at fracture has been reduced.
In one case (void nucleation during prestraining) the damage
is permanent and cannot be recovered; while in the other case
(residual stresses and reduced work hardening rates) the
damage could be completely recovered by stress relieving.
Both Knott. [Ref. 22], and Iricibar et al, [Ref. 26], have
shown that stress relieving prestrained steels at about 950°F
will restore the work hardening rate, will increase the strain
at fracture and will restore the fracture toughness of the
prestrained material to its original value.

It is postulated that the fracture toughness of the HY-
series steels, subsequent to prestraining, could be restored
by a stress relieving treatment. Further, it is believed
that the reduction in toughness is due to a reduction in
the plane strain fracture strain, $\epsilon_{f,ps}$. This combined with
the observation that $\epsilon_{f,ps}^p + \epsilon_p = \epsilon_{f,ps}^{np}$ makes it possible
to estimate the change in J_{1C} as it was shown that:

$$J_{1C} = (\frac{1 - \nu^2}{\alpha^4}) \sigma_y (\epsilon_{f,ps})$$

50

As an example of the use of the equation, the J_{1C} for 10%
prestrain for HY-100 is estimated to be 504 (in-lbs/(in*in)),
assuming σ_y = 120.0 ksi. and $\varepsilon_{f,ps}^{.1} = \varepsilon_{f,ps}^{0}$ -0.1 = 0.458 and
$\varepsilon_{f,ps}^{0}$ = 0.558 from Table IX.

The only information required to make this prediction
was the J_{1C} value for the non-prestrained material and the
stress-strain curve for HY-100.

The reduction in the tearing modulus with the increase
in prestrain follows a similar path. Since the tearing
modulus is proportional to the slope of the J versus crack
extension curve and is inversely proportional to the flow
stress squared, an increase in the yield stress will result
in a increase in the flow stress and thus a decrease in the
tearing modulus; and it is suspected that the reduction in
the plane strain tensile ductility will reduce the slope of
the J curve similar to its effect on the reduction of J_{1C}.

VI. SUMMARY AND CONCLUSIONS

The following observations have been made:

1. Prestraining of HY-80 and HY-100 to about 5% reduces the fracture toughness by about 41.0% for HY-80 and 32.0% for HY-100.

2. The fracture surfaces of the prestrained samples show less plasticity than those on the non-prestrained samples, but all samples fractured by microvoid coalescence.

3. Large elongated dimples that appear as troughs of low ductility are observed much more frequently on the fracture surfaces of the prestrained samples. These regions are high in inclusions and are regions of segregation where at least the amounts of Ni, Cr and Mo are higher than the surrounding regions. However, even assuming that these regions can carry no load the reduction in fracture toughness or the tearing modulus would be only on the order of several per cent instead of the observed reduction of at least 32.0%.

4. Transformation twinning was observed in all samples independent of their prior strain history.

5. The dislocation density increased markedly with prestrain.

6. Fracture resistance decreased with increasing hardness (due to prestrain), but this is a rather insensitive means to predict the reduction of fracture resistance, because these materials do not exhibit much strain hardening.

The tearing modulus is reduced by prestraining similar to J_{1C}. The mechanism for this is expected to be identical to that responsible for the reduction in J_{1C}.

From the above observations the following conclusions were reached:

1. Prestraining results in a reduction in the plane strain fracture strain ($\varepsilon_{f,ps}$) as calculated from K_{1C}, COD, and J_{1C} relationships.

2. The plane strain fracture strain for prestrained samples is equal to the plane strain fracture strain of a non-prestrained sample minus the amount of plastic strain induced by the prestraining.

3. The prestraining has resulted in an increase in the yield stress due to an increase in the dislocation density.

4. J_{1C} is shown to be related to the yield strength and $\varepsilon_{f,ps}$ as follows

$$J_{1C} \propto \sigma_y \, (\varepsilon_{f,ps})^4$$

Thus, although the reduction of the non-prestrained value for $\varepsilon_{f,ps}$ is small, large reductions in J_{1C} can occur.

5. A method to predict the reduction in J_{1C} due to prestraining that only requires a knowledge of the J_{1C} of a non-prestrained sample and the stress-strain bahavior of that material is presented.

6. The damage mechanism associated with the prestraining is believed to be one in which stress relieving treatments can be used to restore the fracture toughness of the material to its original, non-prestrained value.

VII. RECOMMENDATIONS FOR FUTURE STUDY

1. Complete stress-strain curves for all materials should be obtained. From this, both accurate yield stresses and the effect of prestrain on the true strain at fracture can be determined.

2. Tensile tests interrupted with stress relieving treatments should be performed to determine the effect of the stress relieving on the strain hardening rate and the true fracture strain.

3. Additional thin foil transmission electron microscopy should be completed to carefully examine the interactions between carbides/inclusions and dislocations.

4. Metallographic examination of the crack tip region of 1T compact tension specimens, after crack growth but before final fracture, should be conducted to verify the changes in the crack tip plasticity due to prestrain proposed in this work.

5. Experiments necessary to verify the relationships below should be performed.

$$J_{1C} \propto \sigma_y \, (\varepsilon_{f,ps})$$

and

$$\varepsilon_{f,ps}^{p} + \varepsilon_{p} = \varepsilon_{f,ps}^{np}$$

TABLE I

HY-80 and HY-100, Composition and Properties

ELEMENT	MIL-S-16216 HY-80	HY-100	COMMERCIAL AS43 GRADE A	GRADE B	AS TESTED HY-80	HY-100
Carbon[a]	0.18 max	0.20 max	0.23 max	0.23 max	.16	.16
Manganese	0.10-0.40	0.10-0.40	0.40 max	0.40 max	.28	.27
Silicon	0.15-0.35	0.15-0.35	0.20-0.35	0.20-0.35	.21	.24
Nickel	2.00-3.25	2.25-3.50	2.60-3.25	2.60-3.25	2.09	3.22
Chromium	1.00-1.80	1.00-1.80	1.50-2.00	1.5-2.0	1.23	1.58
Molybdenum	0.20-0.60	0.20-0.60	0.45-0.60	0.45-0.60	.23	.39
Phosphorus[b]	0.025 max	0.025 max	0.035 max	0.02 max	.005	.009
Sulfur[b]	0.025 max	0.025 max	0.040 max	0.020 max	.018	.018
Titanium	0.02 max	0.02 max	--	--	.002	.002
Vanadium	0.03 max	0.03 max	0.03 max	0.03 max	.003	.003
Copper	0.25 max	0.25 max	--	--	.16	.13
Iron	Remainder	Remainder	Remainder	Remainder	Remainder	Remainder

a. 0.20 max for plates 6 in. thick and over.
b. The per cent of combined phosphorus and sulfur shall be 0.045 max.

HY-80 Manufactured by LUKENS STEEL Company

MATERIAL	YIELD KSI	TENSILE KSI	% ELONG IN 2 INCHES	% R.A.	LONG V-NOTCH (-120°F)
HY-80	86.6	100.0	22	20.5	70, 72, 76, ft-lb
	90.7	103.6	21	71.1	
HY-100	111.2	124.4	22	62.7	113, 115, 116
	108.7	120.9	23	64.2	

TABLE II

DTNSRDC J-Integral Results

ALLOY	PRESTRAIN %	DTNSRDC SPECIMEN NUMBER	NEW ID NUMBER	J_{1C} (IN-LBS/IN^2)	AVG J_{1C}
HY-80 2-INCH PLATE	0	FVM 2 FVM 3	L P	862 786	824
	3	FVM 50 FVM 51	C D	596 638	617
	6.3 7.5	FVM 63 FVM 60	E B	601 505	553
HY-100 2-INCH PLATE	0	FVO 2 FVO 4	I A	981 1017	999
	3	FVO 32 FVO 33	S T	790 680	735
	5	FVO 42 FVO 43	U W	689 713	701

57

TABLE III

DTNSRDC Tearing Modulus Instability Results

ALLOY	PRESTRAIN %	DTNSRDC SPECIMEN NUMBER	NEW ID NUMBER	$\frac{dJ}{da}$	T TEARING MODULUS	AVG T
HY-80 2-INCH PLATE	0	FVM 2 FVM 3	L P	15835 14153	54.7 48.9	51.8
	3	FVM 50 FVM 51	C D	11585 7907	31.2 21.3	26.3
	6.3 7.5	FVM 63 FVM 60	E B	5288 4593	14.2 12.4	13.3
HY-100 2-INCH PLATE	0	FVO 2 FVO 4	I A	12643 8373	29.3 19.4	24.4
	3	FVO 32 FVO 33	S T	8760 6975	20.3 16.1	18.2
	5	FVO 42 FVO 43	U W	6544 6123	15.1 14.2	14.7

58

TABLE IV

Yield Stress Effects on J_{1C} and Calculated
Values of Local Applied Stress

MATERIAL	a (INCHES)	c X 10^7 (LBS/IN)	σ_y X10^3 psi	J_{1C} EXP	σ_f X10^{-4} psi	J_{1C} σ_f=CONST	$\dfrac{\Delta J_{1C}(\text{CAL})}{\Delta J_{1C}(\text{EXP})}$
L	1.313	1.277	81.0	862	7.664	862	
P	1.319	1.283	81.0	786	7.341	-	
C	1.248	1.214	100.0	596	6.755	783	.297
D	1.270	1.235	100.0	638	6.917	796	.295
B	1.284	1.249	120.0	505	6.221	783	.221
E	1.264	1.229	114.5	601	6.796	776	.330
I	1.312	1.276	110.0	981	8.373	1017	
A	1.318	1.282	110.0	1017	8.495		
S	1.268	1.228	112.5	790	7.723	970	.207
T	1.267	1.232	112.5	680	7.189	974	.128
U	1.263	1.228	115.0	689	7.254	967	.152
W	1.272	1.237	115.0	713	7.346	974	.141

$\nu = .3$

$E = 29.4 \times 10^6$ psi

$C = \left(\dfrac{1-\nu^2}{E}\right)\pi a$ [lbs/in]

$\sigma_f^2 = -3\sigma_y^2 + \sqrt{9\sigma_y^4 + \dfrac{6\sigma_y^2 J_{1C}}{C}}$

$J_{1C} = C\left[\sigma_f^2 + \dfrac{\sigma_f^4}{6\sigma_y^2}\right]$

59

TABLE V

DPH Scan Results for HY-80

REGION	SPECIMEN					
	L	P	C	D	E	B
	205.6	198.5	211.0	210.5	235.0	241.6
	205.6	205.0	209.5	224.1	248.5	250.5
	215.1	210.5	216.6	241.0	247.9	245.4
LIGHT	209.0	218.7	218.7	232.6	240.4	241.0
	207.5	203.2	218.2	230.3	236.2	242.2
	215.1	210.0	233.2	233.2	230.3	239.2
	210.5	201.7	215.1		250.5	236.2
AVE	209.8	206.8	217.5	228.6	241.3	242.3
	231.5	207.0	232.6	241.6	261.2	287.3
	229.8	221.9	255.1	247.3	260.5	274.9
DARK	231.5	229.2	246.0	266.1	264.0	269.0
	235.6	229.2	246.0	259.8	261.2	270.5
	227.5	232.1	263.3	259.2	269.7	262.6
	236.2	225.2	252.4	246.6	272.7	275.7
				252.4		
AVE	232.0	224.1	249.2	253.3	264.9	273.3

60

TABLE VI

DPH Scan Results for HY-100

REGION	SPECIMEN					
	I	A	S	T	U	W
	224.1	224.1	247.3	264.0	254.4	261.2
	228.0	235.0	258.5	253.8	252.4	256.4
	225.2	221.4	238.0	257.1	259.8	241.6
LIGHT	225.2	233.8	250.5	258.5	251.1	256.4
	228.6	235.6	246.6	266.1	253.1	247.3
	228.6	230.3	259.8	255.1	249.2	257.1
			244.7	251.8	255.8	
AVE	226.6	230.0	247.9	258.1	253.7	253.3
	247.9	247.9	275.7	272.7	275.7	285.7
	248.5	238.6	281.8	284.9	266.9	265.4
	253.8	248.5	277.2	291.3	253.1	278.7
DARK	253.1	253.1	269.7	268.3	266.9	263.3
	264.0	259.8	266.1	266.1	264.7	274.9
	249.2	247.9		275.7	274.9	279.5
	249.2	244.7		277.2		270.5
AVE	252.2	248.6	274.1	276.6	267.0	274.0

TABLE VII

Results of Electron Microprobe Analysis

ALLOY	MATERIAL					
	HY-80		HY-100		HY-130	
	LIGHT	DARK	LIGHT	DARK	LIGHT	DARK
NICKEL	4180	4202	6028	6914	8695	8623
	3841	4331	6491	7045	8486	8417
IRON	304736	309158	288106	287582	299765	298926
	308431	307849	288562	289584	300313	299323
MANGANESE	1752	1656	1224	1584	4312	4458
	1696	1849	1345	1738	4460	4470
CHROMIUM	4964	5276	5625	6320	2040	2028
	5170	5385	5796	6395	2138	2086
MOLYBDENUM	79	111	114	192	139	151
	89	134	162	195	164	181
VANADIUM	2	4	32	13	173	192
	11	-14	40	14	177	214
SULFUR	0	8	-6	27	-1	3
	8	40	5	38	-1	14
SILICON	-47	-13	39	140	118	113
	-20	11	54	160	161	183
CARBON	953	1077	1069	974	1088	1064
	1116	1091	1213	991	1213	1223

TABLE VIII

Table of Plane Strain Tensile Ductility Calculations

SPECIMEN/ % PRESTRAIN	J_{1C} IN-LB/IN^2	σ_y KSI	COD X10^2 INCHES	$\epsilon_{\theta ave}$	ϵ_y	ϵ'_y
HY-80						
L/0	862	81.0	1.064	0.365	0.574	0.108
P/0	786	81.0	0.970	0.358	0.563	0.100
C/3	596	100.0	0.596	0.318	0.499	0.062
D/3	638	100.0	0.638	0.324	0.509	0.067
E/6.3	601	114.5	0.525	0.305	0.480	0.053
B/7.5	505	120.0	0.421	0.283	0.444	0.038
HY-100						
I/0	981	110.0	0.892	0.352	0.553	0.094
A/0	1017	110.0	0.925	0.355	0.558	0.097
S/3	790	112.5	0.702	0.332	0.522	0.074
T/3	680	112.5	0.604	0.319	0.501	0.063
U/5	689	115.0	0.599	0.318	0.500	0.062
W/5	713	115.0	0.620	0.321	0.505	0.065

TABLE IX

Plane Strain Tensile Ductility Plus Plastic Strain

MATERIAL		% PRESTRAIN	$\varepsilon_{f,ps}$	ε_p	$\varepsilon_{f,ps} + \varepsilon_p$
HY-80	L	0	0.574	0.0	0.574
	P	0	0.563	0.0	0.563
	C	3	0.499	0.03	0.529
	D	3	0.509	0.03	0.539
	E	6.3	0.480	0.063	0.543
	B	7.5	0.444	0.075	0.519
HY-100	I	0	0.553	0.0	0.553
	A	0	0.55.	0.0	0.558
	S	3	0.522	0.03	0.552
	T	3	0.501	0.03	0.531
	U	5	0.500	0.05	0.550
	W	5	0.505	0.05	0.555

Figure 1. Computer Interactive Test Arrangement

65

Rolling Direction

Prestrain Loading Direction

T-L SPECIMEN

S

L

T

S - Short Transverse
T - Long Transverse
L - Longitudinal Direction
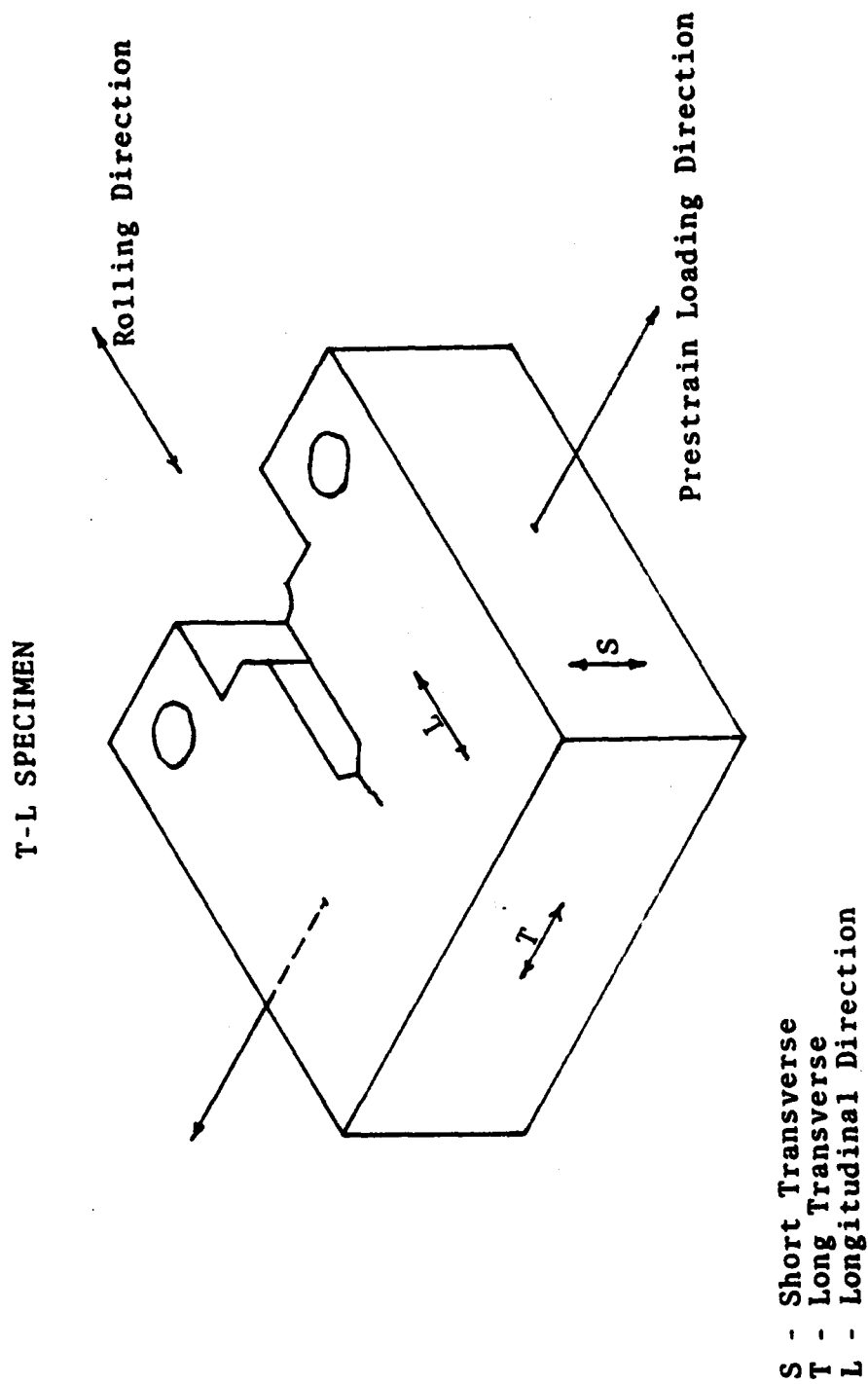
Figure 2. Test Specimen Orientation

66
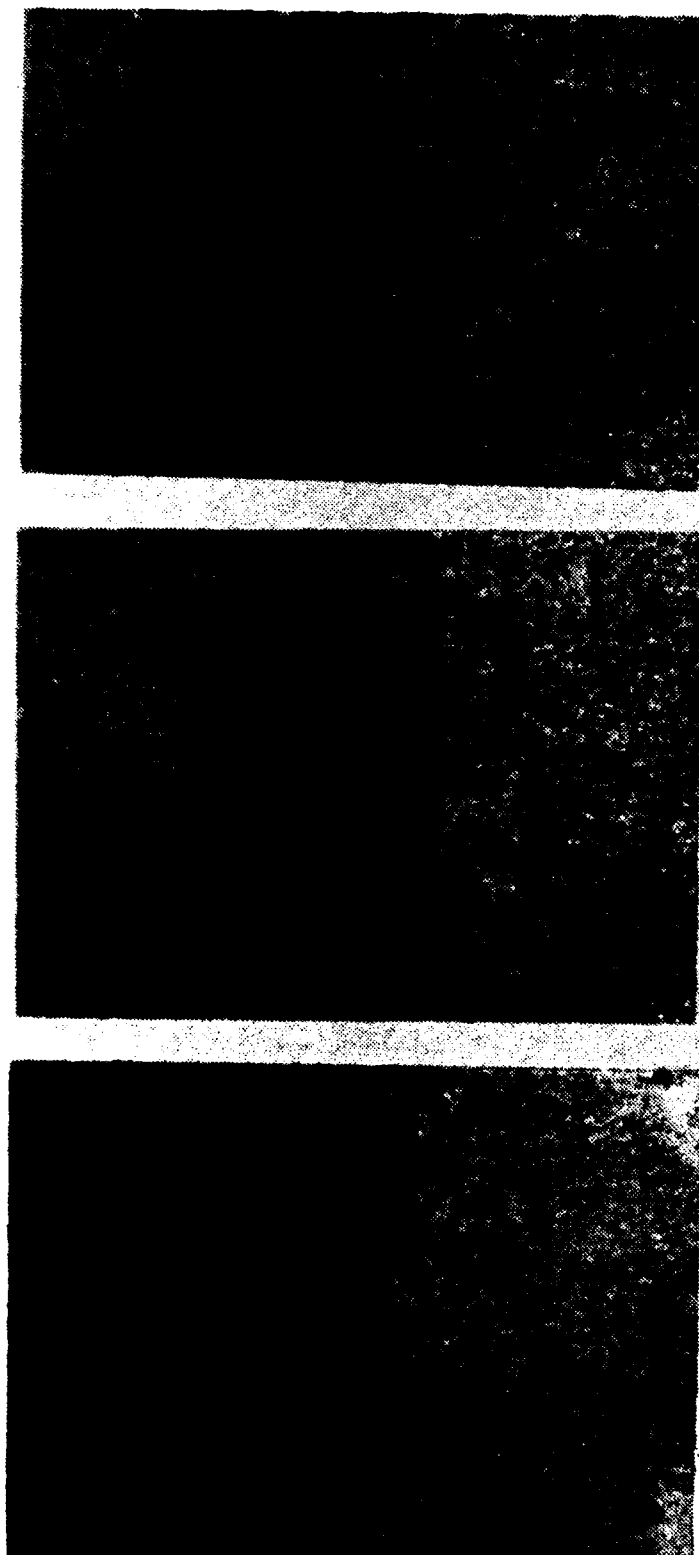
FVM 2, 0%, 7x   FVM 50, 3%, 7x   FVM 60, 7.5%, 7x

Figure 3. HY-80 Heat Tinted Fracture Surfaces
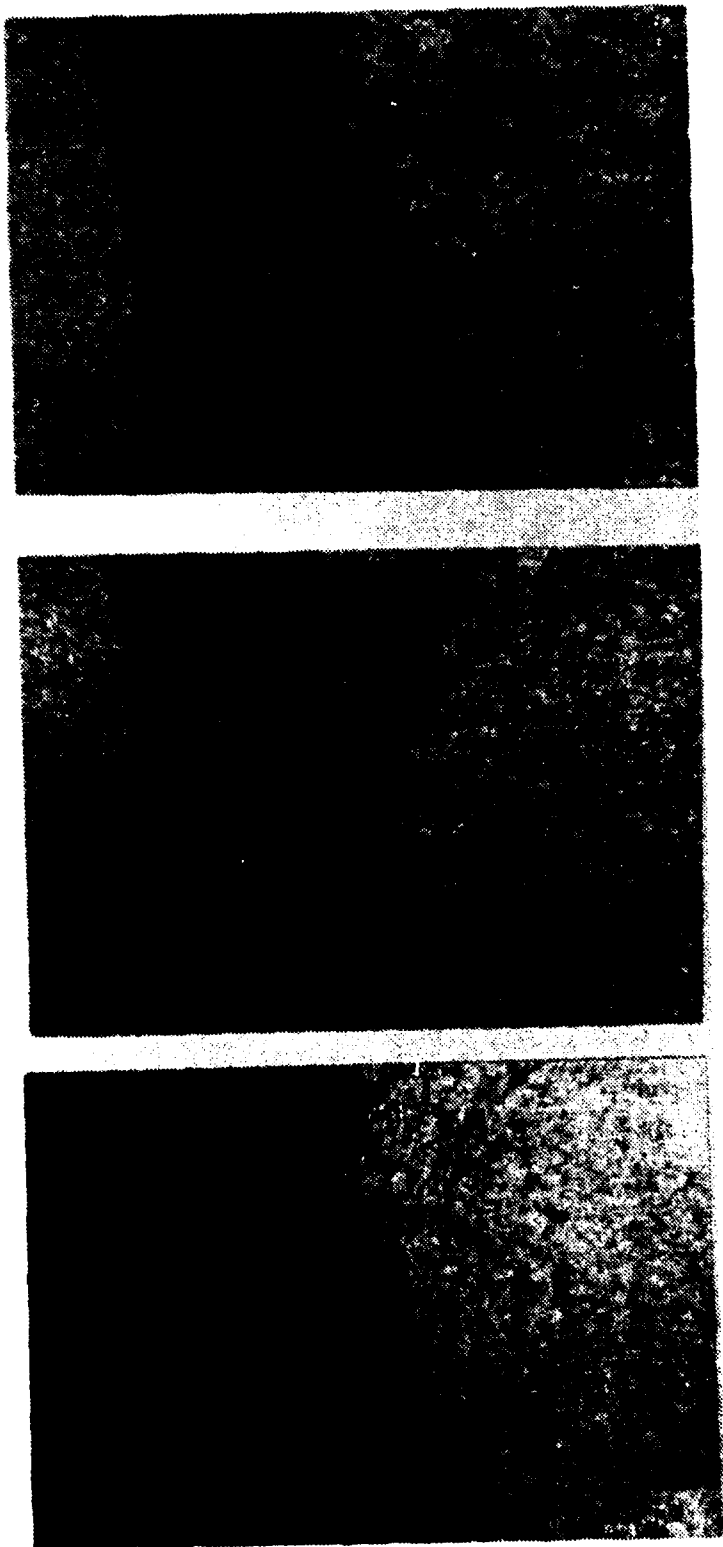
FVM 63, 6.3%, 7x

FVM 51, 3%, 7x

FVM 3, 0%, 7x

Figure 4. HY-80 Heat Tinted Fracture Surfaces
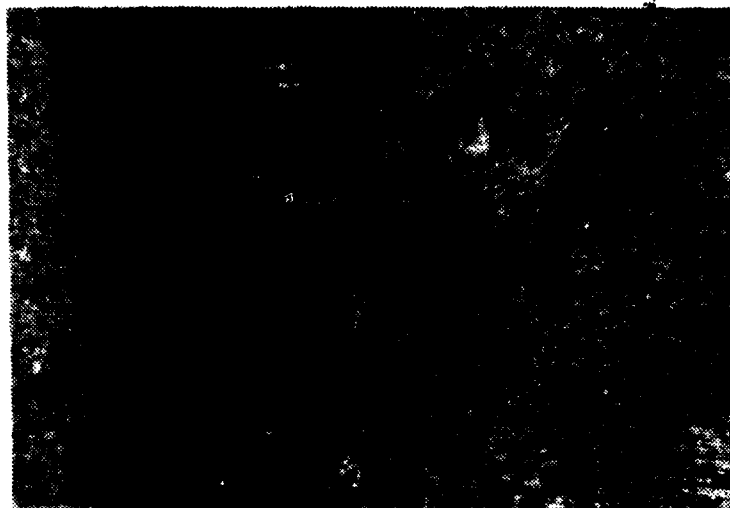
FVO 42, 5%, 7x
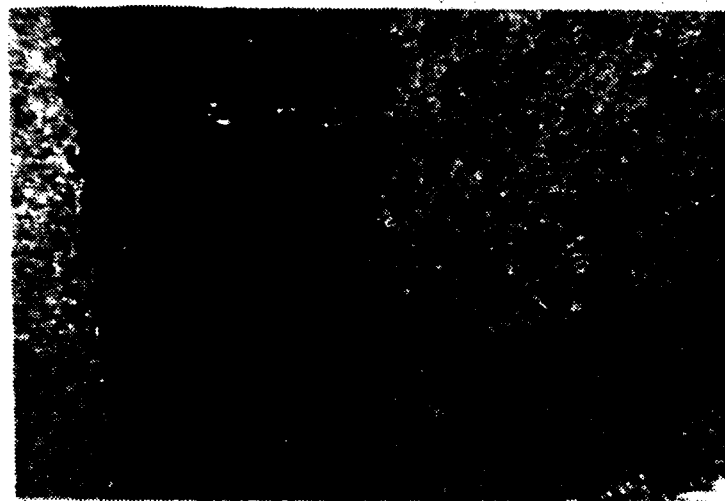
FVO 32, 3%, 7x
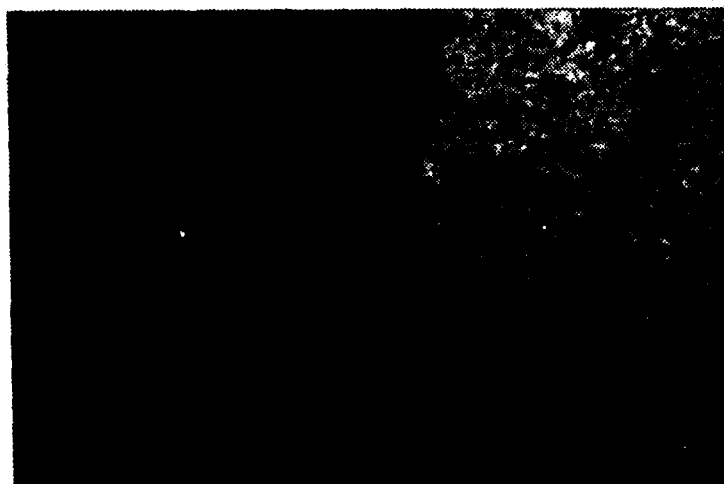
FVO 2, 0%, 7x

Figure 5. HY-100 Heat Tinted Fracture Surfaces

69
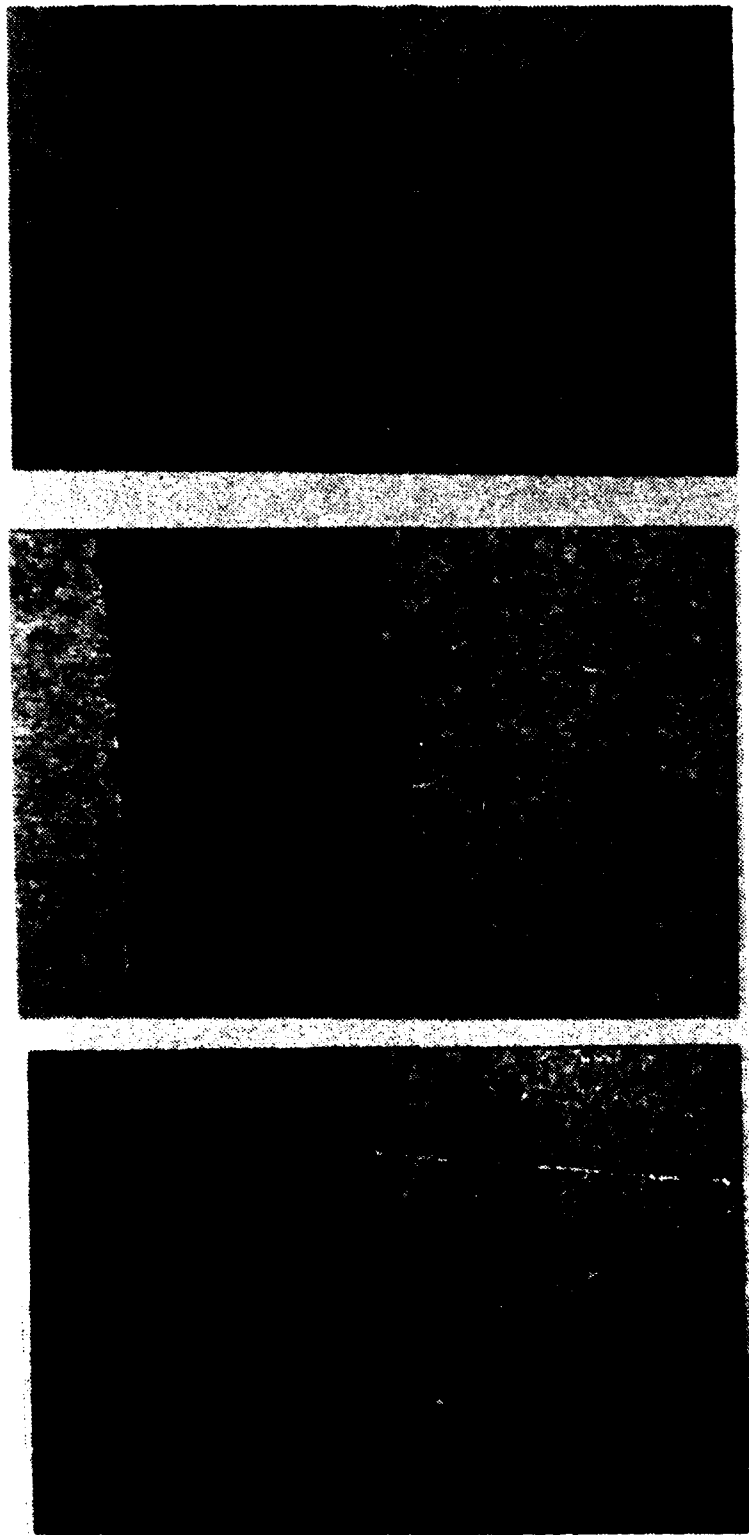
FVO 43, 5%, 7x

FVO 33, 3%, 7x

FVO 4, 0%, 7x

Figure 6. HY-100 Heat Tinted Fracture Surfaces
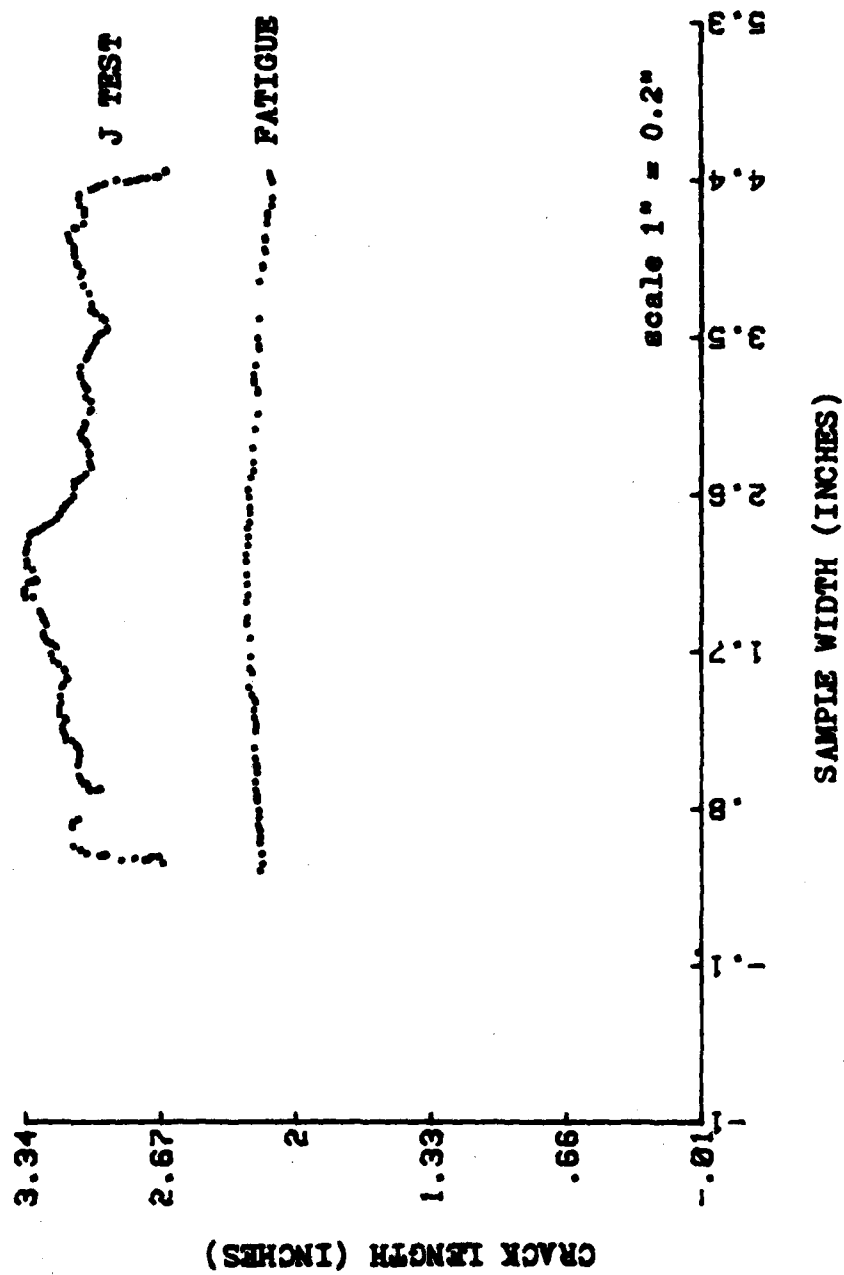
Figure 7. Digitized Fatigue Precrack and J-Integral Fracture Area
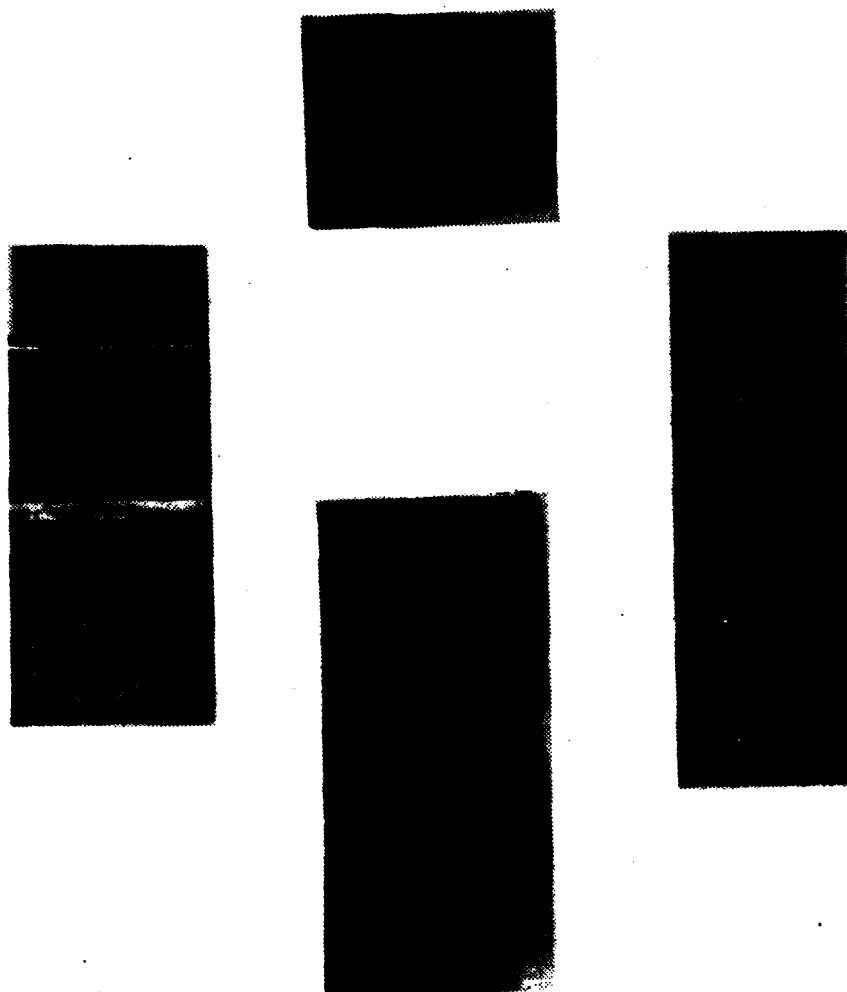
Figure 8. Three Perspectives of a Compact Specimen

FVM 60

FVM 63

FVM 50

FVM51

FVM2

FVM 3

Figure 9. HY-80 Fracture Surfaces at 1.05X

73
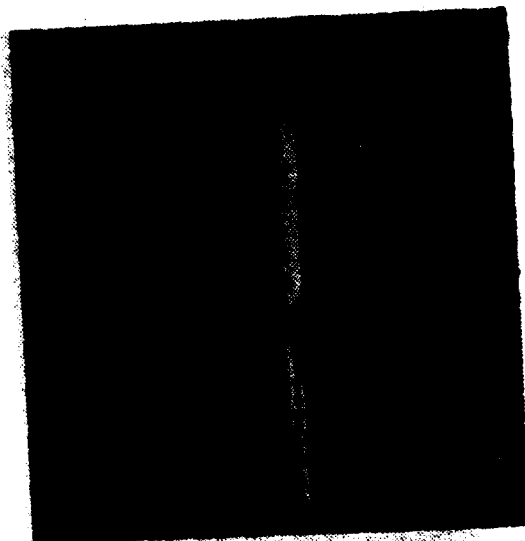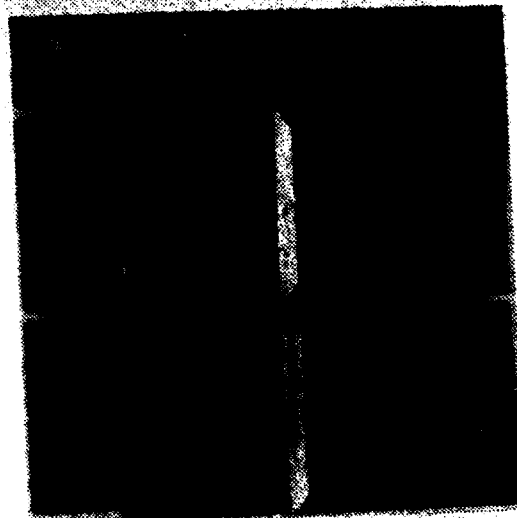
FVO 4   FVO 2

FVO 33   FVO 32
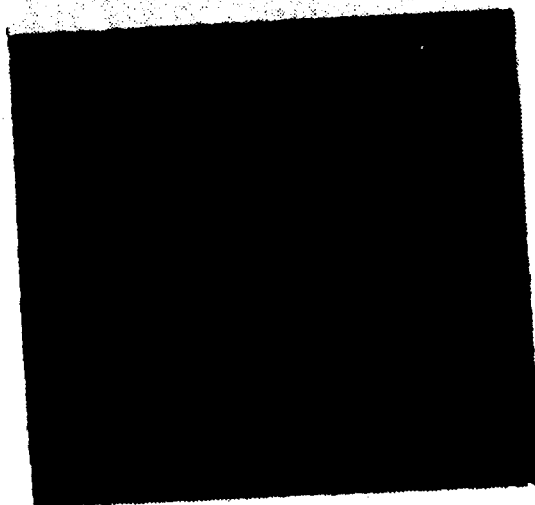
FVO 43   FVO 42

Figure 10.   HY-100 Fracture Surfaces at 1.05X

74

Figure 11. J_{1C} versus Rockwell Hardness
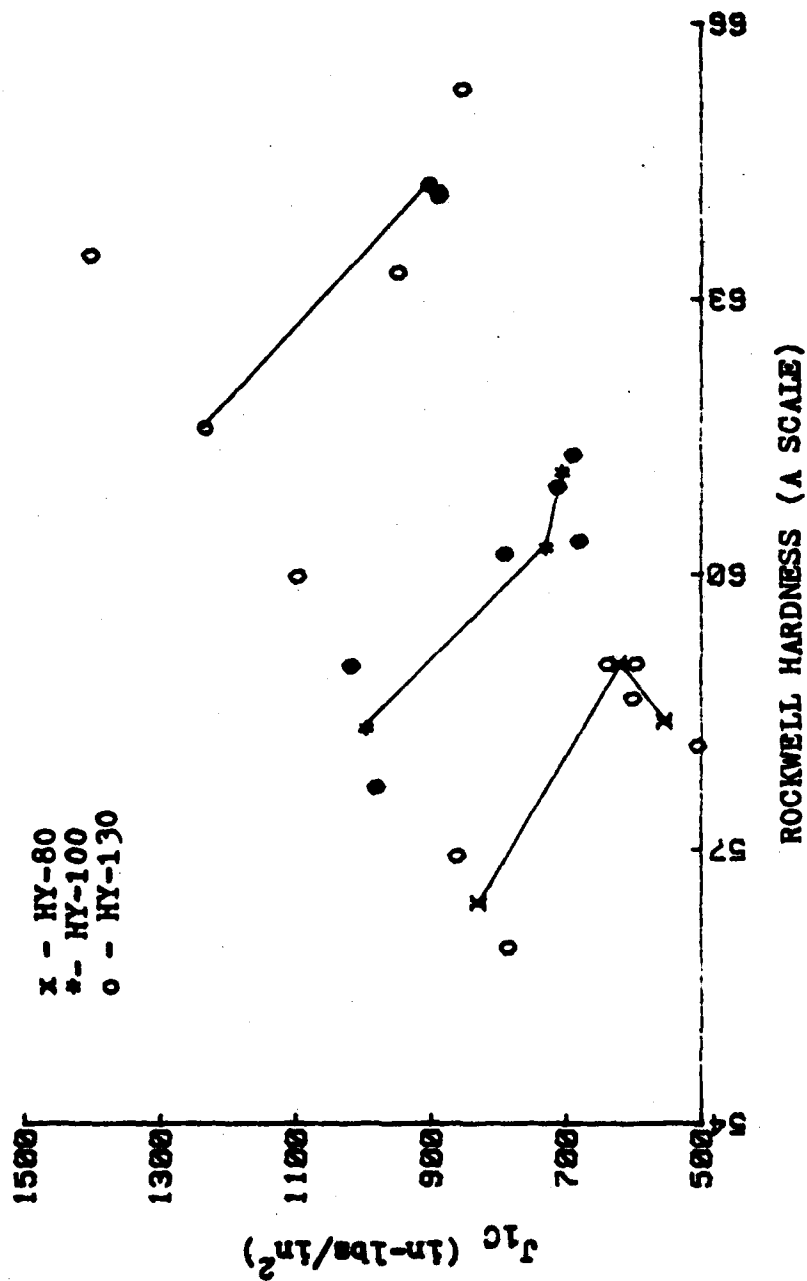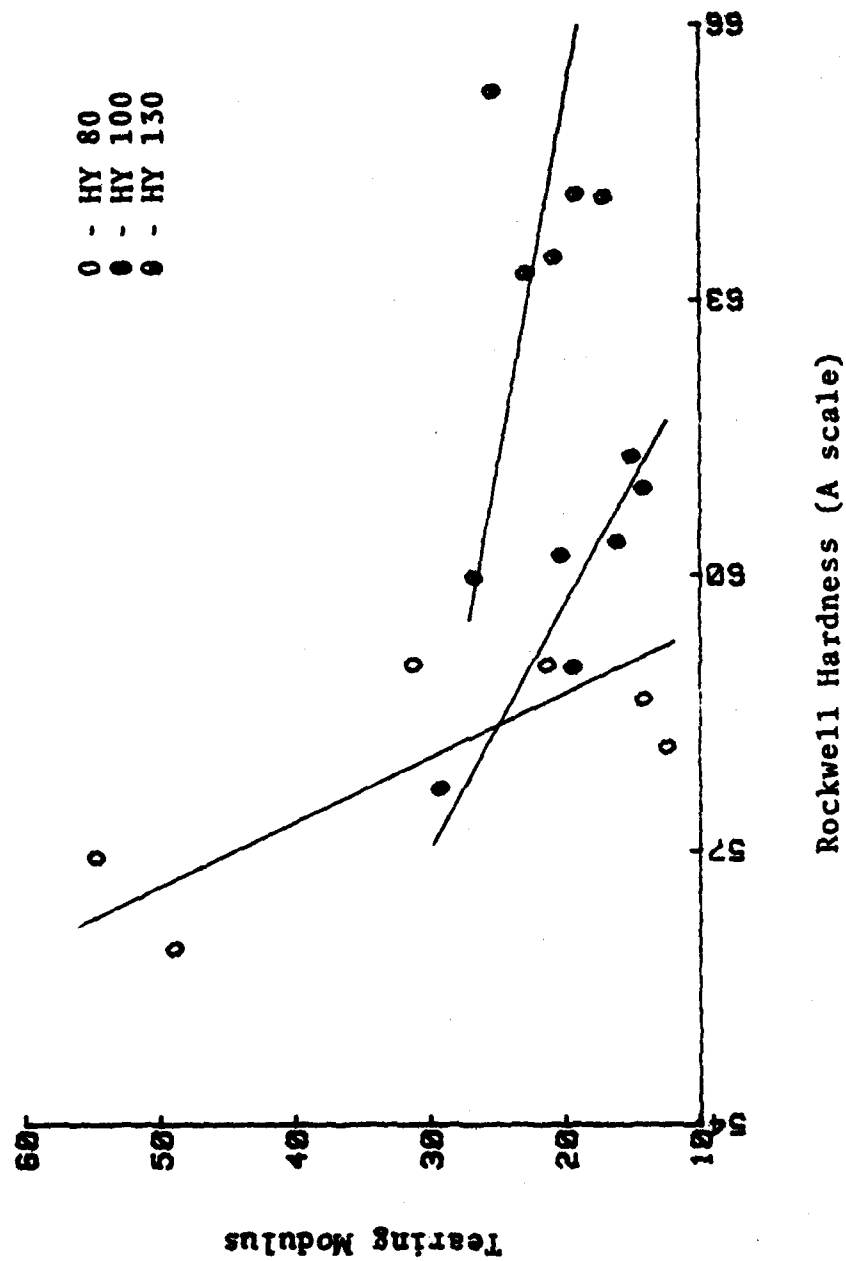
Figure 12. Tearing Modulus versus Rockwell Hardness

76

Electrolyte

700 ml - Ethanol
120 ml - Distilled water
100 ml - Glycerol
80 ml - Perchloric

Voltage (volts)
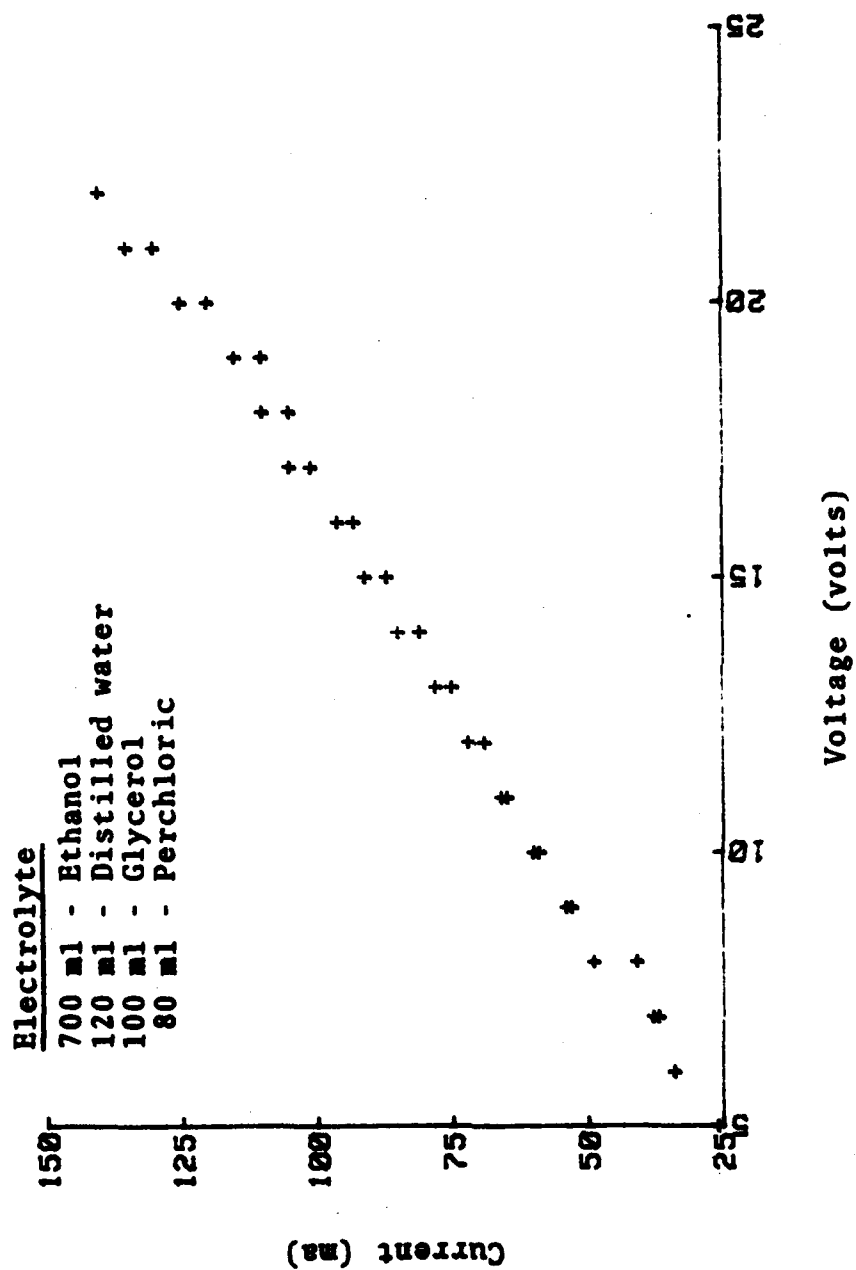
Current (ma)

Figure 13. Electrolyte, Current versus Voltage Curve

77
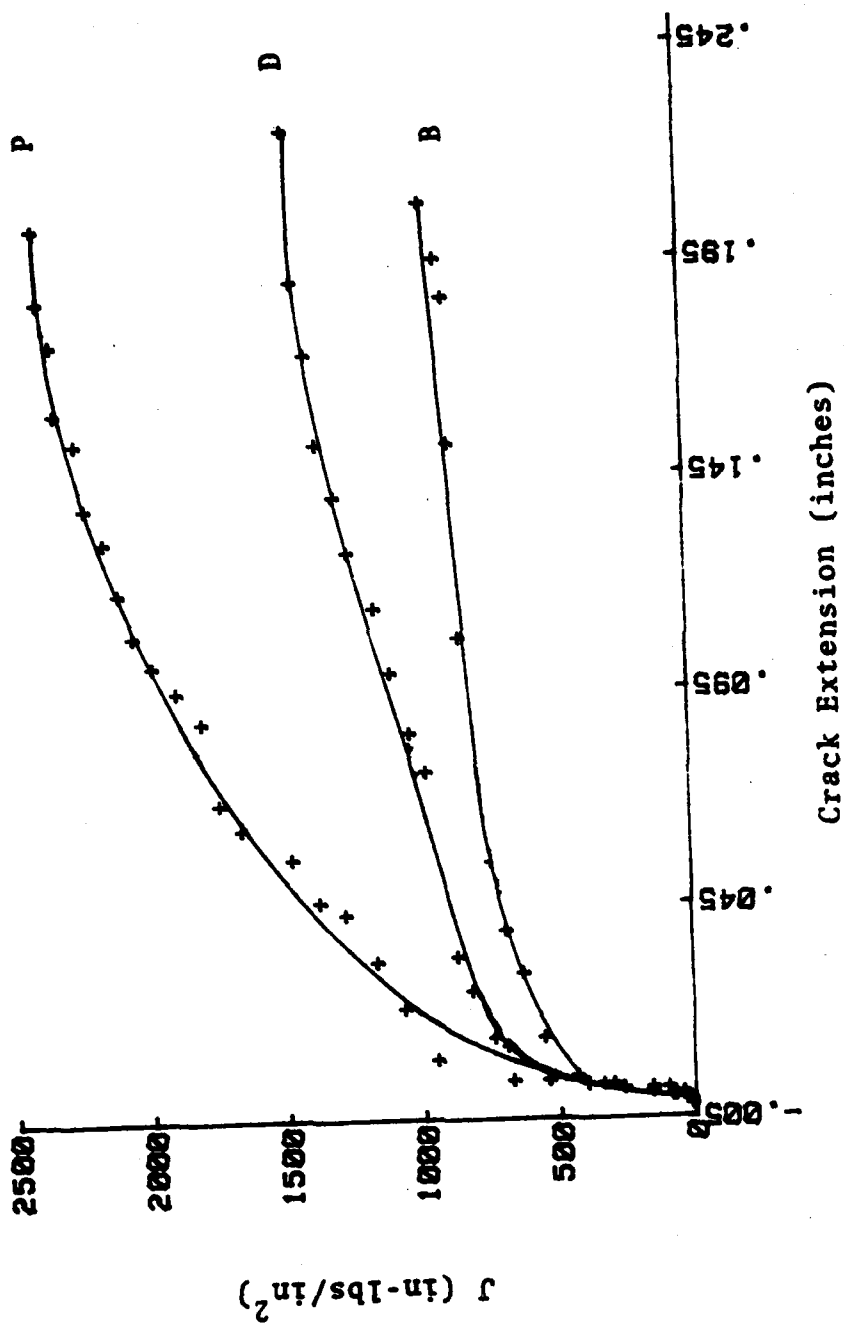
Figure 14. DTNSRDC, HY-80 J-Integral Plots
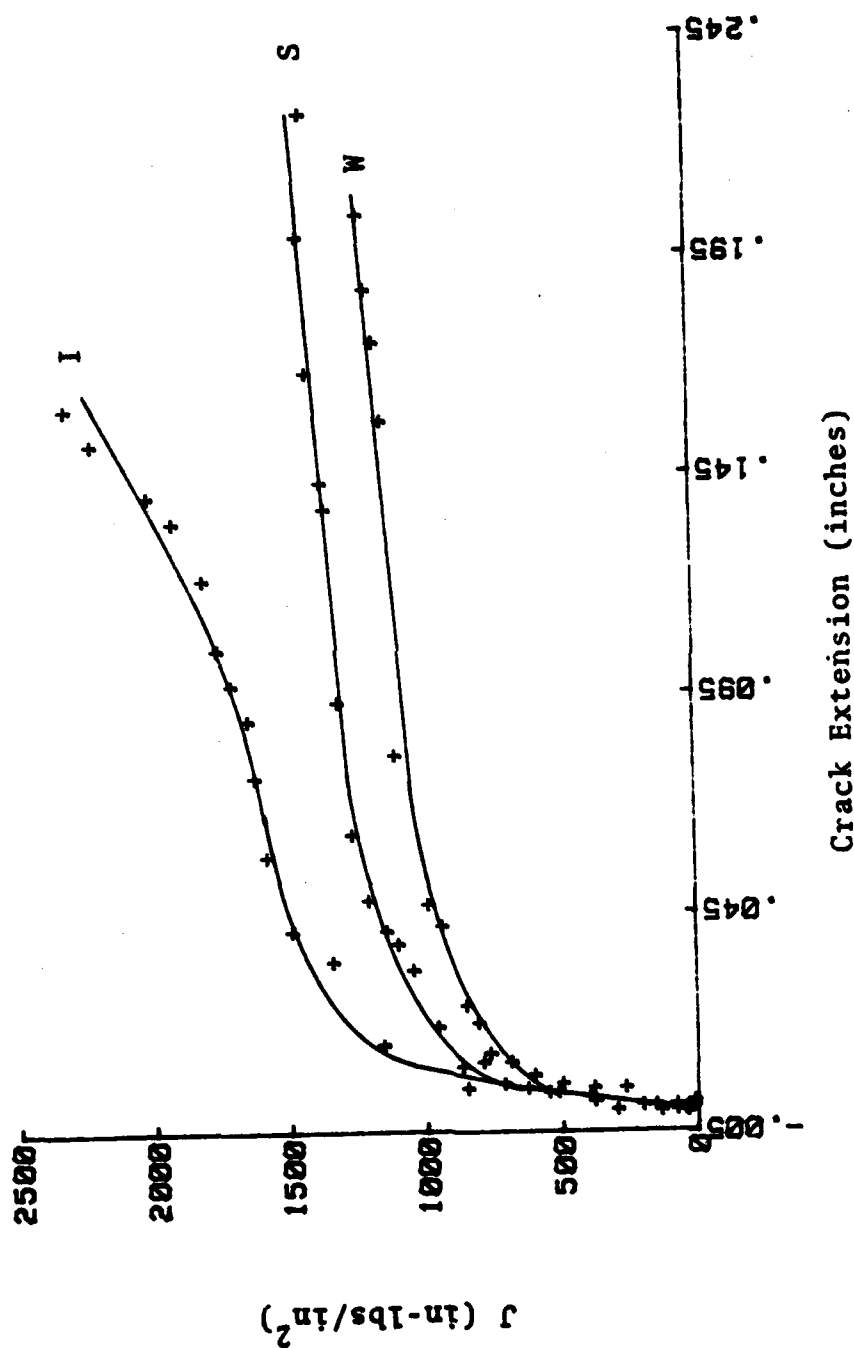
Figure 15. DTNSRDC, HY-100 J-Integral Plots

79
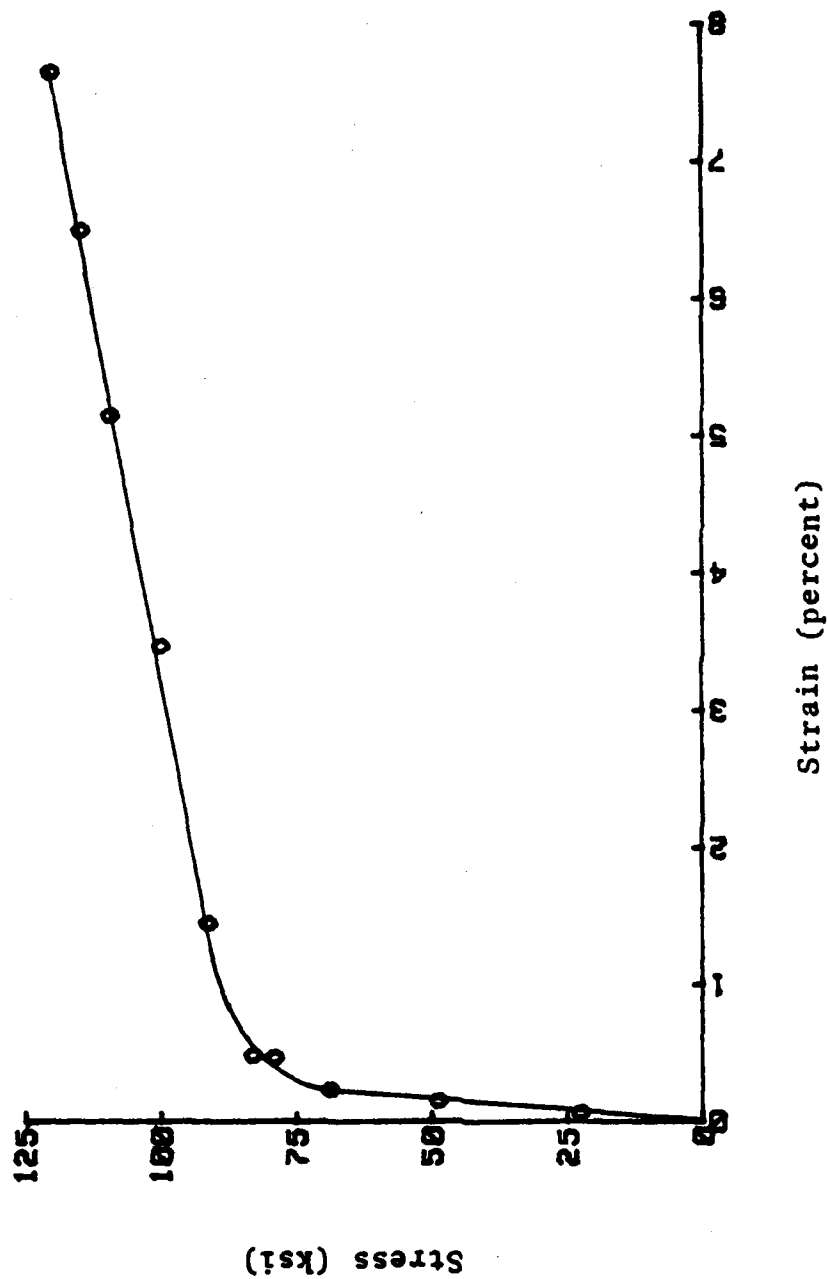
Figure 16. HY-80 Stress-Strain Curve
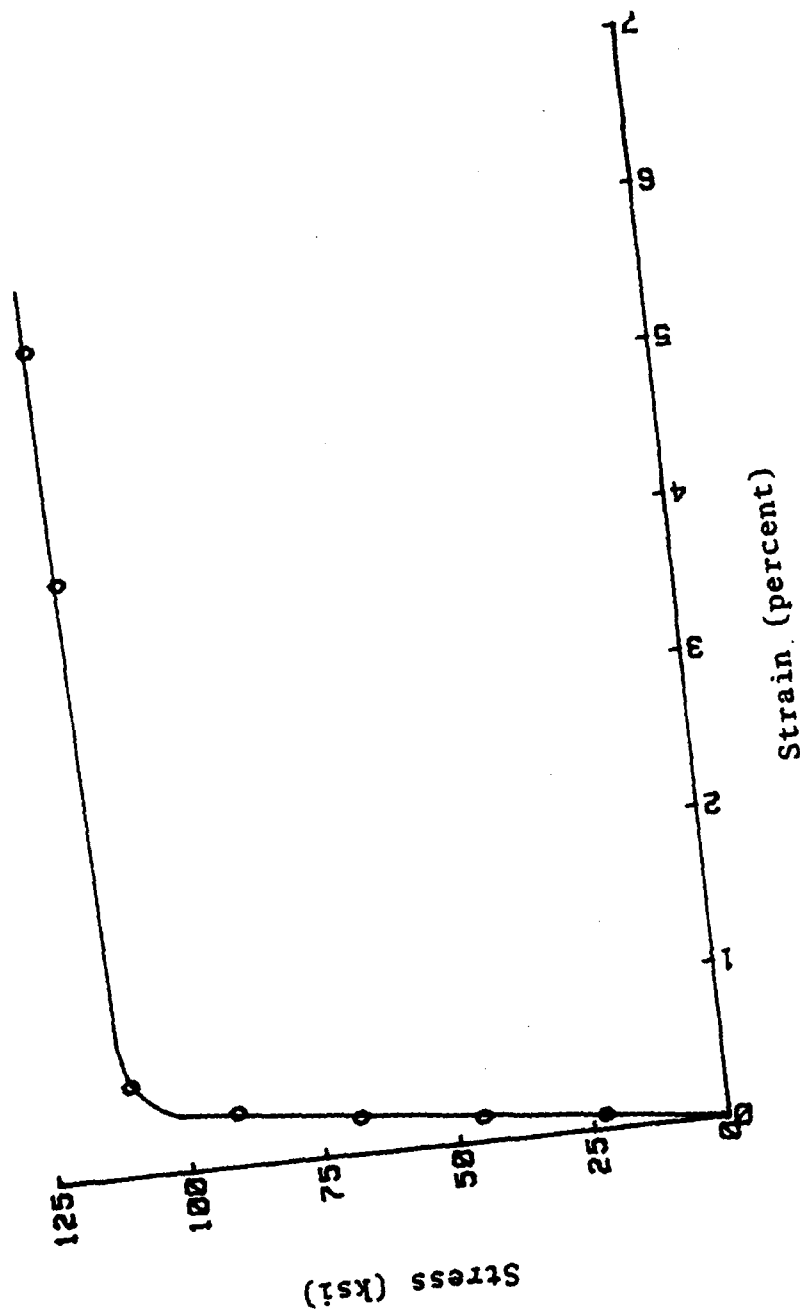
Figure 17. HY-100 Stress-Strain Curve
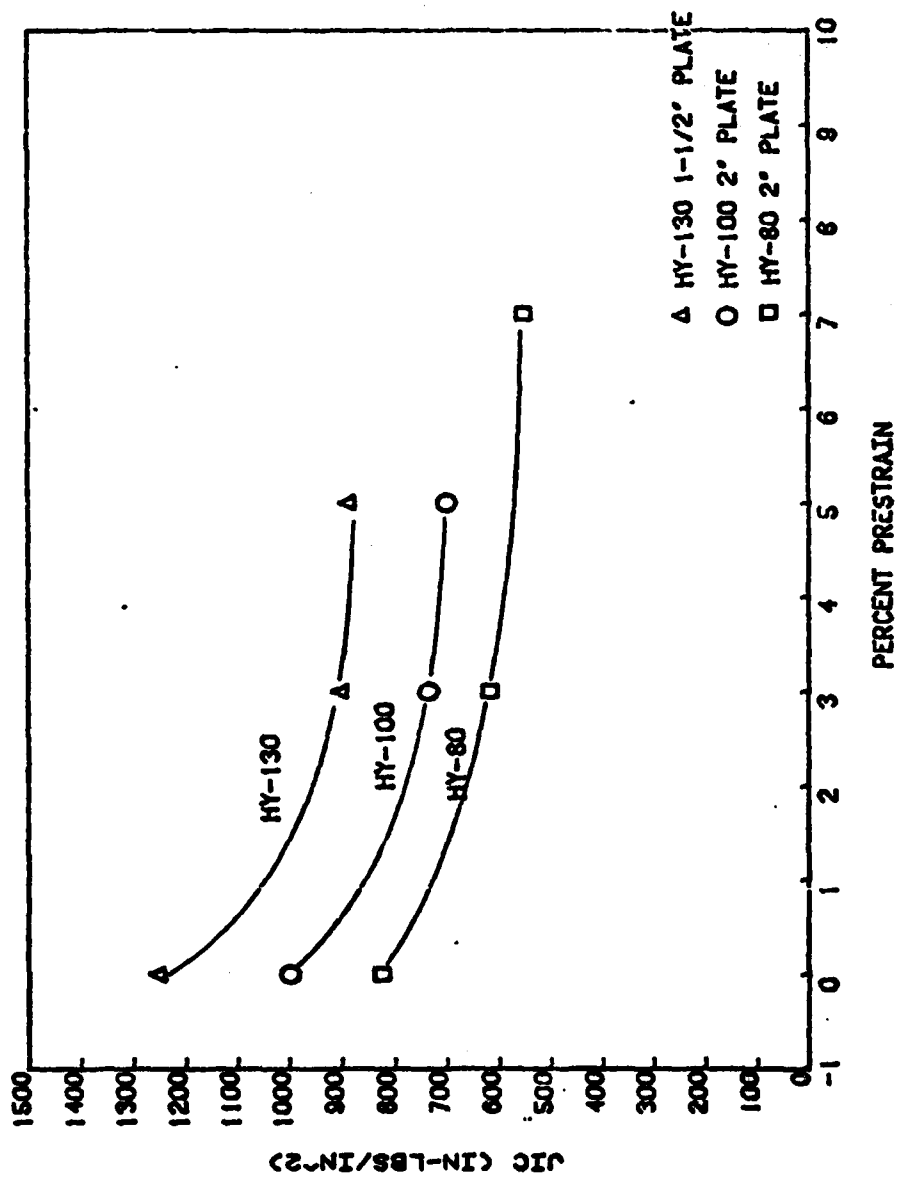
Figure 18. Plot of J_{1C} versus Percent Prestrain
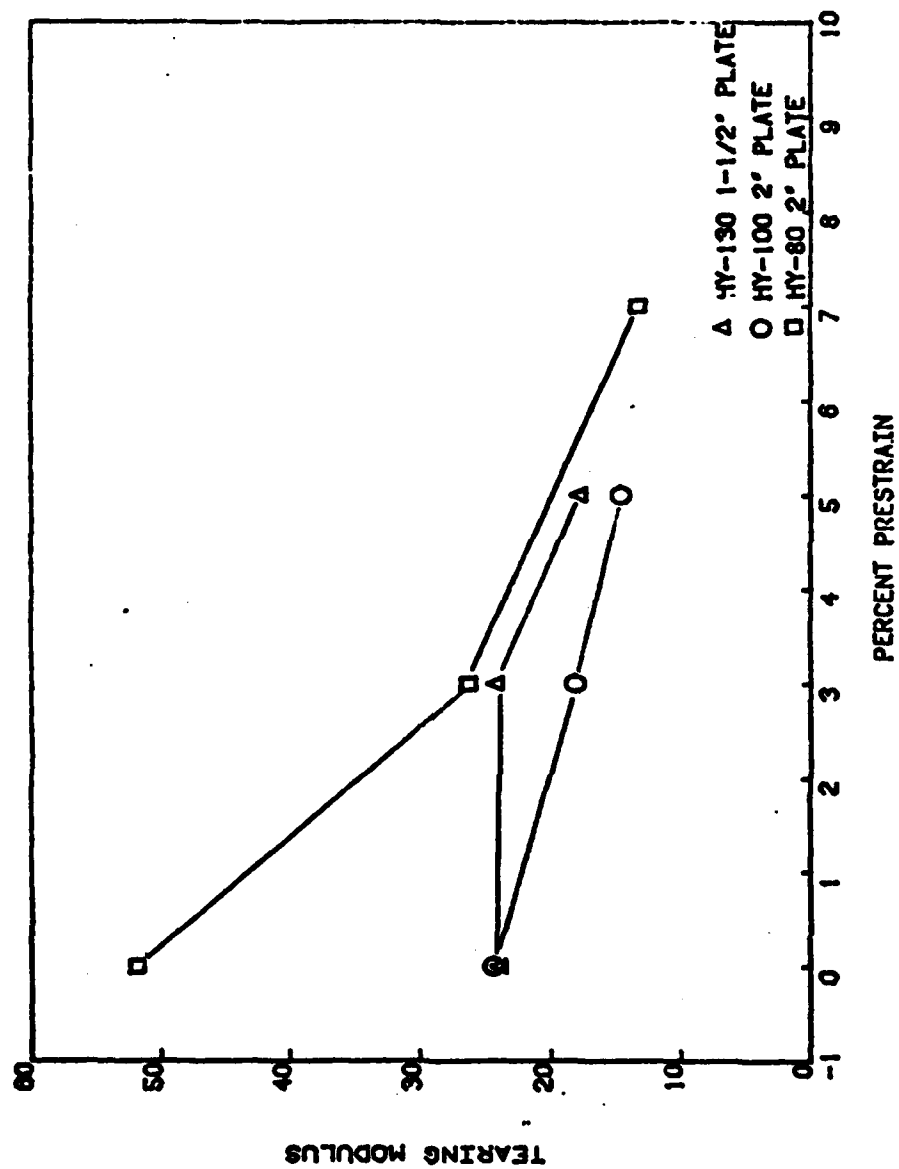
Figure 19. Plot of Tearing Modulus versus Percent Prestrain

83
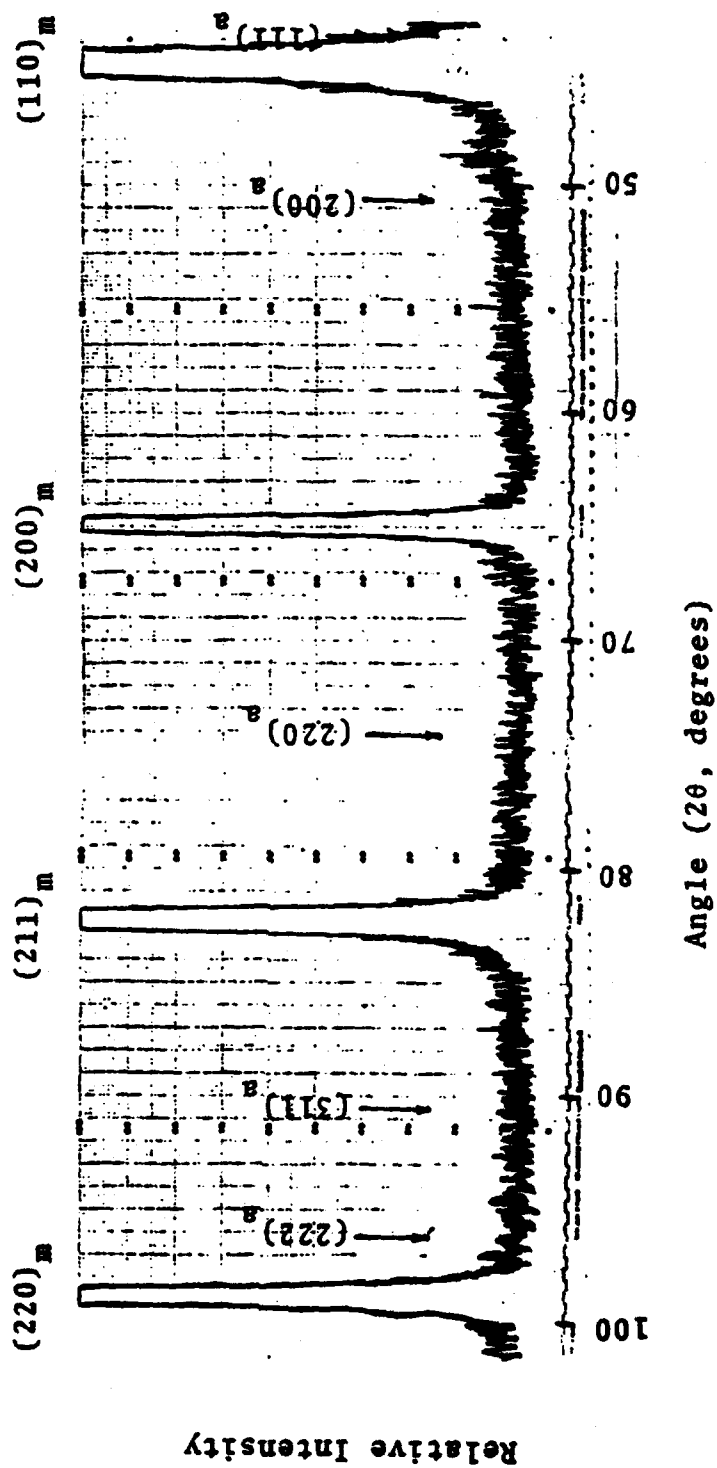
Figure 20. X-ray Diffraction Pattern Specimen E

84

Figure 21. Microstructural Photographs of HY-80 Samples

Figure 22. Microstructural Photographs of HY-100 Samples

Figure 23. Photographs of Surface Etching Variations
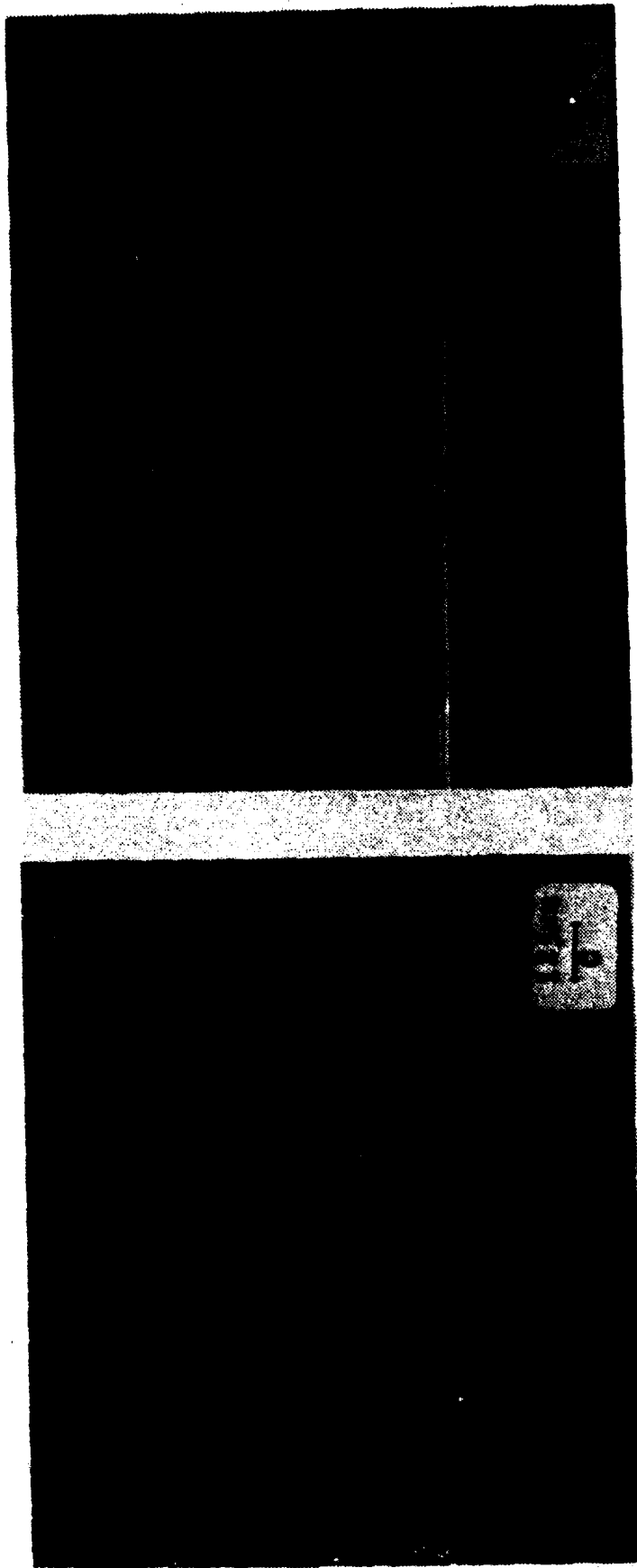
Figure 24. Photographs of Banding with DPH Indentations
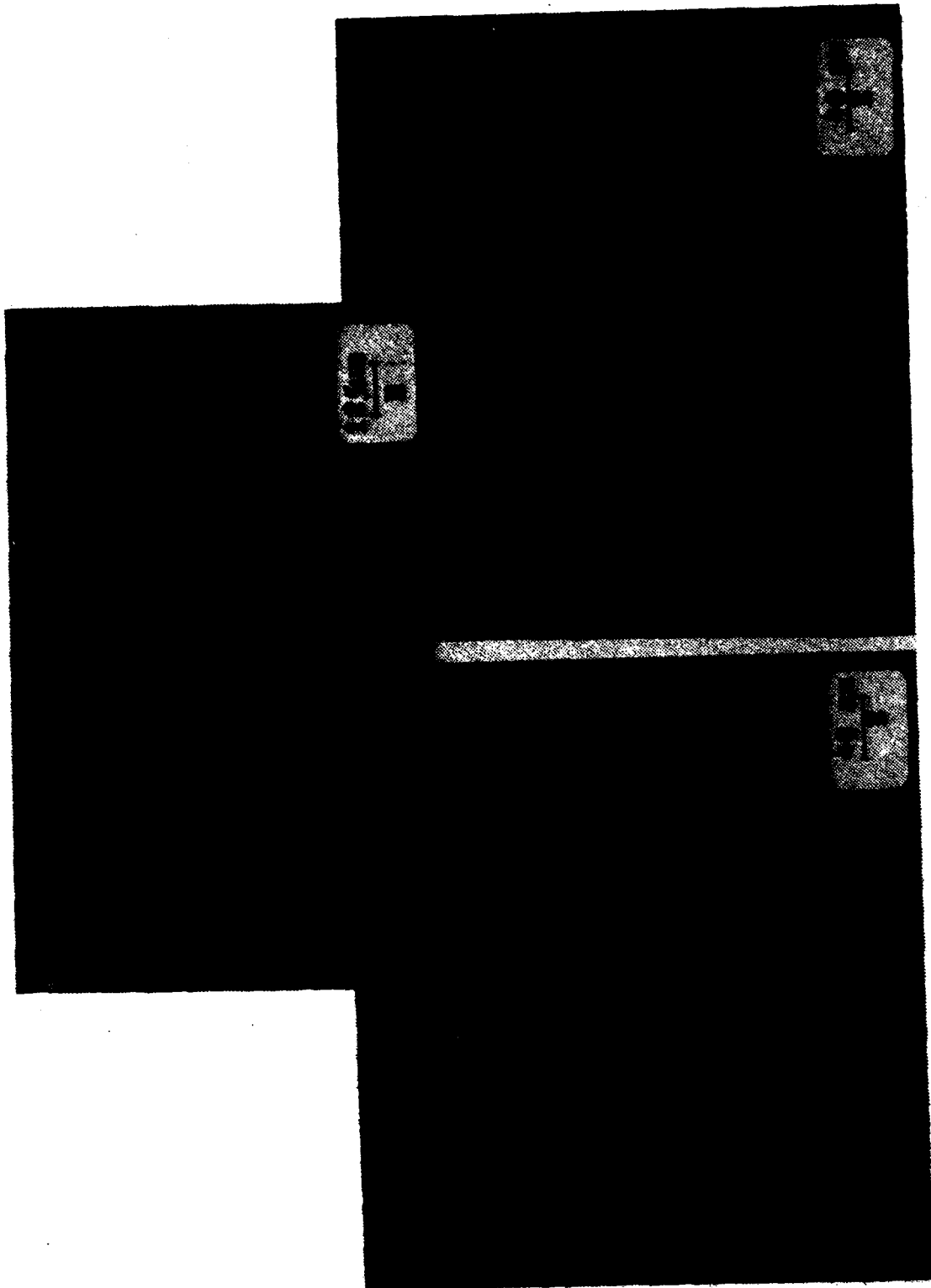
Figure 25. Photos of Regions in HY-80 Containing Inclusions
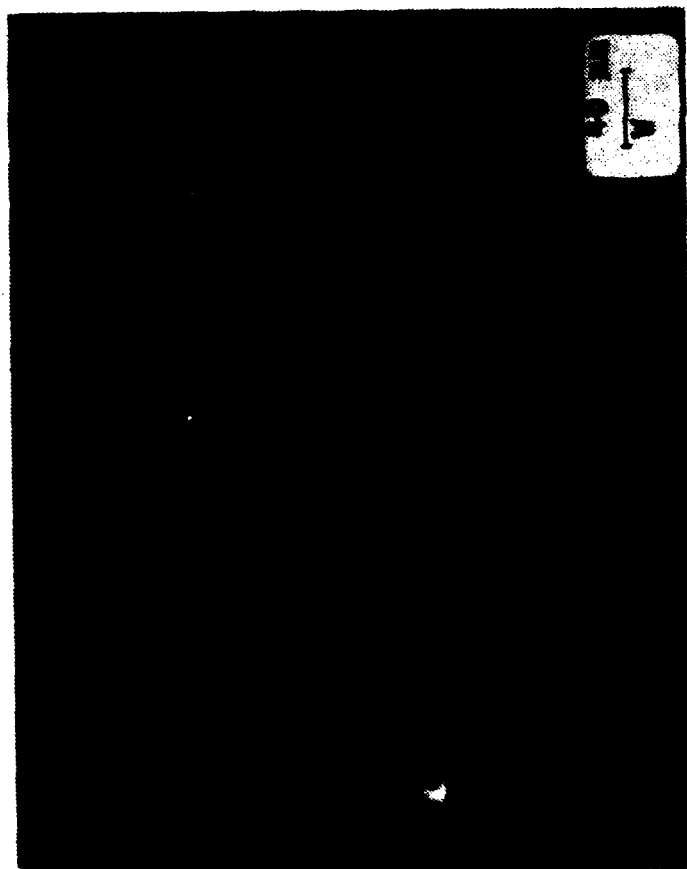
Figure 26. Photos of Regions in HY-100 Containing Inclusions
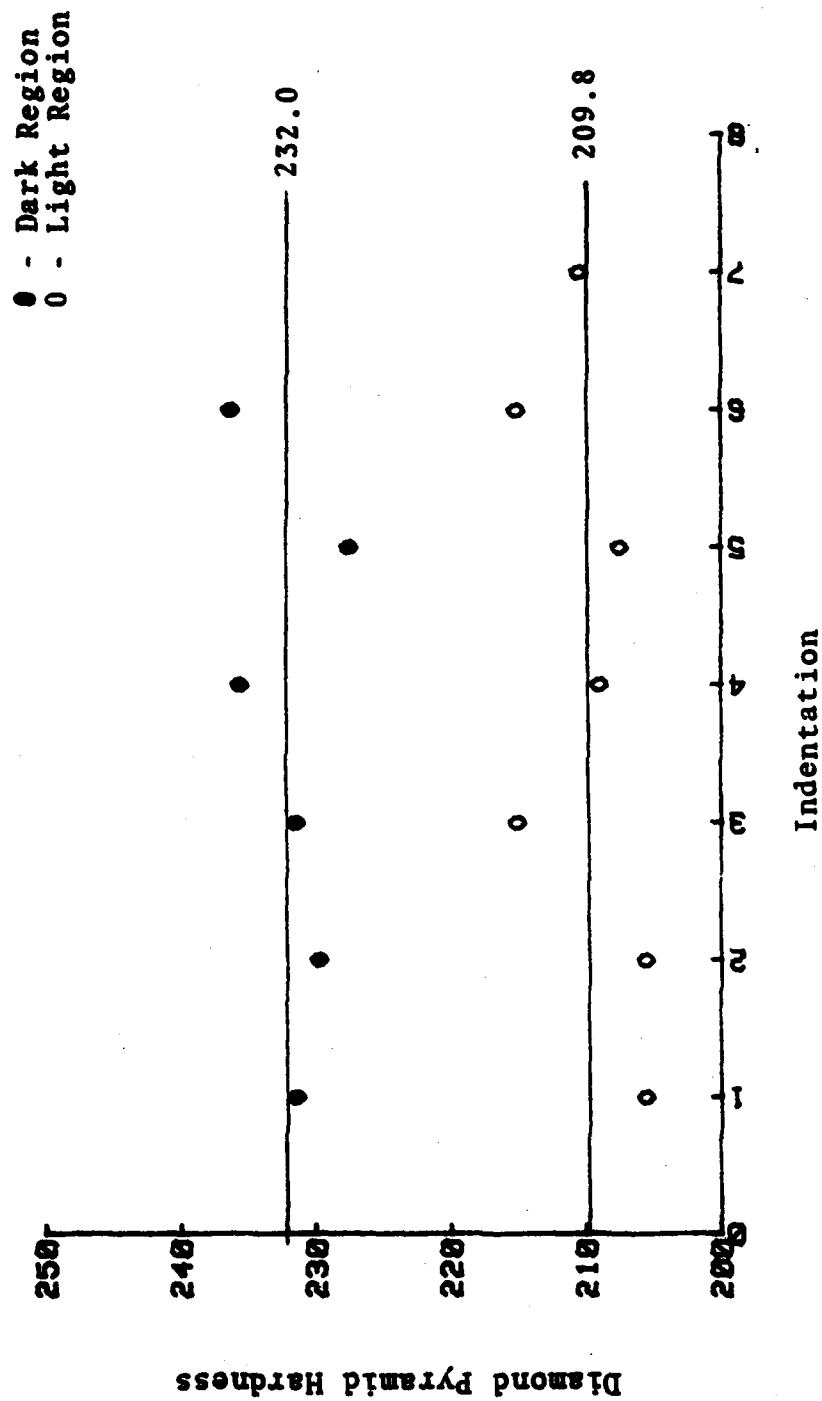
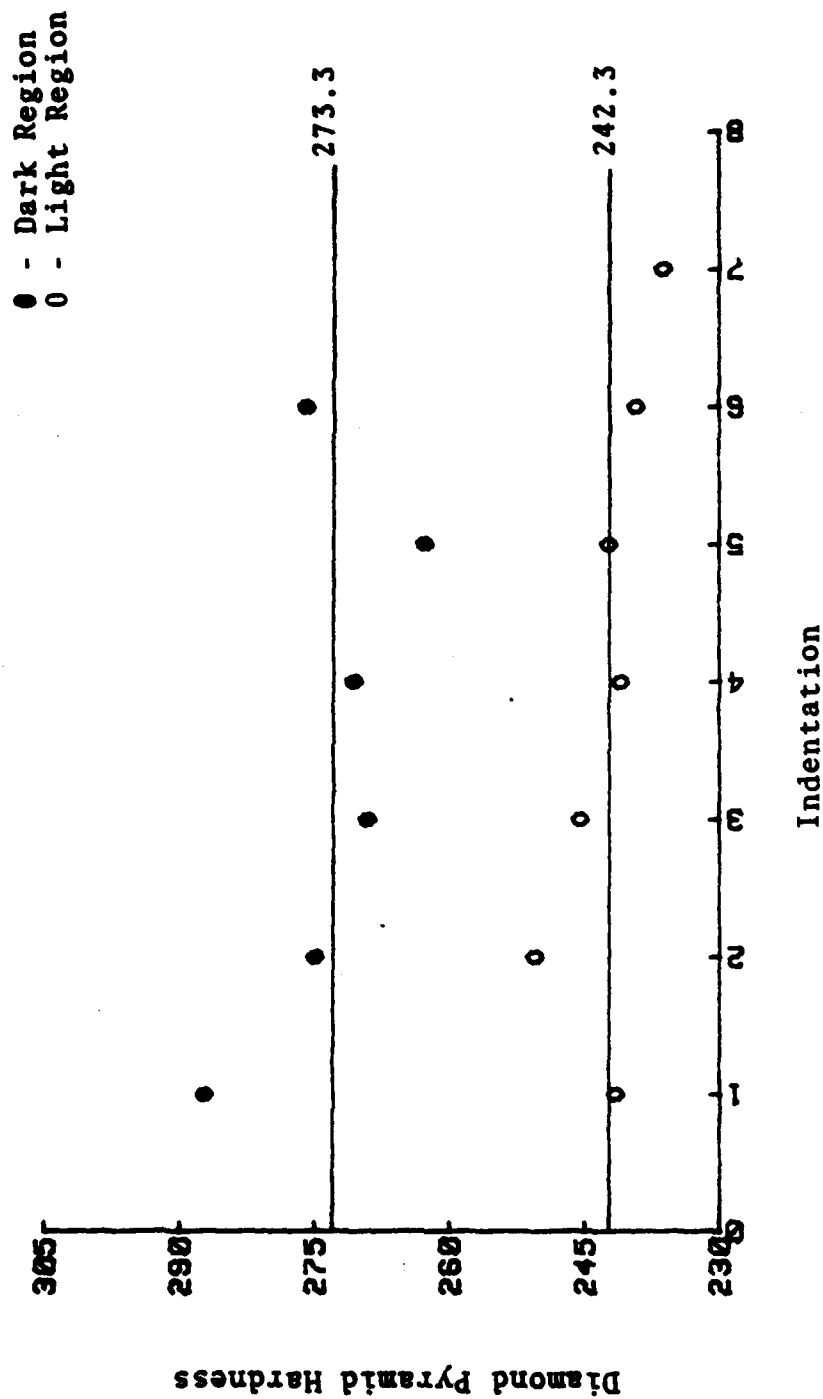Figure 27. DPH Results - HY-80 Specimen L (0%)
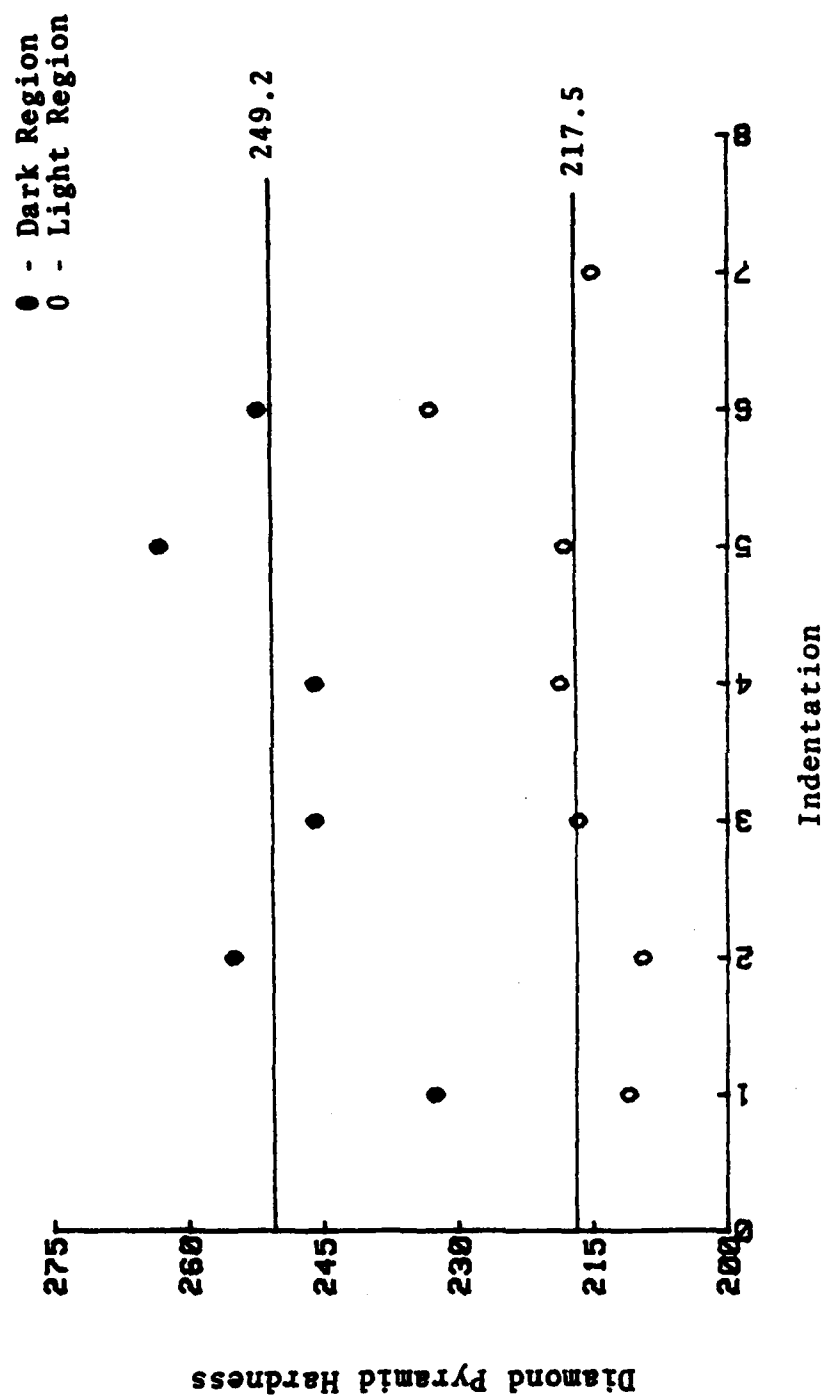
Figure 28. DPH Results - HY-80 Specimen C (3%)
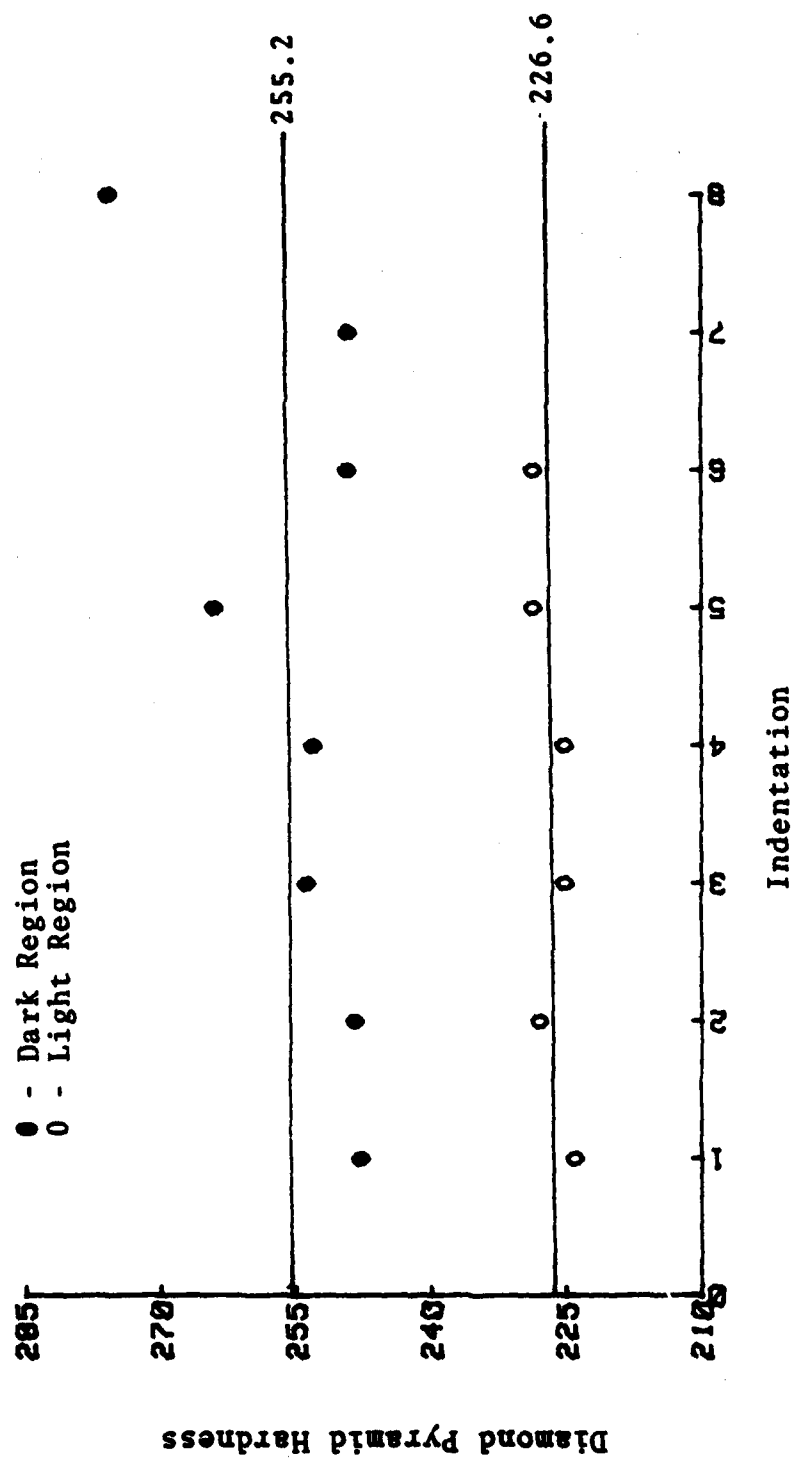
Figure 29. DPH Results - HY-80 Specimen B (7.5%)

Figure 30. DPH Results - HY-100 Specimen I (0%)

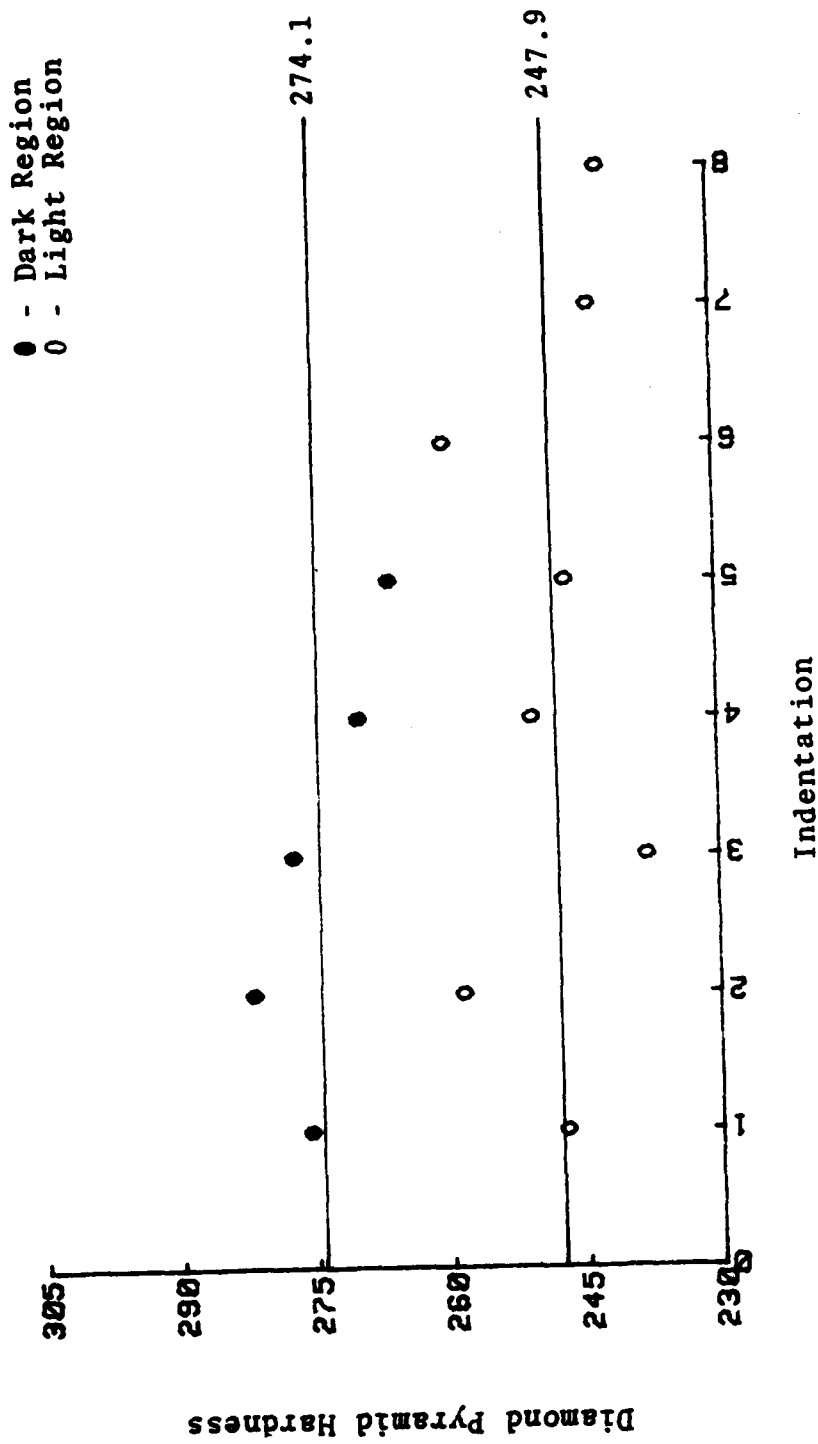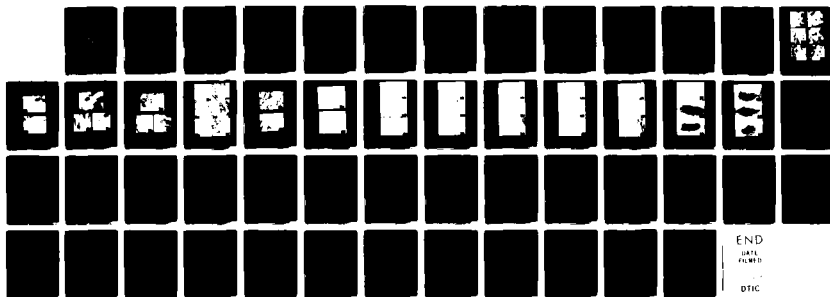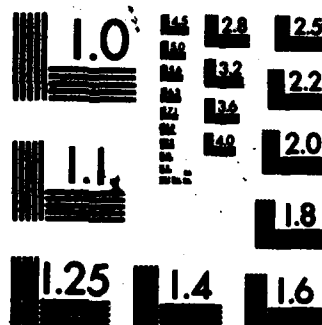94

Figure 31. DPH Results - HY-100 Specimen S (3%)

END

DATE
FILMED

DTIC

MICROCOPY RESOLUTION TEST CHART
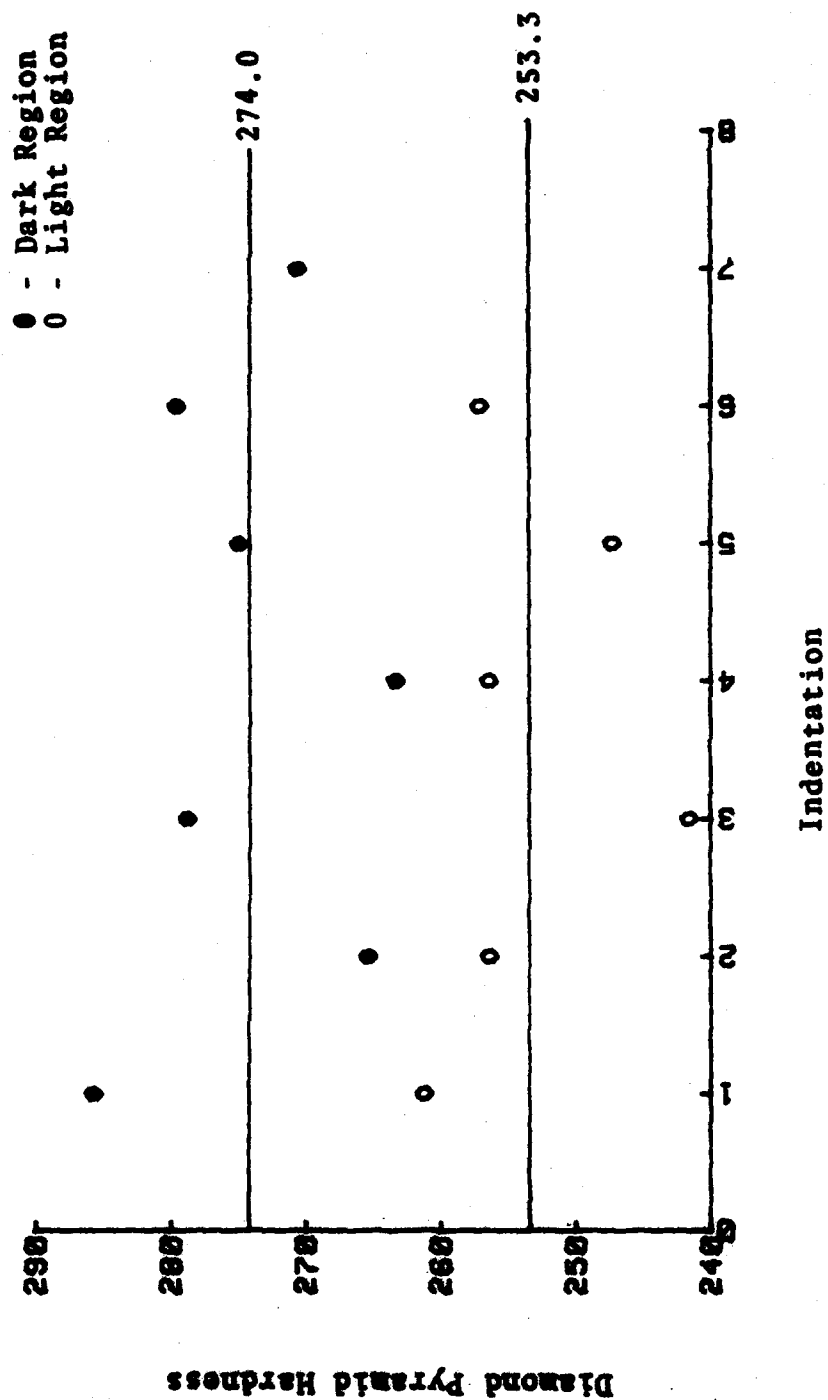
NATIONAL BUREAU OF STANDARDS-1963-A

Figure 32. DPH Results - HY-100 Specimen W (5%)

Figure 33. DPH Results - Light Regions HY-80

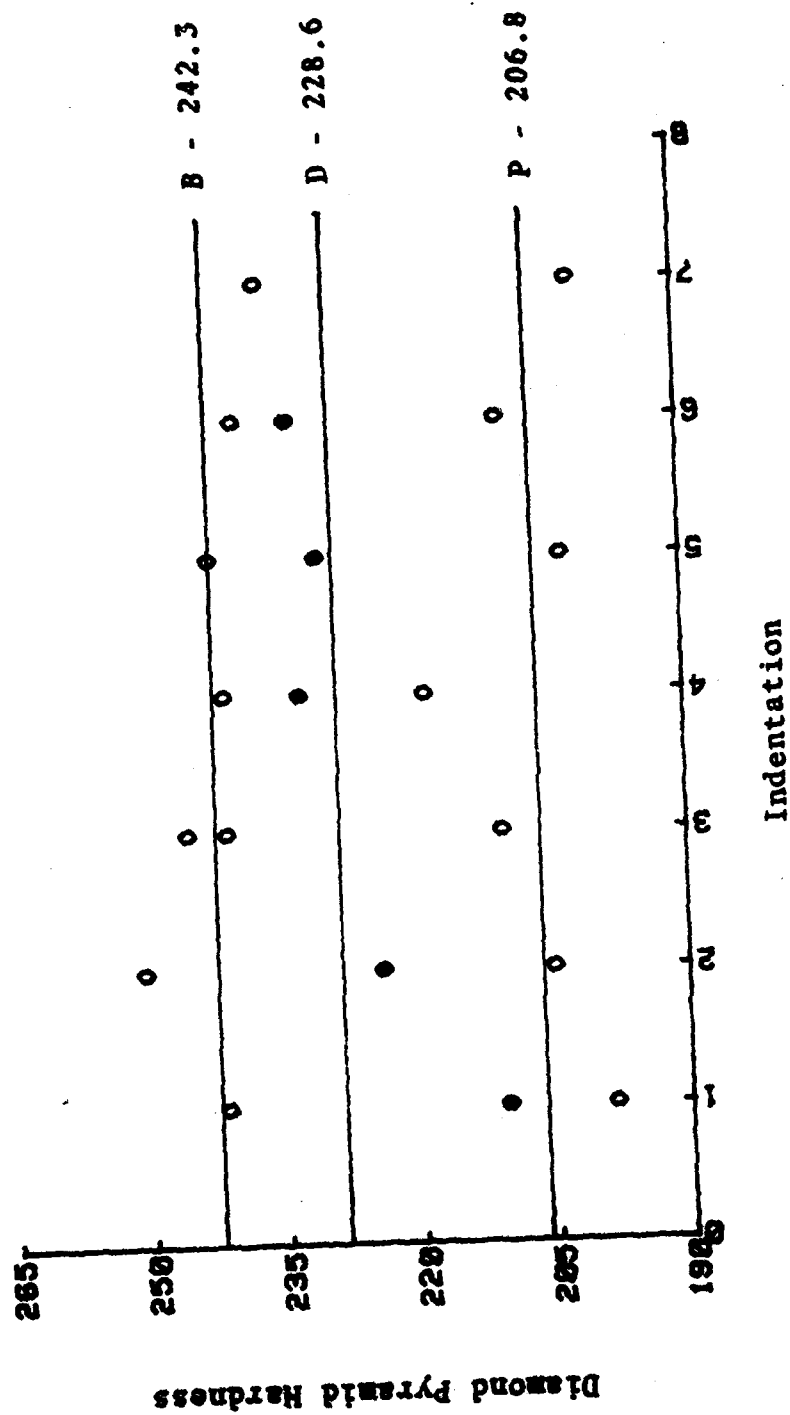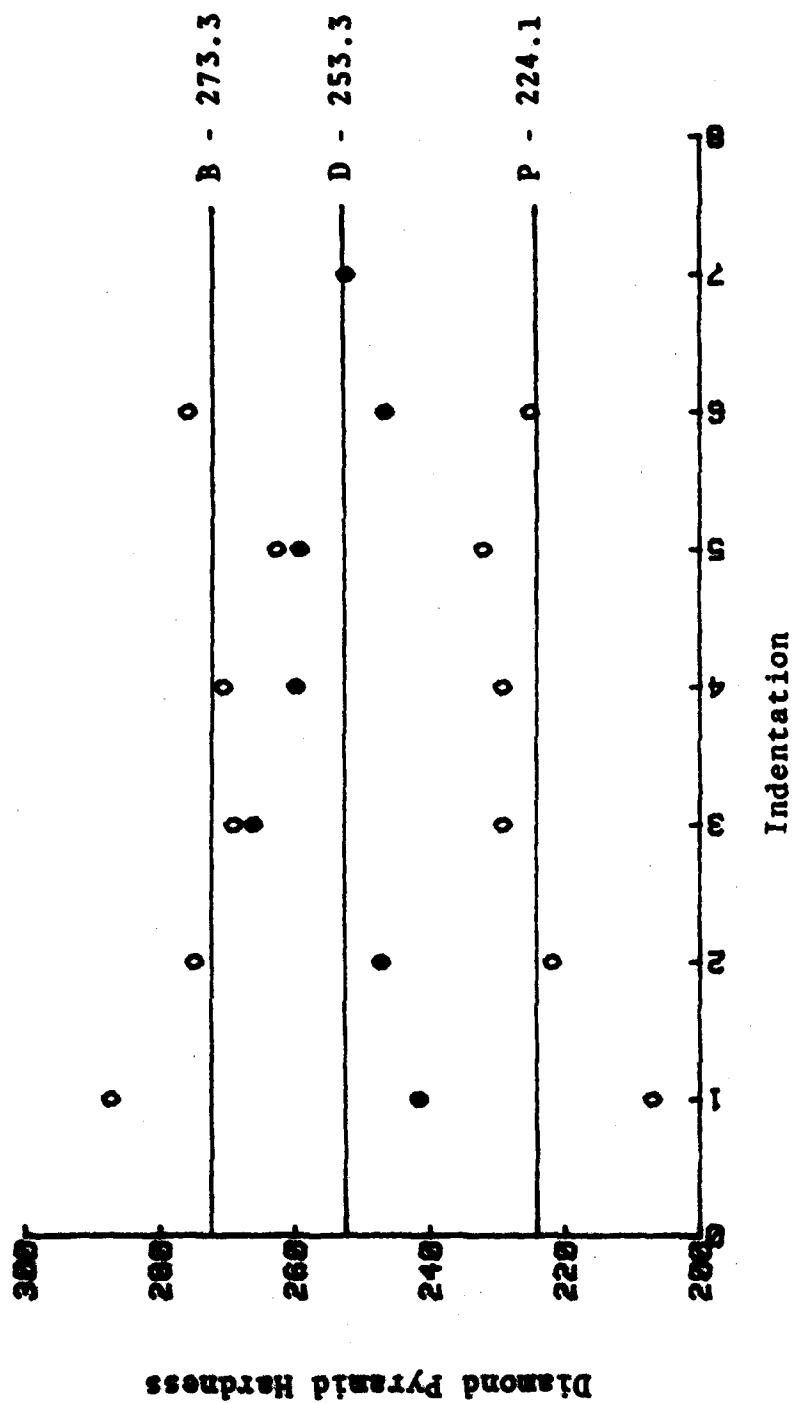Figure 34. DPH Results - Dark Regions HY-80
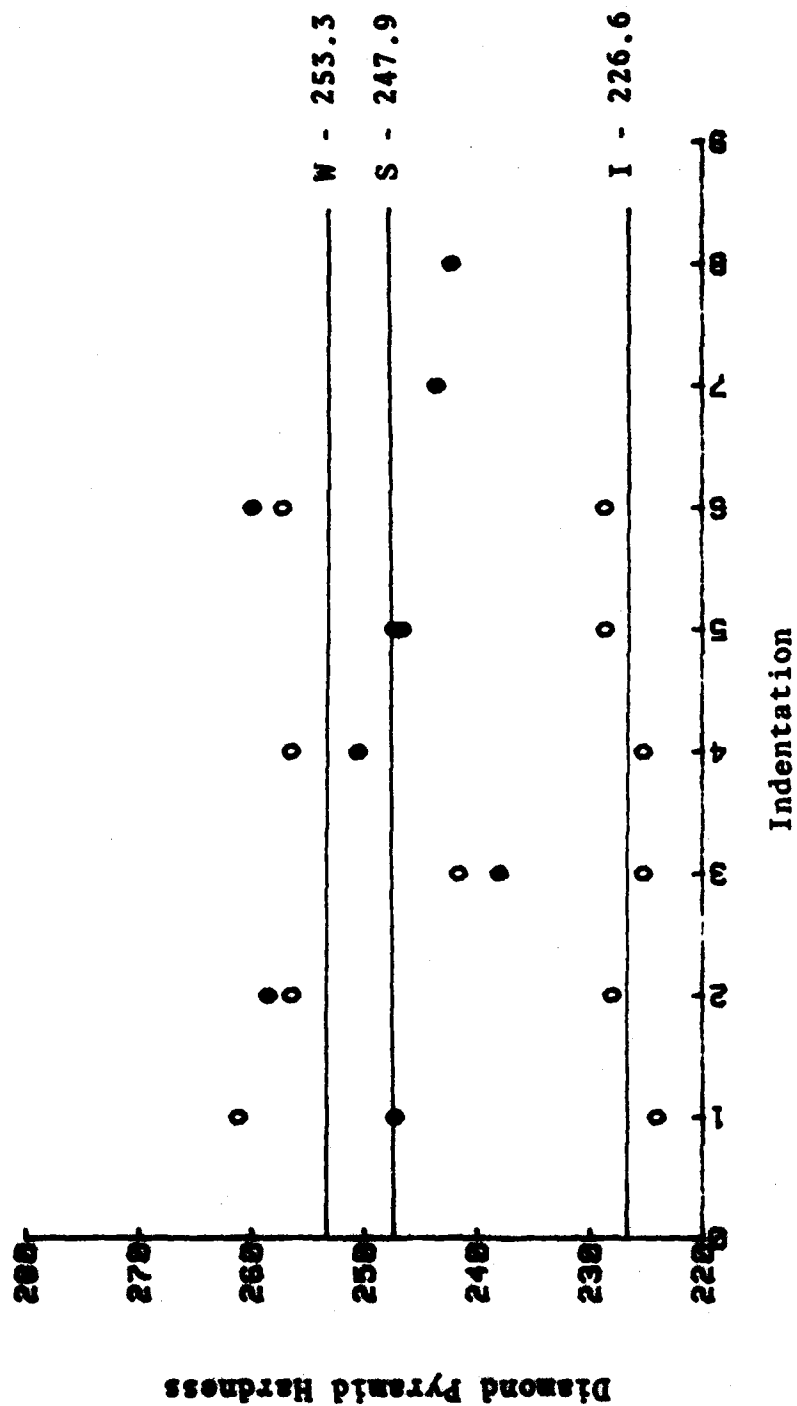
Figure 35. DPH Results - Light Regions HY-100
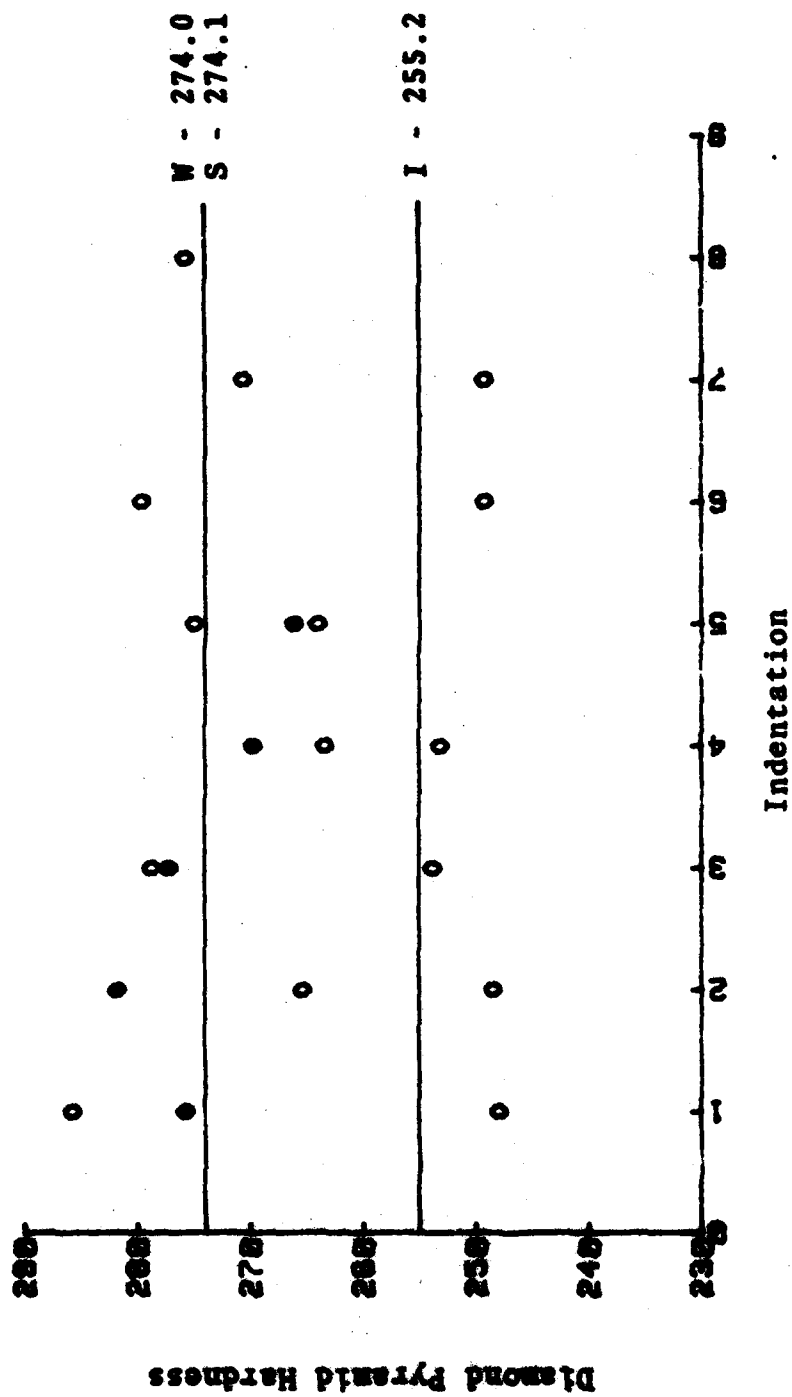
Figure 36. DPH Results - Dark Regions HY-100
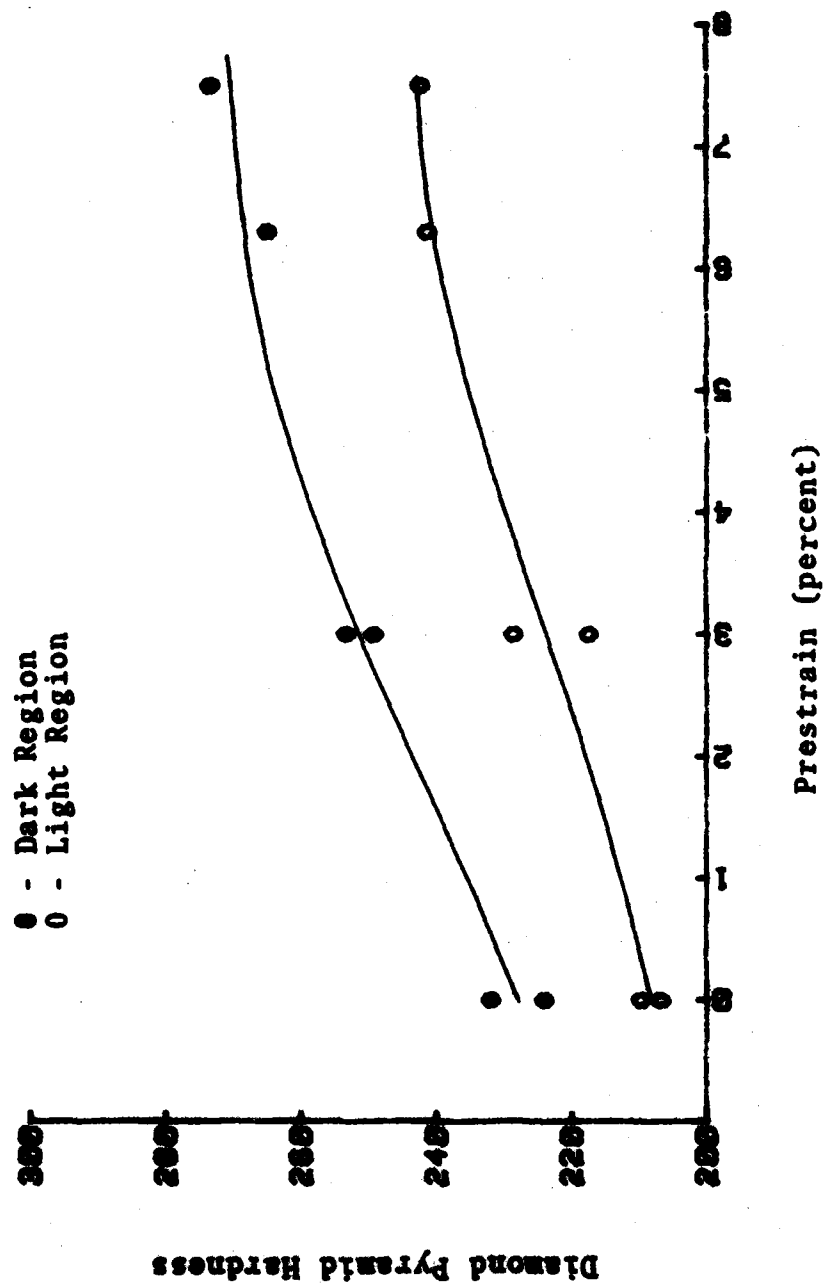
Figure 37. DPH versus Prestrain in HY-80
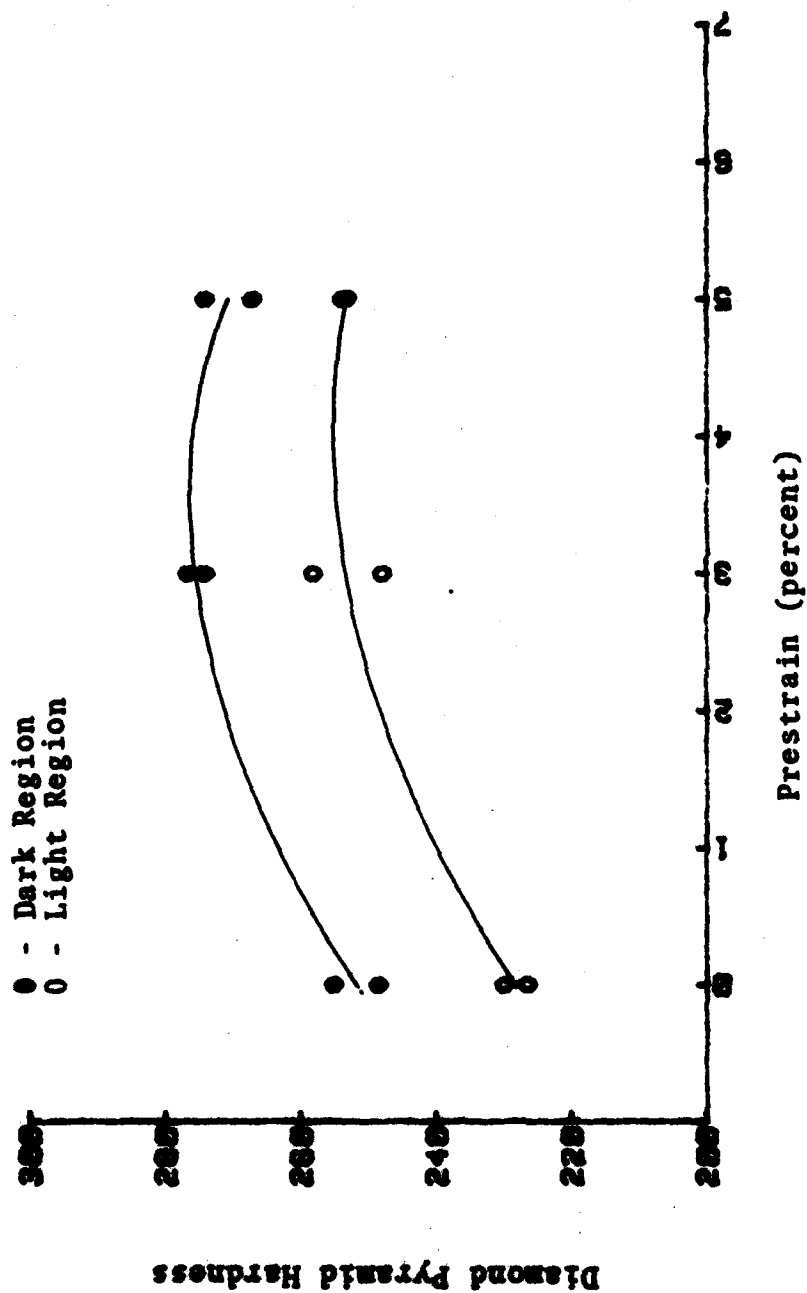
Figure 38. DPH versus Prestrain in HY-100
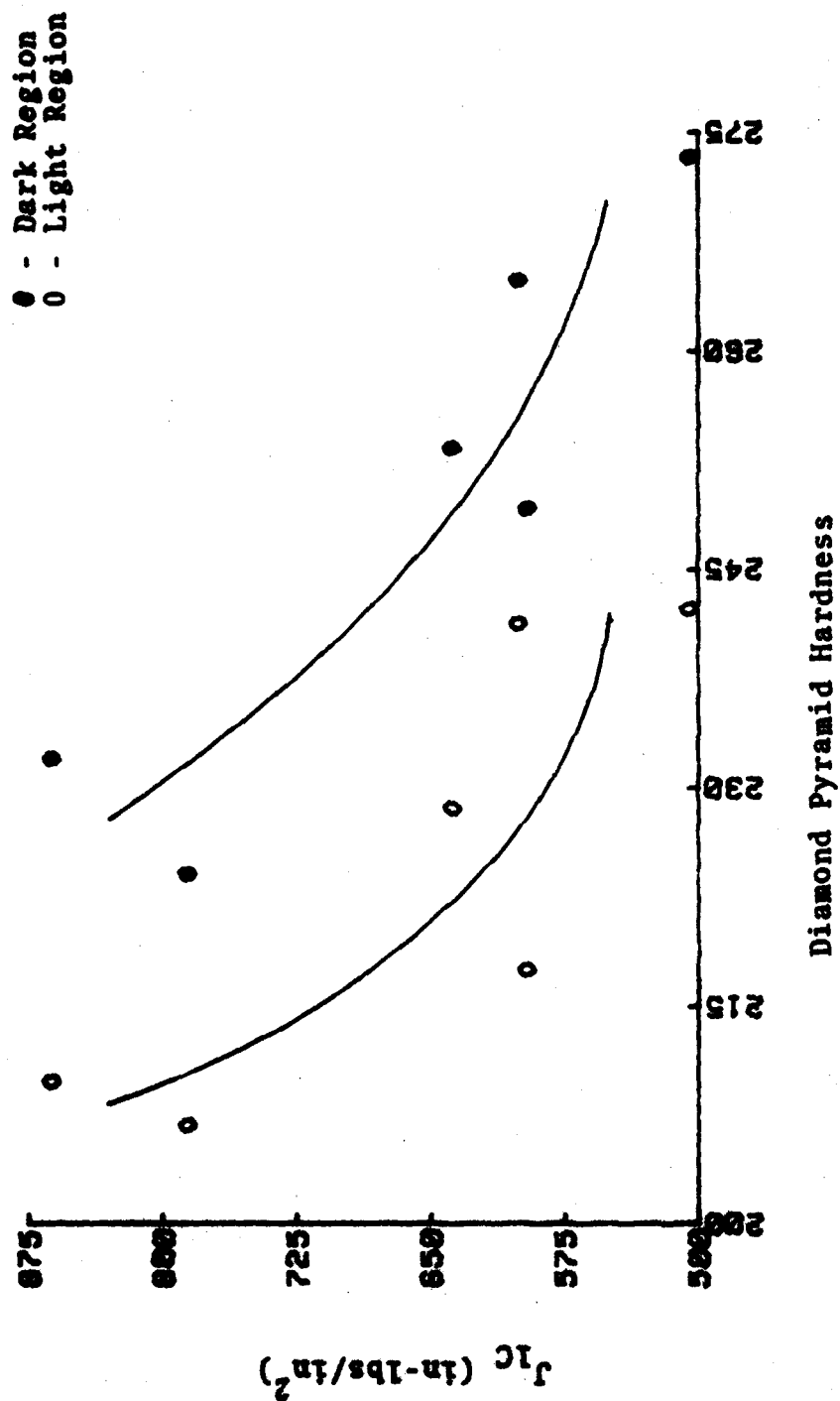
Figure 39. J_{1C} versus DPH in HY-80
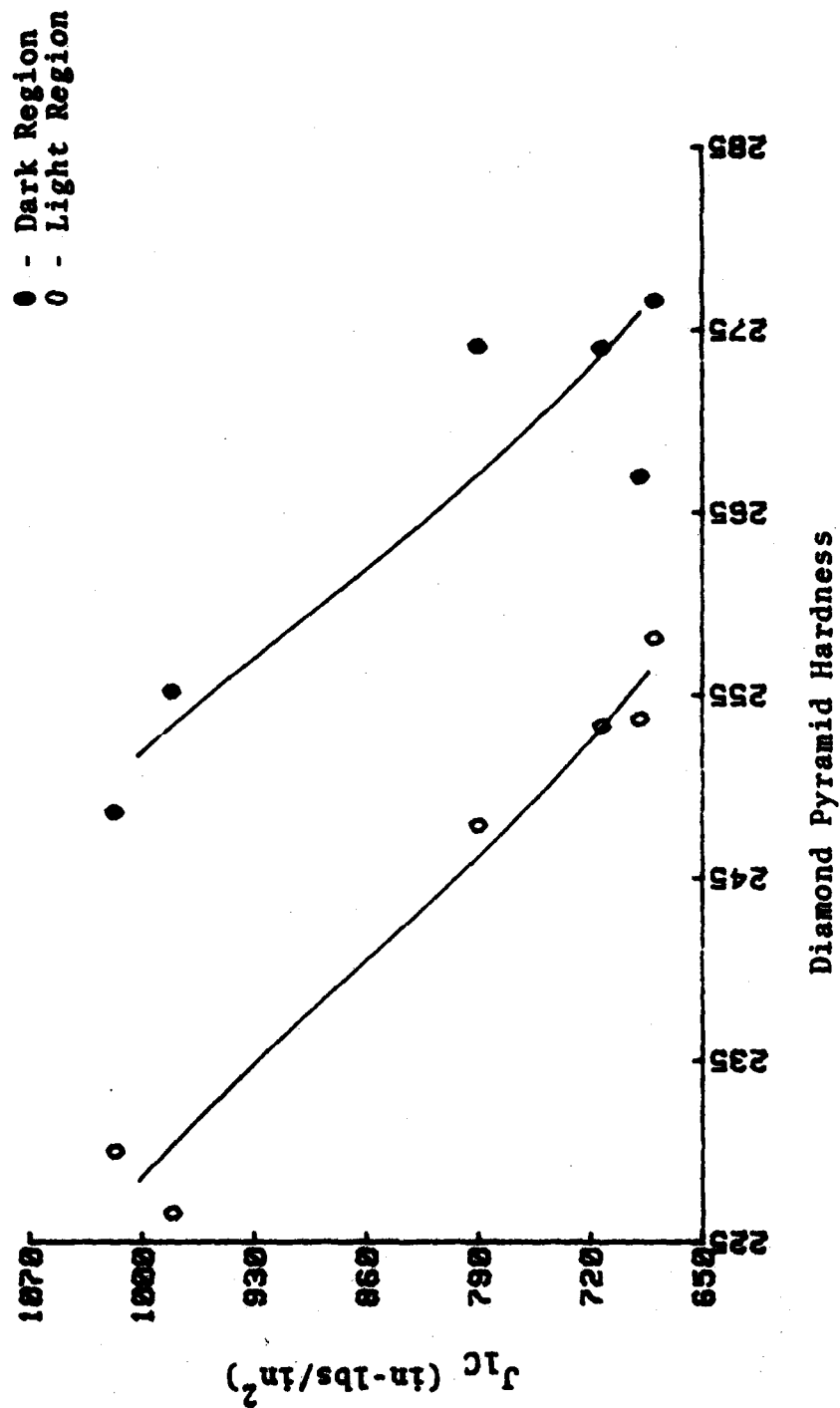
Figure 40. J_{1C} versus DPH in HY-100
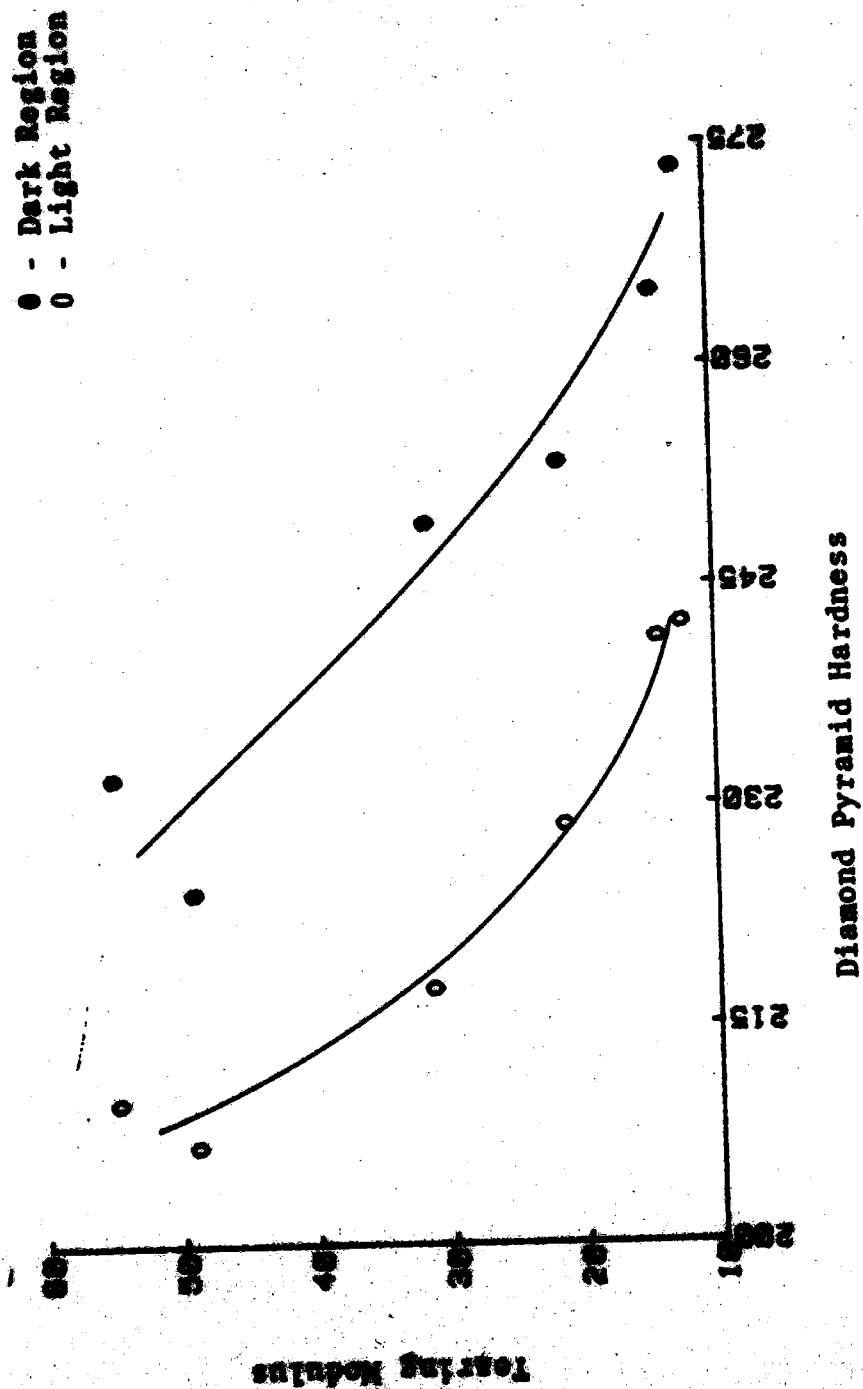
Figure 41. Tearing Modulus versus DPH in HY-80
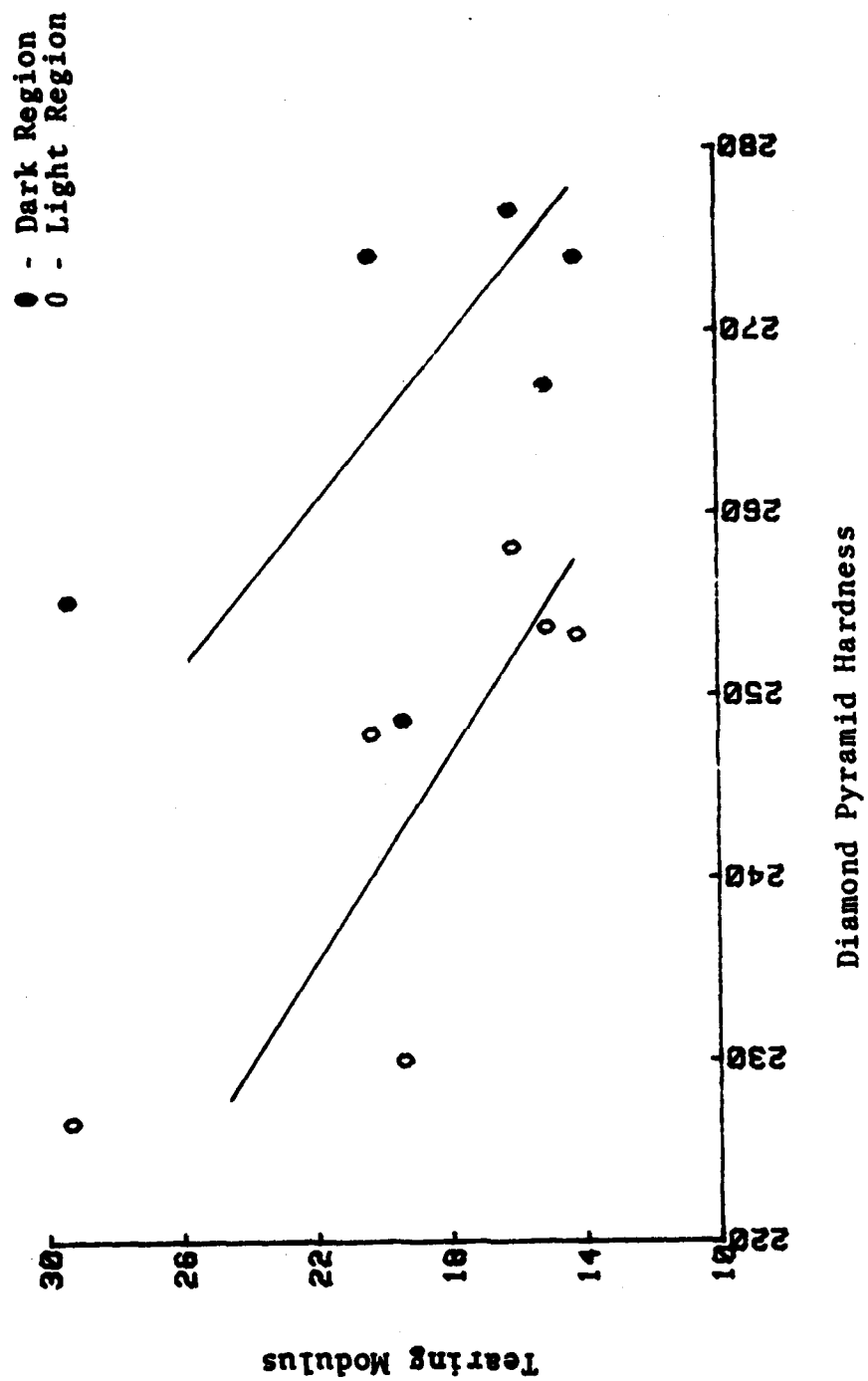
Figure 42. Tearing Modulus versus DPH in HY-100
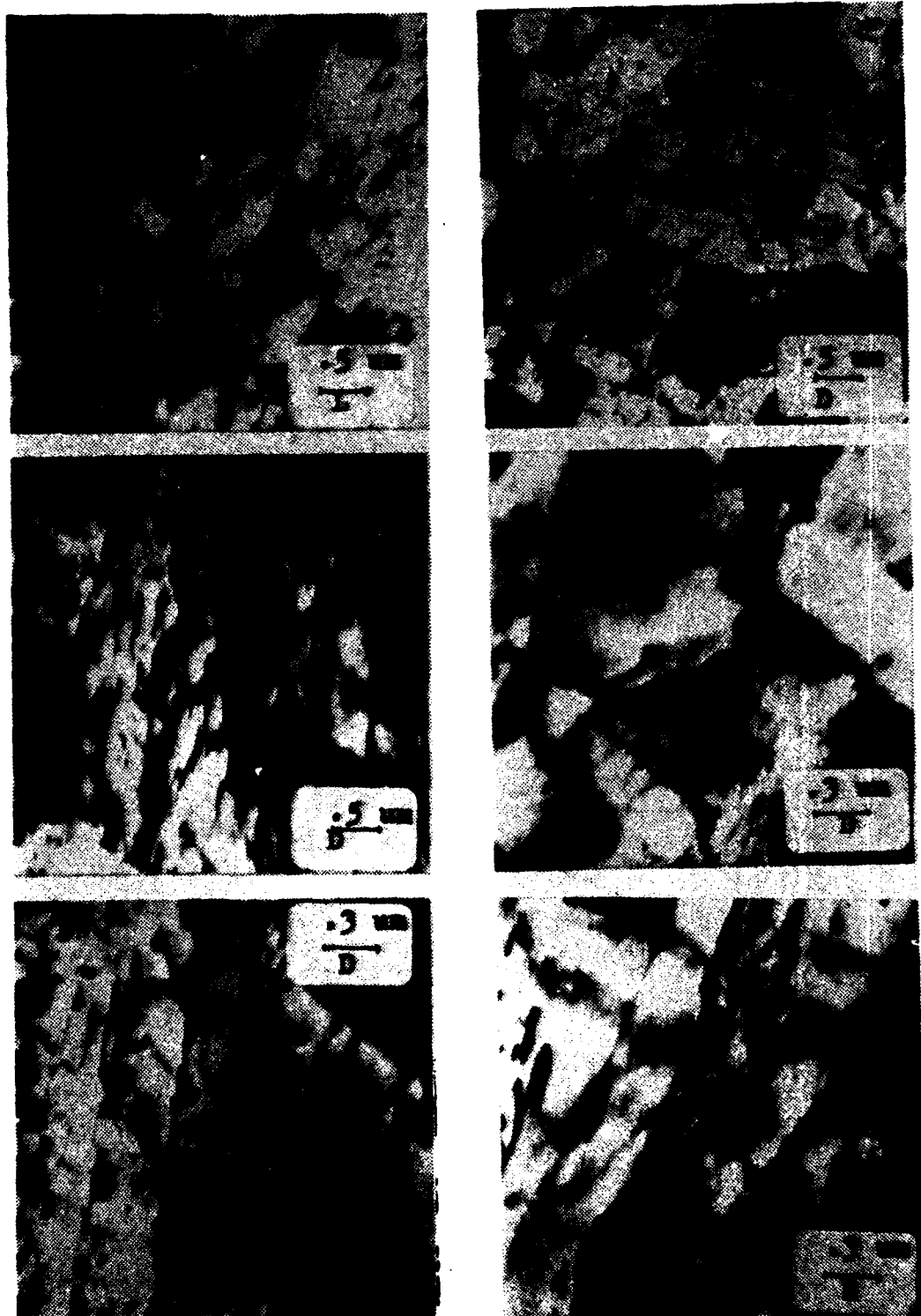
Figure 43.   TEM Photo of HY-80 Microstructure
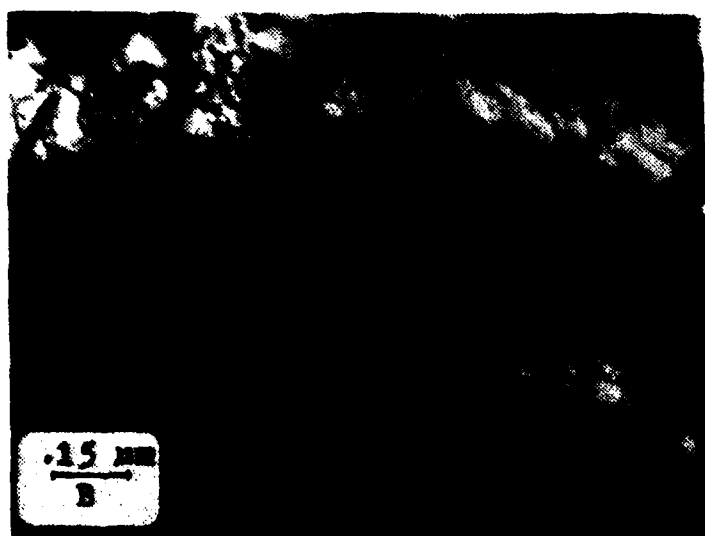
Figure 44. TEM Photo of Dislocations in HY-80

Figure 45.   TEM Photo of Transformation Twinning in HY-80
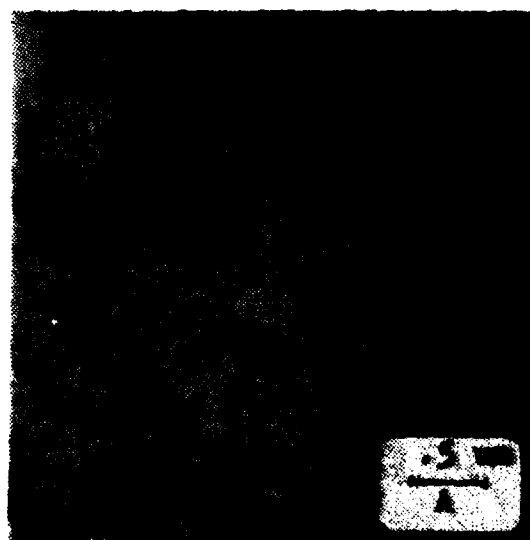
Figure 46. TEM Photo Depicting Carbide Distribution

110

Figure 47. TEM Photo of HY-100 Microstructure

111
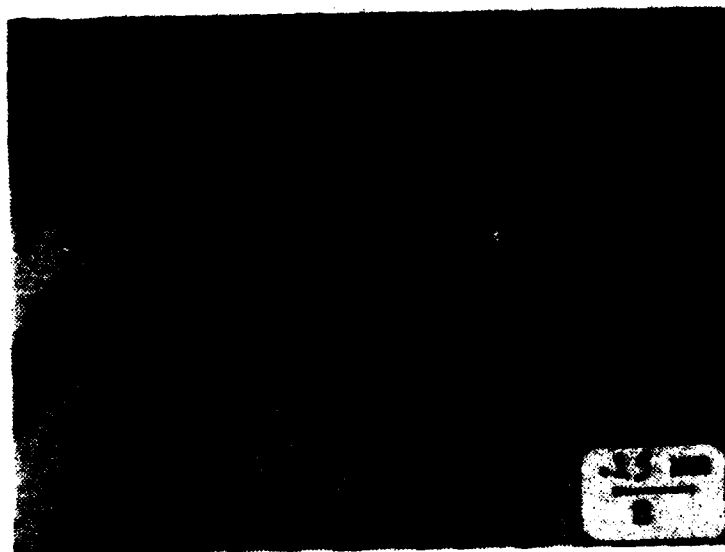
Figure 48.   TEM Photo of Transformation Twinning in HY-100
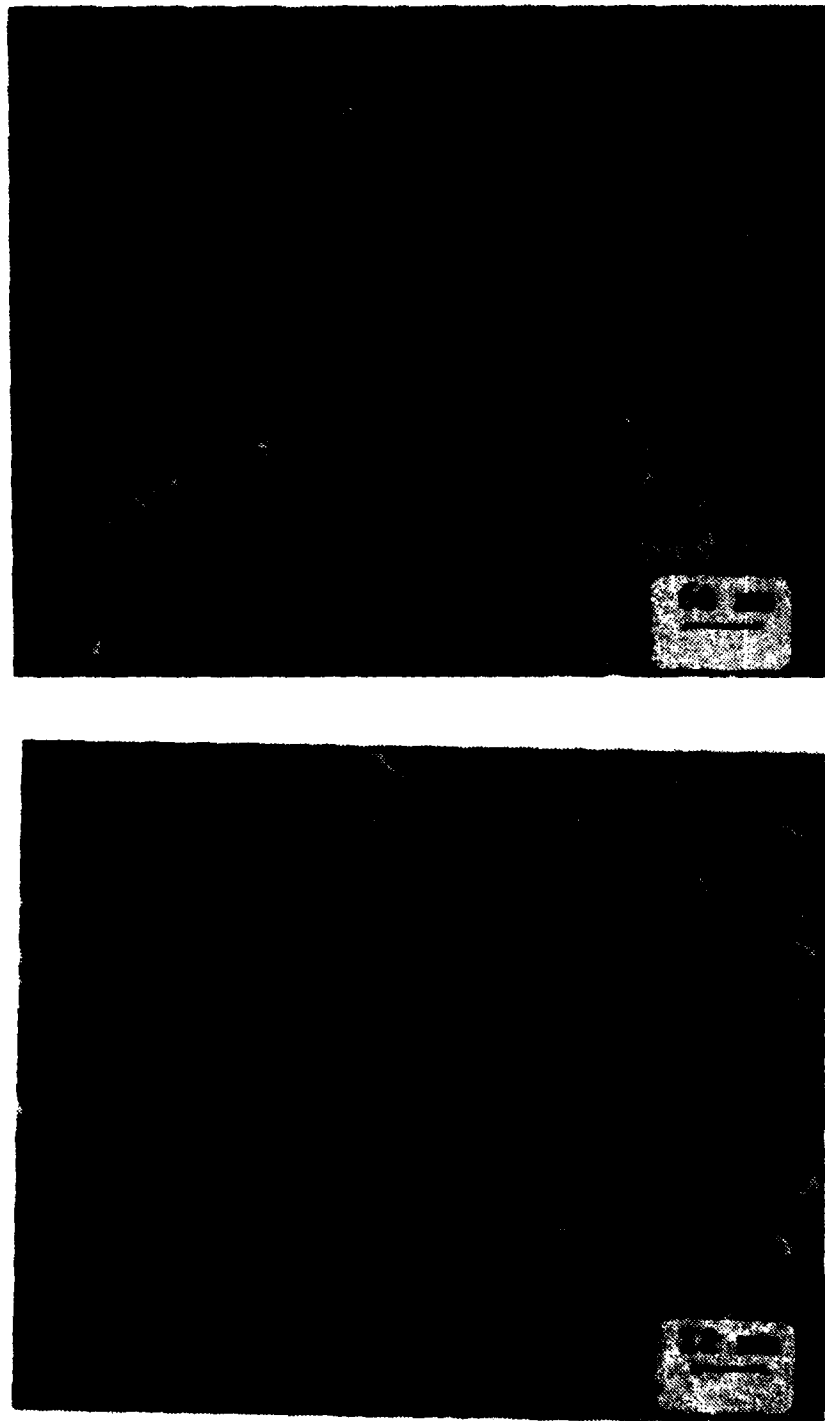
Figure 49.   SEM Photo of Sample P Fracture Surface
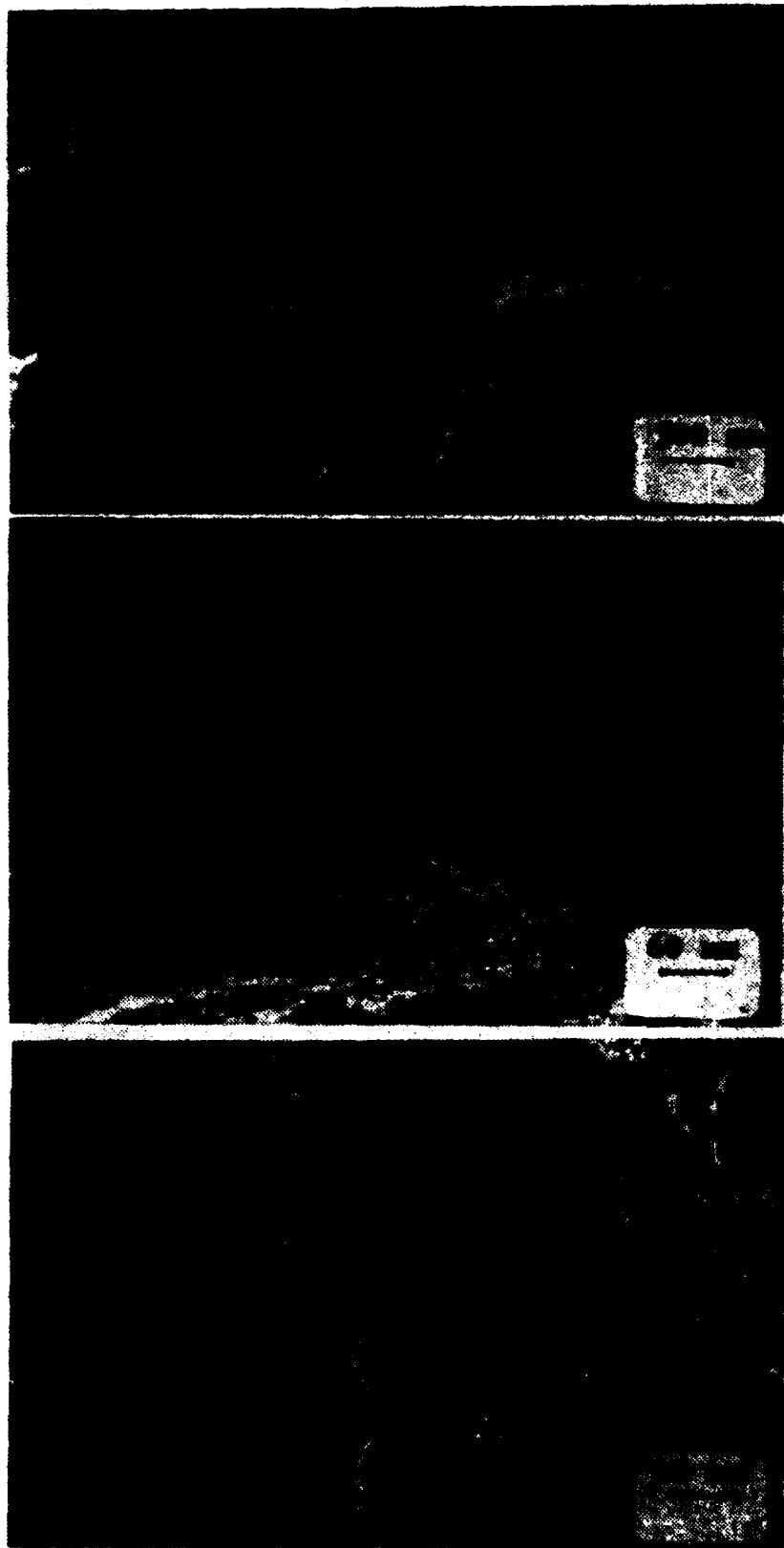
Figure 50.   SEM Photo of Sample D Fracture Surface
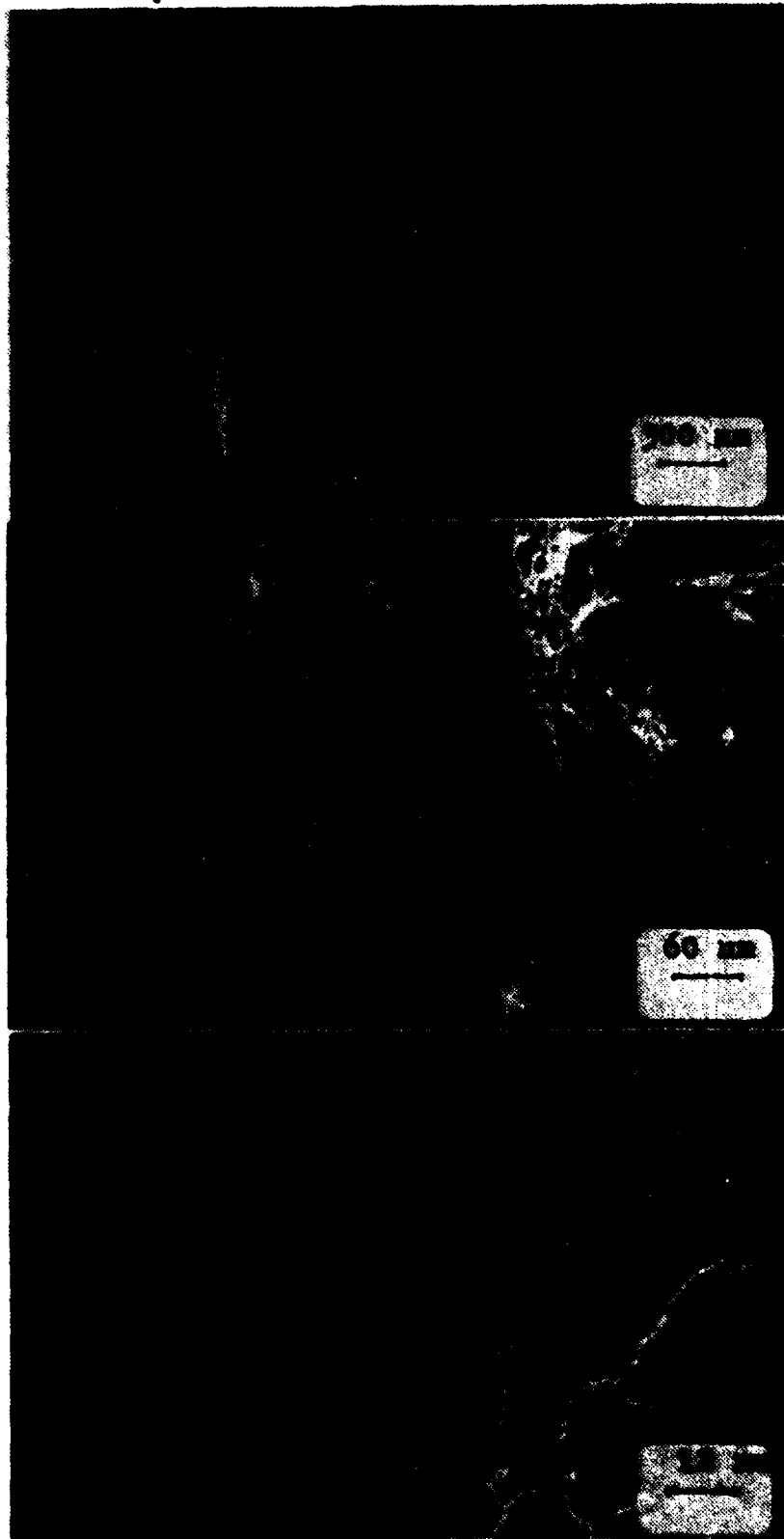
Figure 51.   SEM Photo of Sample B Fracture Surface

115
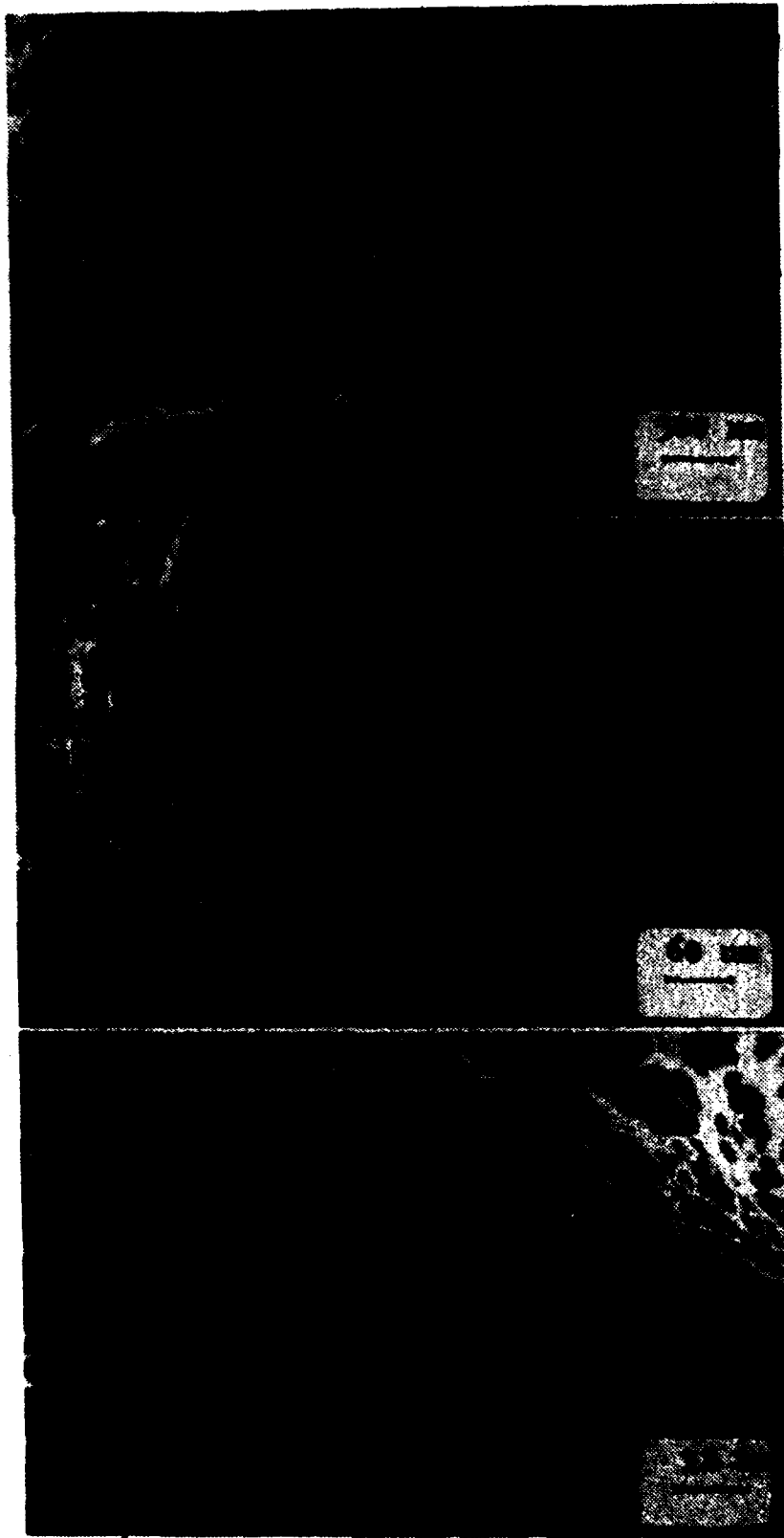
Figure 52. SEM Photo of Sample I Fracture Surface

116
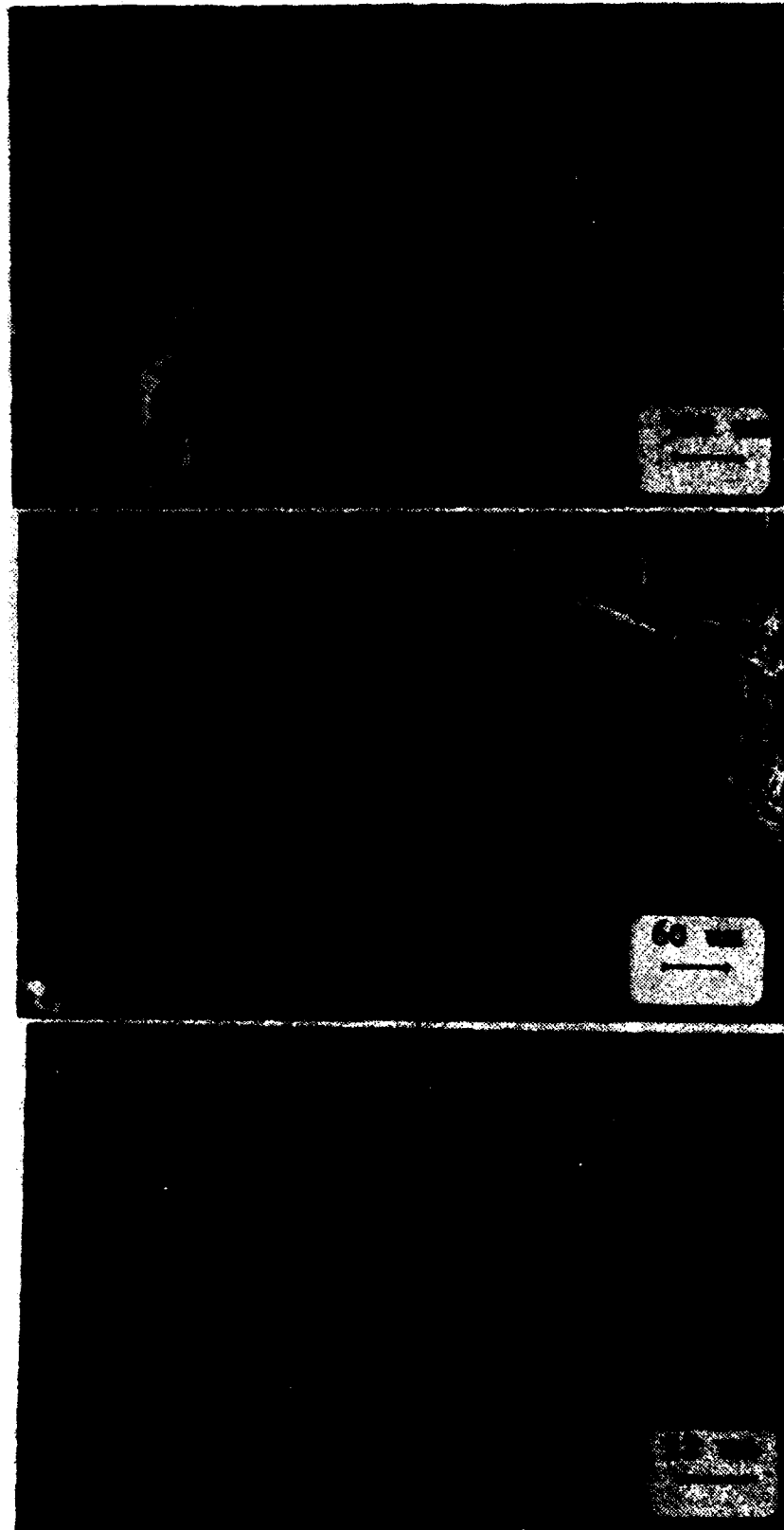
Figure 53.   SEM Photo of Sample T Fracture Surface
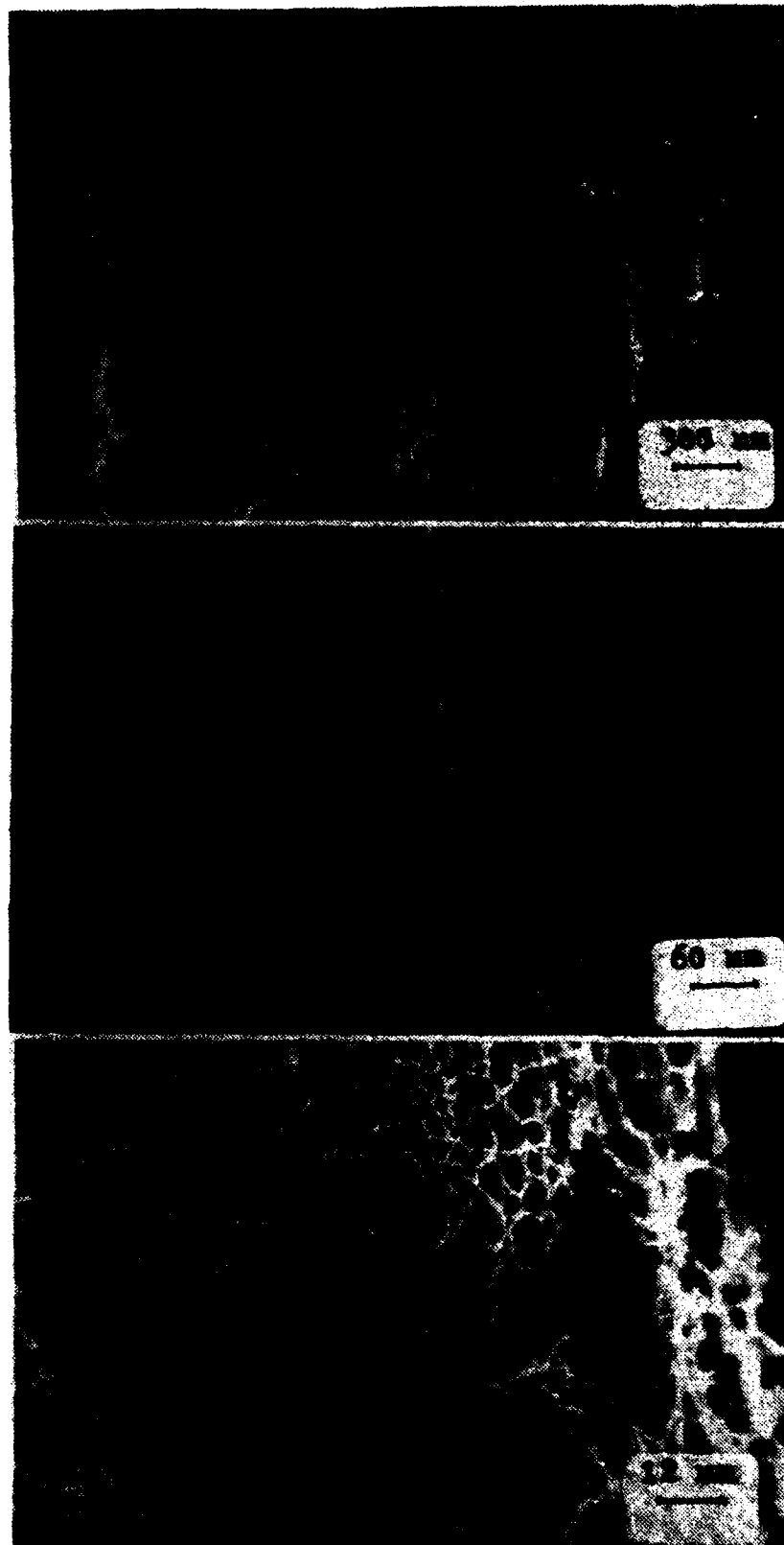
Figure 54. SEM Photo of Sample W Fracture Surface
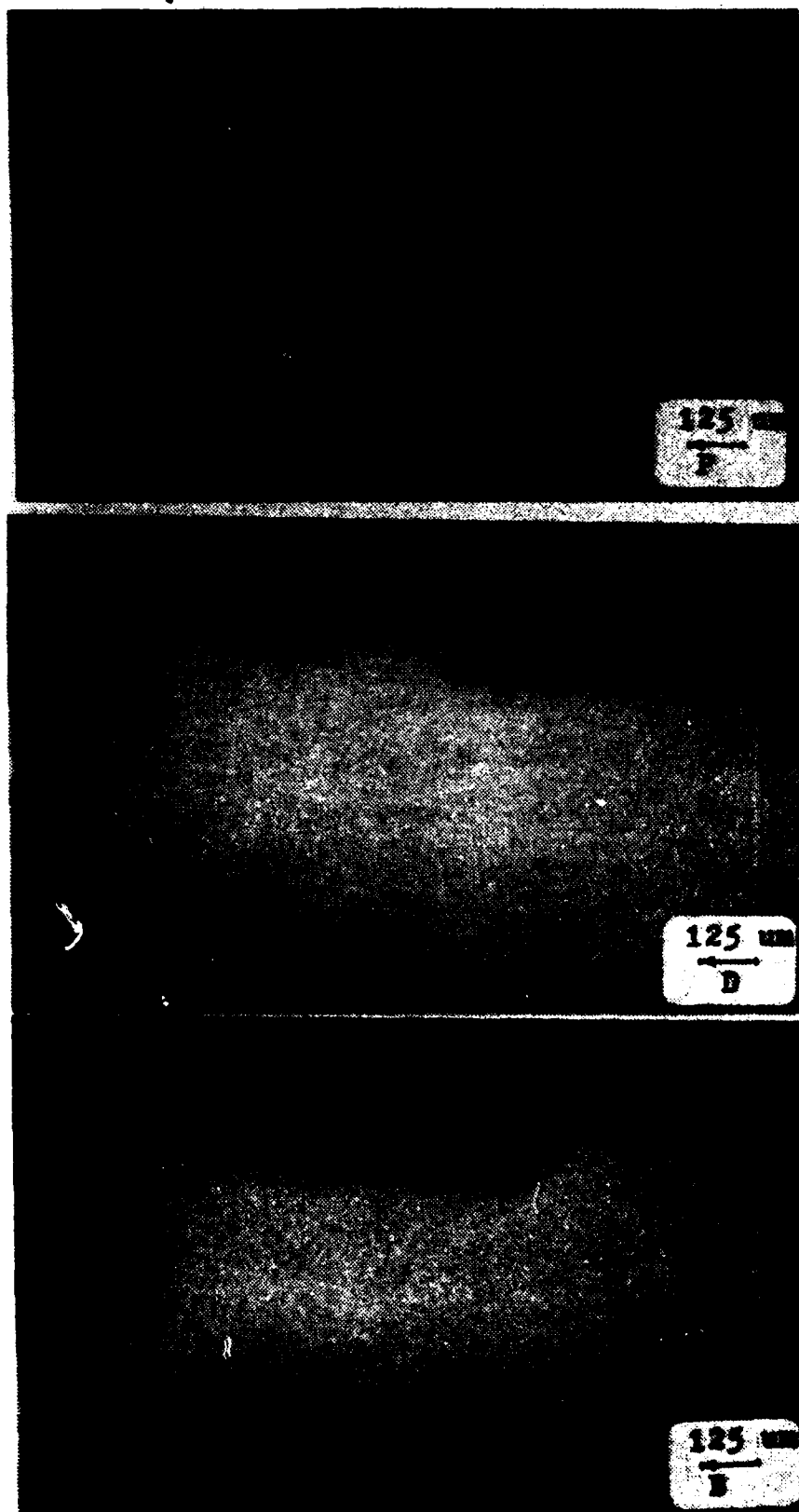
Figure 55. Metallographic Views of HY-80

119
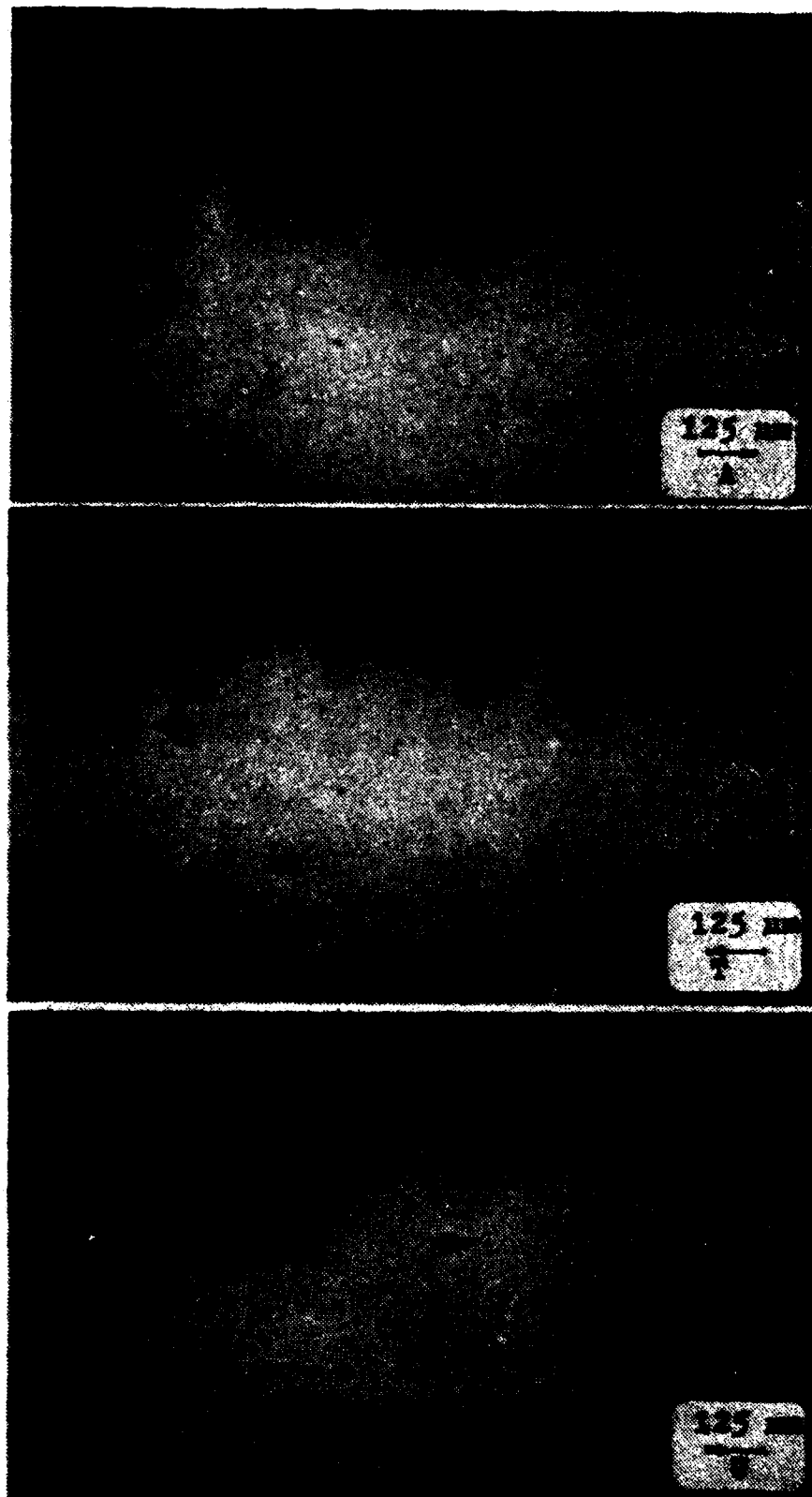
Figure 56. Metallographic Views of HY-100
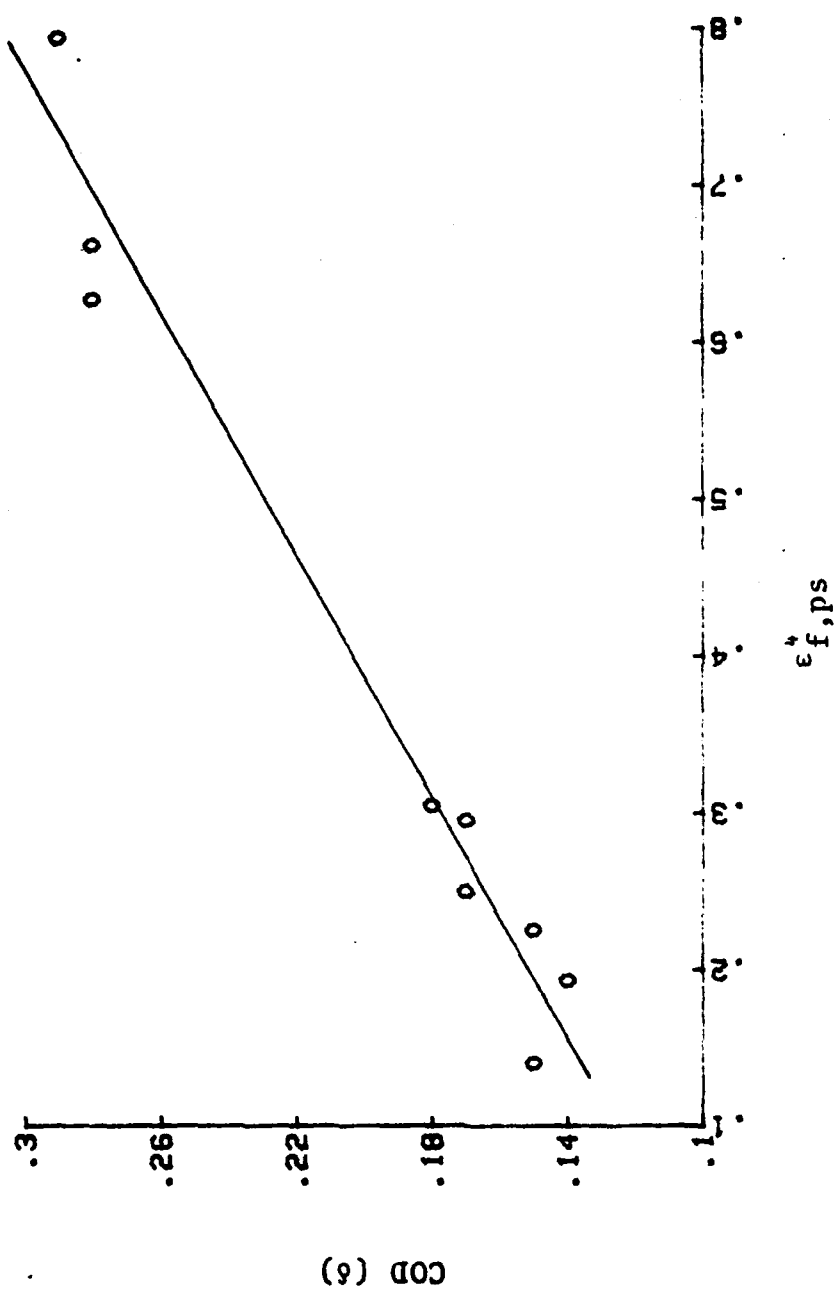
Figure 57. Miller's COD versus Plane Strain Ductility

121
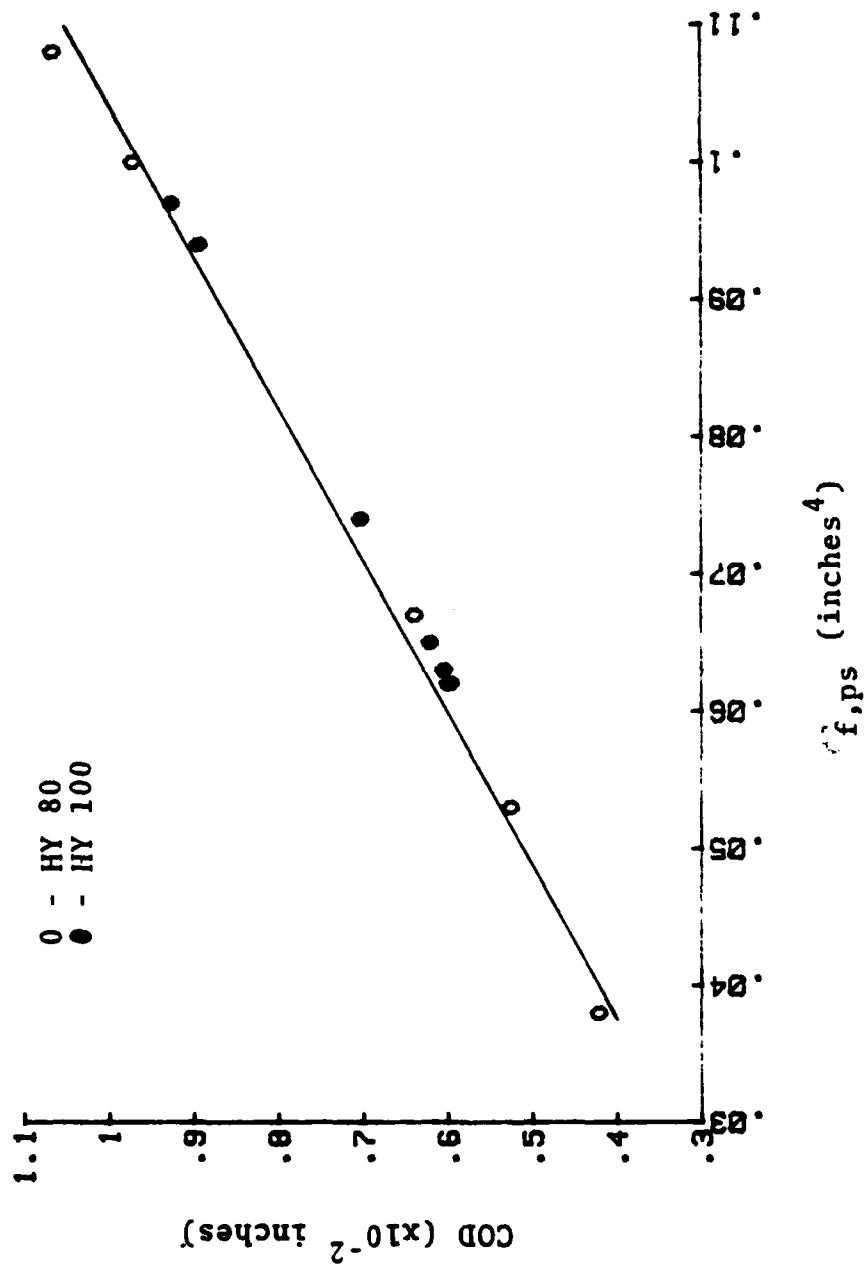
Figure 58. COD versus Plane Strain Tensile Ductility

122
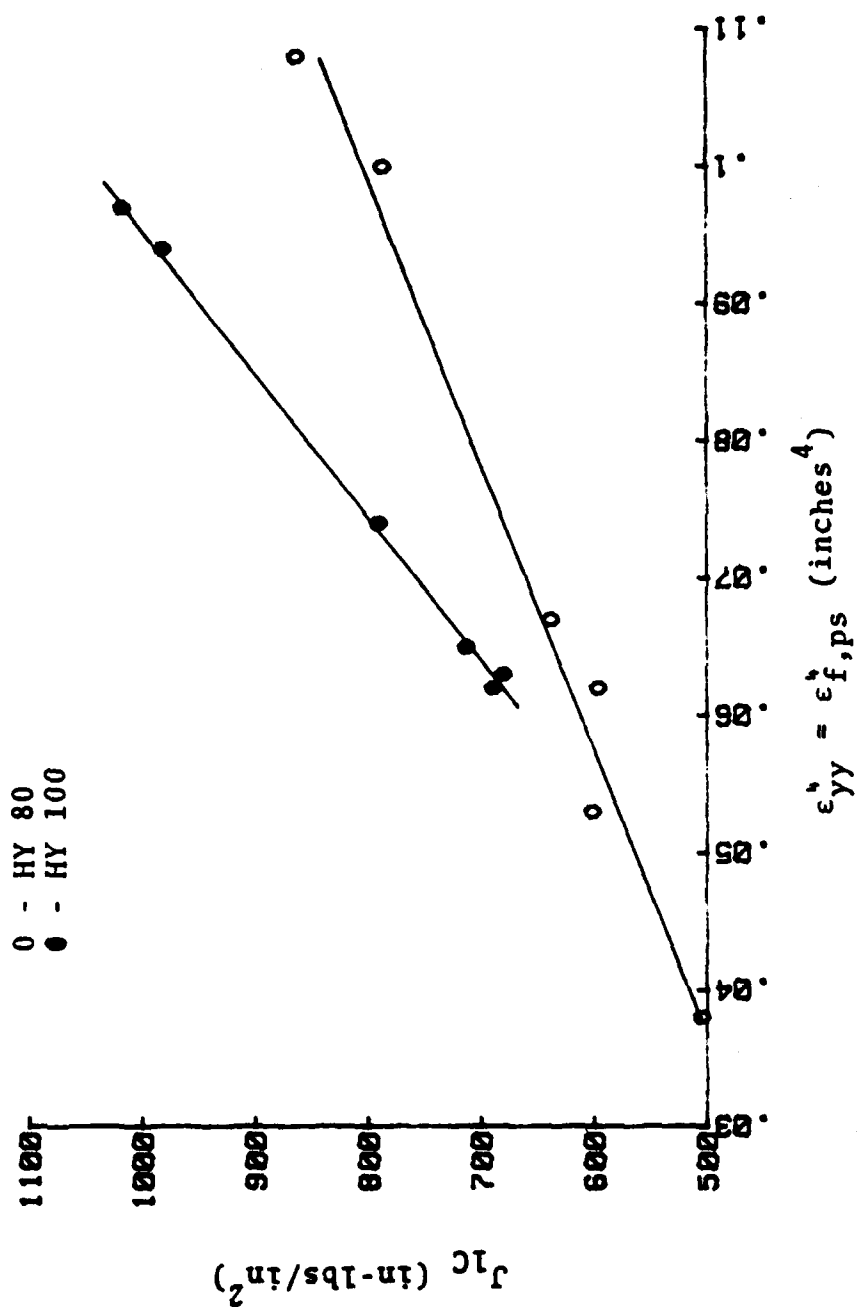
Figure 59. J_{1C} versus Plane Strain Tensile Ductility

APPENDIX A

A. INTRODUCTION

One of the more time consuming aspects of completing a thesis in the materials science area is the development of an adequate faculty in the various laboratory techniques intrinsic to a careful matellurgical study. The purpose of this appendix is to set forth in as explicit a form as possible the specimen preparation procedures utilized by the author during the course of this research. While the steps detailed may directly relate only to the subject alloy system, it is hoped that the general ideas and especially the warnings of potential pitfalls will find more widespread application.

B. FRACTURE SURFACE CLEANING BY A CELLULOSE ACETATE REPLICA PROCESS

1. General Application

On fracture surfaces, lightly oxidized, to be studied using a scanning electron microscope.

2. Equipment/Materials Required

Acetate replicating tape, acetone, cotton swabs.

3. Procedures

a. Cut a piece of heavy cellulose acetate replicating tape from the roll that is large enough to cover the fracture surface to be cleaned.

124

b.   Saturate a cotton swab with acetone and apply to only one side of the tape. Continually flood the tape surface with acetone until it begins to soften and cloud slightly.

c.   Using a thumb or finger work the wet side of the tape thoroughly into the surface to be cleaned. It is permissible to use the stick end of the swab to push the softened tape into small features which cannot be reached otherwise. Do not use anything harder than the stick however, as surface damage may result.

d.   Set aside and let dry completely. This usually takes at least twenty minutes.

e.   Carefully pull the tape free of the surface, ensuring that all the tape is removed.

f.   Repeat steps a) through e) until no visible oxides or contaminants are pulled off with the replica.

g.   Ultrasonically clean the specimen in acetone for 10-20 minutes. This will soften and remove any traces of the tape left in the surface.

4. Discussion

A general rule of thumb with fracture surfaces is the less done to them to expose the requisite detail the better. Each cleaning method leaves its imprint on the surface and this is especially true with any form of chemical cleaning. Accordingly, less drastic methods should be

125

employed before replica stripping is attempted. Further, acetone attacks some alloys, so ensure the material being examined is not susceptible to this before this technique is tried. Replica cleaning has been used successfully on many low alloy steels at the Naval Postgraduate School. This technique was used exclusively on all fracture surfaces examined in this study.

C. FRACTURE SURFACE CLEANING BY AN ACID CLEANING TECHNIQUE

1. General Application

On fracture surfaces, heavily oxidized, to be studied using a scanning electron microscope.

2. Equipment/Materials Required

Concentrated HCl, distilled water, hexamethylene tetramine, ultrasonic cleaner.

3. Procedures

a. Into 50 cc of distilled water slowly pour 50 cc concentrated HCl. Add 0.2 gm hexamethylene tetramine and stir until completely dissolved.

b. Place approximately one inch of the solution in a small beaker and ultrasonically clean the specimen for approximately 10 seconds in the solution at room temperature.

c. Rinse the specimen thoroughly in ethanol and visually inspect the surface. An adequately cleaned steel surface will have a grayish cast.

126

d. If the surface is still badly contaminated, repeat steps a) through c) until satisfactory results are obtained. Cleaning times greater than 30 seconds are unusual and will probably damage the specimen.

e. Replica clean the surface in accordance with the previously described technique.

4. Discussion

This is a last resort technique and should only be used if all else fails. It has been included only for completeness. Note that a fairly concentrated acid solution is called for and even though the hexamethylene tetramine serves as an organic inhibitor, the solution is still very reactive. The caveats proffered in the replica cleaning discussion cannot be overstated. Excessive use of this technique will definitely eradicate much surface detail. This inhibited HCl cleaning method has been used successfully on several low alloy steels. For further information on cleaning techniques see the SEM/TEM Fractography Handbook, published by Battelle Columbus Laboratories, Columbus, Ohio in December 1975.

D. THIN FOIL SPECIMEN PREPARATION TECHNIQUE

1. General Application

Microstructural studies using a transmission electron microscope.

2. Equipment/Materials Required

Low speed diamond saw, wet sandpaper units (flat pads), micrometer, acetone, ethanol, distilled water, Servomet Spark Machine, 3mm inside diameter thin wall copper tubing, jet polishing assembly (Struers Polipower Rectifier Unit and Tenupol), low power microscope, electrolyte, small tweezers.

3. Procedures

a. Using a low speed diamond saw, cut a wafer of the material to be examined about .009 - .012 inch thick. This requires the first saw cut to square one side, and the second cut to produce a wafer with nearly parallel surfaces.

b. Clean the wafer thoroughly to remove all traces of cutting oil/saw coolant with acetone, taking extreme care not to bend the wafer.

c. Mount the wafer on a thin brass strip using double stick tape. Ensure that the strip and wafer surface are absolutely dry and try not to touch the tape with your fingers. Press firmly to obtain good adhesion. Mounting the specimen on the strip allows for spark cutting without movement or loss of the 3mm disk.

d. Follow the steps outlined in Appendix B for the use of the Servomet Spark Machine for cutting 3mm diameter disk. When removing the disk from the adhesive caution must be exercised to ensure that the disk is not bent.

Bending the sample induces gross plastic deformation which will invalidate any microstructural features observed. Tweezers are used to remove the 3mm disk.

e. Once the wafer is free, ultrasonically clean the thin 3mm disk in acetone to remove the dielectric (kerosene) and any mastic residue. Again, the importance of not bending the specimen cannot be over emphasized.

f. Lightly sand each side of the 3mm disk with 600 grit paper to remove the burrs around the edges. This will greatly improve the seal obtained in the specimen holder and will also prolong the life of the holder.

g. Wash the disk in ethanol and blow dry using a hand held dryer.

h. Set up the Tenupol and Polipower as described in Appendix B under Tenupol Operations.

i. Record electrolyte temperature, pump flow rate, rectifier voltage and current settings. Electrolyte selection is covered in detail in the experimental section of this thesis.

j. After jet polishing has created a small hole in the 3mm disk, rapidly remove specimen holder and immerse it in a beaker of distilled water. While immersed, open the holder and allow the specimen to fall free.

k. Remove sample from the distilled water and place it in a watch glass filled with ethanol. During all handling, do not bend or scratch the sample.

129

1. After rinsing the sample, place it on dry filter paper or lens paper to remove all remaining fluids.

m. Place sample on a glass slide and inspect the polished surfaces for a bright shiny appearance, for a small uniform hole with smooth sides, and for no indications of either etching or pitting using a low power light microscope. If etching is present then current must be increased and/or flow rate increased. If pitting is present the current is too high. Macro current changes can be effected by adjusting the voltage setting on the Polipower.

n. With an optically good sample, commence trans-mission electron microscopy. The operating procedures employed on the JEM 100 CXII transmission electron micro-scope by JEOL Ltd are included in Appendix B.

APPENDIX B

A. INTRODUCTION

Safe, efficient operating procedures for all equipment used in a material science research thesis are mandatory. This appendix delineates those procedures used on the major systems employed during the course of this authors research. It is hoped that future material science students will be able to use these procedures to help reduce the time required in equipment familiarization and operations.

B. S4-10 STEREOSCAN SCANNING ELECTRON MICROSCOPE, OPERATING procedures for

    1. Start Up

        a. Room Light......................... ON

        b. Day Switch......................... ON

        c. Chamber Isolation valve........... fully anticlockwise

        d. Specimen Stage Clamp.............. Release

        e. Auto Pump/Spec Change Switch....... Press Spec Change

        f. Carefully withdraw the specimen stage from its housing until the safety catch prevents further movement.

        g. Insert the specimen stub in the its holder and insert the specimen stage.

h. Specimen Stage Clamp............ Latch

i. Auto Pump/Spec Change.......... Press Auto Pump

j. Wait for vacuum Ready Light.... Green

k. Chamber Isolation Valve........ Rotate clockwise
until aperture
detent required is
found. Do not open
until isolation valve
green light is
illuminated.

l. Switch EHT..................... ON

m. Switch PM...................... ON

n. Switch CRT and Collector....... ON

o. Switch the Filament............ ON

p. Turn the FILAMENT CONTROL slowly clockwise until
the working current is 2.5A. Do not exceed 2.8A.

2. <u>Obtaining an Image</u>

a. Scan Generator................. switch to Visual
Raster

b. Scan Generator................. Switch to VERT

c. Magnification Unit............. select 20X

d. Visual Display Unit............ turn BLACK LEVEL
control fully
anticlockwise

e. Visual Display Unit....... turn BLACK LEVEL control clockwise. A defocused image will now be observed

f. Adjust current control to foscus the image.

3. <u>Photographic Recordings</u>

a. Insert film into the Polaroid 545 land film holder.

b. Position final condenser knobs to focus imagine one display screen.

c. Scan Generator; select LINE SET position (knob 2).

d. Scan Generator; vary Y SHIFT knob through full range. Observe signal level on wave form monitor. The majority of the wave amplitude should be within two vertical increments on the screen. Also, signal should not bottom out.

e. Adjust signal amplitude and lower the peak by adjusting both the BLACK LEVEL (knob 3) and the PM VOLTAGE (knob 4).

f. With a proper signal select RECORD RASTER on the Scan Generator (knob 2).

g. Depress the RESET BUTTON on the Scan Generator (button 6).

h. Expose the film.

i. Depress the START button on the Scan Generator (button 7).

j. Once the signal on the Waveform Monitor has disappeared, process the film.

133

k. On the Scan Generator; select VISUAL RASTER position on knob 2.

4. <u>Specimen Change and Securing</u>

    a. Specimen Isolation Valve............. close (anticlockwise)

    b. Magnification Unit................... select 20X

    c. Filament Control..................... REDUCE

    d. Switch EHT (skip if changing specimen).... OFF

    e. Switch PM............................ OFF

    f. Switch CRT and COLLECTOR............ OFF

    g. Switch the Filament................. OFF

    h. Specimen Chamber Clamp.............. RELEASE

    i. AUTO PUMP/SPEC CHANGE............... SPEC CHANGE

    j. Withdraw stage and remove specimen

    k. Stage and Chamber Clamp............. CLOSE and LATCH

    l. AUTO PUMP/SPEC CHANGE............... AUTO PUMP

    m. Return to start up procedure 1j if only changing specimen, otherwise continue

    n. NIGHT SWITCH........................ ON

5. <u>Additional Information</u>

    a. For additional operating procedures see:

OPERATING INSTRUCTIONS S4-10 STEREOSCAN SEM MANUAL NUMBER TL 1116-0M-96118-0002

C. SERVOMET SPARK MACHINE, OPERATING PROCEDURES FOR

    1. Normal Operations

        a. POWER switch.......................... ON

        b. Work Position control............... select RAISE

        c. Work Position control............... select WORK

        d. POWER switch.......................... OFF

        e. Clamp sample in position and attach HT lead to
the sample. Ensure alligator clip is in contact with piece
to be cut.

        f. Place electrode into the modified lathe holder.

        g. Position the electrode over the area to be cut by
adjusting the position of the holder. The holder moves radi-
ally along the slide bars, and the slide bars can also be
rotated.

        h. POWER switch.......................... ON

        i. Work Position control............... LOWER

        j. Work Position control............... select WORK

        k. Electrode position switch .... select CUT

        l. HT switch............................. ON

        m. HT level switch...................... select 5

        n. For automatic timed operation pull out the TIMER
switch.

        o. Serve control switch................. ON

        p. Timed sequence will cycle through position 7
before turning the machine off.

q. If not timed, TIMER switch off, a cutting position
must be selected and the operator must periodically check the
sample to obtain an estimate of the time required to cut the
disk. Otherwise the operator runs the risk that the sample
will release and will be lost in the dielectric or will bend
up into the 3mm inside diameter electrode and become egg shaped.

r. After the sample is cut or when inspection of the
cutting, progress is required HT switch.......... select OFF

s. SERVO................................. OFF

t. HT level switch....................... OFF

u. Work Position control................. select RAISE

v. Work Position control................. select WORK

w. Electrode position switch............. select UP

x. Servo control switch................. select ON

When enough clearance exist to remove or inspect the
sample continue.

y. Servo control switch................. select OFF

z. Power switch......................... OFF

WARNING WARNING WARNING. The dielectric is kerosene
and if the table is raised or lowered with the HT switch ON
an explosion is possible.

aa. Additional information see THE SERVOMET SPARK
MACHINE Manual.

D. STRUERS TENUPOL AND POLIPOWER, OPERATIONS OF

1. <u>Normal Operations</u>

a. Ensure all components are clean. A contaminated tank or component on the Tenupol unit can result in an improperly polished surface and loss of sample.

b. Place the electrolyte in the tank.

c. Set the Tenupol unit in place atop the tank.

d. Electrically connect the Tenupol to the Polipower at the polishing cell jack.

e. Plug in both the Polipower and the Tenupol.

f. Position the 3mm jets in the Tenupol.

g. Attach the photocell.

h. Increase the bulb current to maximum.

i. Connect the black leads to the jets.

j. Mount the specimen in the 3mm specimen holder and position the holder between the jets.

k. Turn on the MAINS and the THINN switches on the Tenupol and rotate the photocell sensitivity knob until an audible alarm sounds.

l. Back off on the sensitivity knob 1-1.5 increments and repeat the previous step and this step until the alarm remains silent.

m. Turn off the MAINS and the THINN switches.

n. Set the pump flow rate on the Tenupol.

o. Turn on the MAINS and pump switch on the polipower.

p. Adjust the voltage level by rotating the voltage regulation knob to the desired level.

q. Connect the red lead to the specimen holder.

r. Turn on the MAINS and the THINN switches.

s. Allow sufficient time for the fluid level to stablize approximately 20 seconds at a flow rate of .5.

t. Turn on the Current switch on the Polipower.

u. As soon as an audible alarm sounds indicating a hole in the specimen, rapidly remove the specimen holder and immerse it in distilled water.

v. Turn-off MAINS and PUMP switch, the Current switch, the MAINS switch, and the THINN switch.

w. For additional information see the STRUERS TENUPOL INSTRUCTION Manual.

E. JEOL TRANSMISSION ELECTRON MICROSCOPE MODEL JEM 100CX II operating procedures for

1. <u>Normal Operations</u>

a. Turn POWER key on microscope fully clockwise to START and release.

b. After 15 minutes DP/HIGH/READY green lights will illuminate.

c. Fill cold trap with liquid nitrogen.

CAUTION: Insure all glass observation ports are closed and covered with a cloth towel. The liquid nitrogen will damage the glass viewing ports.

d. Press HT button and 60KV accelerating voltage button, then 80KV and finally the 100KV. NOTE: watch the beam current meter till stable before increasing the accelerating voltage.

e. Check all apertures are withdrawn except the condenser aperture.

f. Note the condenser system alignment, the current center adjustment, the image forming system alignment and the dark field mode alignment should not be required. If suspected contact the technician or your thesis advisor.

g. Check the specimen is secure in the holder by turning the holder upside down and tapping gently.

h. Turn FILAMENT EMISSION knob fully anticlockwise.

i. STAND UP never insert specimen holder while sitting at console.

j. Check goniometer is at 0 degrees and engage the clutch.

k. Line up slot in Goniometer and the pin on specimen holder shaft and then push in the holder until it stops.

l. Apply light pressure to the holder until a click is heard and the red light on the goniometer illuminates. The airlock will now be evacuated.

m. When the red light extinguishes turn holder fully clockwise and then allow to slide slowly into the microscope. Hold onto it!

n. Turn FILAMENT EMISSION knob to saturation.

o. Defocus beam by rotating the coarse CONDENSER knob 5 clicks anticlockwise.

p. Press function button SCAN.

q. Rotate the right hand specimen positioning knob 20 turns from either stop position.

r. Turn on the Specimen Position Indicator.

s. Position spot on the specimen position indicator in the center using both position translate knobs.

t. Start search for the hole in the specimen using the translate knobs. You may use the specimen positioning knob to help find the lightest region.

u. Check OBJECTIVE aperture is out.

v. The magnification is changed by means of the small MAGNIFICATION knob.

w. Condense the beam.

x. Move the edge of the sample over the condensed beam using the specimen positioning knobs.

y. Select SADIFF

z. Insert the objective aperture 1

aa. Focus the center spot of the diffraction pattern using the small knob on the SA/HADIFF camera length knob.

ab. Center the objective beam around the diffraction pattern center spot by means of the objective aperture translation screws.

ac. Depress MAG to return to a bright field image.

2. **Focussing**

a. The image is focussed by means of three knobs on the right hand console. As a focussing aid use the image wobbler as follows:

b. Turn on the image wobbler switch.

c. If image brightness fluctuates press SCAN button and condense beam to smallest spot.

d. Eliminate beam oscillation with image wobbler A and B knobs (right hand upper door).

e. Reselect MAG mode.

f. Tilt flourescent screen and observe image through binoculars.

g. Adjust focus until image doubling is completely eliminated.

h. Turn off image wobbler.

3. **Objective Astigmatism**

a. The objective astigmator controls are located in the upper left door. There are two sets of controls labelled 1 and 2, selected by a switch. Either may be used.

b. Obtain the best focussed image as above.

c. Adjust appropriate OBJ STIGMATOR coarse and fine X and Y knobs to eliminate astigmatism and obtain best image quality.

4. **Taking Photographs**

a. Only the area included within the four corner marks on the screen can be photographed.

b.   Check CAMERA: AIRLOCK OPEN lamp is illuminate.

c.   Focus desired area of specimen using tilted screen and binoculars.

d.   Lower the viewing screen.

e.   Depress SHUTTER AUTO and FILM ADVANCE SINGLE buttons.

f.   Adjust exposure: SHUTTER SPEED knob until green light is lit.

g.   Depress CAMERA FILM ADVANCE button.   The file will advance, the photograph number will be printed on the film.

h.   When the CAMERA: FILM ADVANCE button is illuminated raise the screen by the lower button.

i.   The correct exposure will be made automatically. While this happens the red EXPOSURE light is lit.

j.   When the exposure is finished lower the screen by the button.

5.   Switching Off

a.   Turn FILAMENT EMISSION knob to OFF.

b.   Zero specimen tilt.

c.   Remove specimen holder from microscope and return to box; remember to stand up when removing the specimen holder.

d.   Remove objectives and selected area diffraction apertures.

e.   Turn FILAMENT EMISSION knob to saturation.

f.   Adjust illumination so that screen is filled at magnification of 2.7K.

g.   Turn FILAMENT EMISSION knob to OFF.

h.   Depress ACCELERATING VOLTAGE OFF button.

i.   At end of the day turn POWER key OFF.

j.   For additional information or particulars in a given area see the JEOL JEM 100CX II manual. There are three different sets of operating procedures within the manual.

LIST OF REFERENCES

1. Heller, S. R., Jr., "An Evaluation of HY-80 Steel as a Structural Material for Submarines, Part II:" _Naval Engineers Journal_, pp. 193-200, April 1965.

2. ASTM Special Technical Publication 494, _Welding the HY Steels_, by R. W. Flax, R. E. Keith, and M. D. Randall, pp. 7-9, April 1971.

3. Department of the Navy Military Specification MIL-S-1162 16H (SHIPS), _Military Specification Steel Plate, Alloy, Structural, High Yield Strength (HY-80 and HY-100)_, 15 March 1972.

4. Heller, S. R., Jr., "An Evaluation of HY-80 Steel as a Structural Material for Submarines, Part I:" _Naval Engineers Journal_, pp. 29-44, February 1965.

5. "Modern Alloying Theory Upgrades Engineering Materials," _Metals and Materials_, pp. 39-43, November 1976.

6. Dancoisne, P. L., "Spotlight on Manganese," _Metals and Materials_, pp. 18-24, June 1978.

7. Brick, R. M., Pense, A. W., and Gordon, R. B., _Structure and Properties of Engineering Materials_, pp. 250-277, McGraw-Hill Book Company, 1977.

8. Hertzburg, R. W., _Deformation and Fracture Mechanics of Engineering Materials_, pp. 348-354, John Wiley and Sons, 1976.

9. _The Determination of the Elastic-Plastic Toughness Parameter_, J_{1C}, working document for the ASTM Standards Committee, undated.

10. Joyce, J. A., Gudas, J. P., "Computer Interactive J_{1C} Testing of Navy Alloys," _Elastic-Plastic Fracture_, ASTM STP 668, pp. 451-468, 1979.

11. Gudas, J. P., Joyce, J. A., and Davis, D. A., "Investigation of Specimen Geometry Modifications to Determine the Conservative J_{1C} - R Curve Tearing Modulus Using the HY-130 Steel System," _Fracture Mechanics, ASTM STP 677_, pp. 474-485, 1979.

144

12. U.S. Nuclear Regulatory Commission, NUREG Report Number 0311, A Treatment of the Subject of Tearing Instability, Paris, P. C., Tada, H., Zahoor, A., and Ernest, H., August 1977.

13. David W. Taylor Naval Ship Research and Development Center Report DTNSRDC-81/029, An Experimental Evaluation of Tearing Instability Using the Compact Specimen, by M. G. Vassilaros and J. A. Joyce, pp. 1-20, November 1981.

14. Structure Probe Technical Report N5392, WDS Analysis of Three Banded Steel Samples (HY-80, HY-100, HY-130), by Norman M. Walter, pp. 1-8, 25 January 1983.

15. Clayton, J. O. and Knott, J. F., "Observations of Fibrous Modes in a Prestrained Low-Alloy Steel," Metal Science, v. 10, no. 2, pp. 63-71, February 1976.

16. Mills, W. J., "The Room Temperature and Elevated Temperature Fracture Toughness Response of Alloy A-286," Journal of Engineering Materials and Technology, v. 100, pp. 195-199, April 1978.

17. Naval Research Laboratory Report 4696, Thickness and Temperature Effects on the J-Integral COD Relationship, by V. Provenzano, C. M. Hawthorne, pp. 1-23, 31 December 1981.

18. Begley, J. A. and Landes, J. D., The J-Integral as a Fracture Criterion, Fracture Toughness Proceedings of the 1971 National Symposium on Fracture Mechanics, Part II, ASTM STP 514, American Society for Testing and Materials, 1972.

19. Rice, J. R., "A Path Independent Integral and the Approximate Analysis of Strain Concentration by Notches and Cracks." Journal of Applied Mechanics, Transactions of the American Society of Mechanical Engineers, pp. 379-386, June 1968.

20. Knott, J. F., Fundamentals of Fracture Mechanics, pp. 167-175, John Whiley and Sons, 1973.

21. Barsom, J. M., and Pellegrino, J. V., "Relationship Between K_{1C} and Plane-Strain Tensile Ductility and Microscopic Mode of Fracture," Engineering Fracture Mechanics, v. 5, no. 2, pp. 209-221, 1973.

22. Knott, J. F., "Micromechanisms of Fibrous Crack Extension in Engineering Alloys," Metal Science, pp. 327-336, August-September 1980.

145

23. ASTM Special Technical Publication 559, The Measurement of K_{1C} on small Specimens Using Critical Crack Tip Opening Displacement, by J. N. Robinson and A. S. Tetelman, p. 139, 1974.

24. Fields, B. A. and Miller, K. J., "Fibrous Crack Initiation and Propagation in Prestrained HY-100 Steel," Journal of Mechanical Engineering, C91/78, pp. 133-143, 1978.

25. Bates, R. C. and Santhanam, A. T., "Relationship Between Notch Tip Strain and Crack-Opening Displacement," Materials Science and Engineering, v. 46, pp. 159-165, 1980.

26. Iricibar, R., IeRoy, G., and Embury, J. D., "Relationship of Strain Hardening and Damage in Ductile Fracture," Metal Science, v. 14, pp. 337-343, August-September 1980.

27. Tracey, D. M., "Strain Hardening and Interaction Effects on the Growth of Voids in Ductile Fracture," Engineering Fracture Mechanics, v. 3, pp. 301-315, 1971.

INITIAL DISTRIBUTION LIST

		No. Copies
1.	Defense Technical Information Center Cameron Station Alexandria, Virginia 22314	2
2.	Library, Code 0142 Naval Postgraduate School Monterey, California 93940	2
3.	Department Chairman, Code 69 Department of Mechanical Engineering Naval Postgraduate School Monterey, California 93940	1
4.	Professor K. D. Challenger, Code 69Ch Department of Mechanical Engineering Naval Postgraduate School Monterey, California 93940	5
5.	Mr. John P. Gudas, Code 2814 David W. Taylor Naval Ship Research and Development Center Annapolis, Maryland 21402	1
6.	Mr. Dave R. Anderson, Code 2814 David W. Taylor Naval Ship Research and Development Center Annapolis, Maryland 21402	1
7.	LCDR James N. Mullican 3790 Queens Road Chattanooga, Tennessee 37416	3